國 立 交 通 大 學

機 械 工 程 學 系
碩士論文

以平行化直接模擬蒙地卡羅法模擬自由分子流到近連續流的空穴

超音速流場

Parallel Monte Carlo Simulation of Supersonic Driven Cavity

Flows from Free-molecular to Near-continuum Regime

研 究 生：謝昇汎

指導教授：吳宗信 博士

中華民國九十六年七月

致謝

　　碩士班的生活將要畫上句點，馬上要開始的是另一個階段的生活，在交大的這兩年的求知路程，特別感謝指導教授吳宗信老師的諄諄教誨，吳老師悉心指導與督促，在遭遇瓶頸時總是幫我渡過難關，解決心中的疑問，讓我能順利的完成研究並且不斷地成長。另外特別感謝曾坤璋學長，在研究過程中所遭遇到問題時給予幫助，並時時督促著我前進，感謝你。還要感謝實驗室的每一位成員，李允民、周欣芸、李富利、洪捷粲、許哲維、鄭凱文、胡孟樺、陳育進、邱沅明、江明鴻學長姊，及洪維呈、盧勁全、陳又寧、王柏勝、林宗漢同學，還有正勤、士傑、志良、玟琪、政霖、育宗、丞志等學弟妹和來自紐西蘭的瓦片(Hadley M. Cave)的幫助，和你們共同在這實驗室相處的點點滴滴我會好好留在我記憶中。最後特別感謝我的父母對於我在交大念研究所這兩年的支持；另外也深深感謝女友雅筑的陪伴與鼓勵，感謝她在我低落的時候給我打氣，我將與她共同分享這分榮耀。

　　兩年很快地過去了，在交大的求學時光即將落幕，即將要邁向另一個人生的舞台，再一次感謝吳宗信老師以及交通大學對我的培育。希望大家都有美好前程以及璀璨的未來。

以平行化直接模擬蒙地卡羅法模擬自由分子流到近連續流的空穴超音速流場

學生: 謝昇汎   指導教授: 吳宗信

國立交通大學機械工程學系

摘要

空穴流場是很基本的流體力學問題,在過去也有很多人做過相關的研究。但是大多數人都是討論連續及不可壓縮流的流場,較少數人針對近連續流到稀薄流體區的流場作研究。因此我們對此做一有系統的探討

本文描述使用直接模擬蒙地卡羅法來模擬從稀薄流體區到接近連續流體範圍的二維上板空穴流場。為了確保能在較鄰近的分子發生碰撞,運用 transient sub-cells [Tesng, *et al.*, 2007] 的功能,使得同時降低計算負荷及記憶體使用量。比較使用 transient sub-cells 功能和不使用 transient sub-cells 功能之模擬結果來驗證正確性。驗證結果顯示出使用 transient sub-cells 功能可以使用大約平均自由路徑大小的網格且擁有正確性,並且大量減少計算負荷,特別是在接近連續流體範圍。流動結構被詳細討論包含上板驅動速度由馬赫數 1.1 到 4 和 Kn 數(與平均自由路徑和 cavity 大小有關)由 10 到 0.0033。

由結果顯示出速度滑動現象會在 Kn 的影響中表現的較 M 的影響為明顯。在 Kn=0.01 和 0.0033 的模擬結果, 都有再右下角出現第二渦流; 且 Kn=0.0033 在 M=4

的情況下會在左下角也出現第三渦流。固定 Kn=0.01 與 0.0033，當馬赫數升高時渦流中

心點會往左下方移動；但是當固定於高 Kn，隨著馬赫數增加渦流中心卻往相反方向移

動。

Parallel Monte Carlo Simulation of Supersonic Driven-Cavity Flow from Free-molecular to Near-continuum Regime
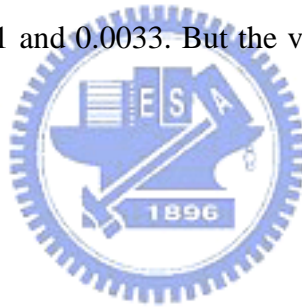
Student : Sheng-Fan Hsien   Advisor : Dr. Jong-Shinn Wu

Department of Mechanical Engineering
National Chiao-Tung University

Abstract

The driven cavity flow is one of the fundamental fluid flow problems with simple geometry that was often used as the benchmark test problem in computational fluid dynamics. Although they have been thoroughly studied in the literature, most of them were focused on incompressible or continuum compressible regime. Very few have been done in the rarefied and near continuum regimes. It may serve as the benchmarking problem for extending numerical scheme into flow in these regimes. Thus, this thesis describes the simulation of a two-dimensional supersonic driven cavity flow from free-molecular to near-continuum regime by directly solving the Boltzmann equation using the parallel direct simulation Monte Carlo method. Transient sub-cells [Tesng, *et al.*, 2007] were implemented on a general unstructured grid to meet the nearest-neighbor collision requirement, while keeping minimal computational overhead and memory requirement simultaneously. Accuracy of simulation of transient sub-cells using larger sampling cell size was verified by comparing the results with that using much finer sampling cell size. Results show that transient sub-cells can greatly reduce the

computational cost, which is especially important in the near-continuum regime. Flow

structures within a driven cavity flow are then discussed in detail by varying the top plate

speed (Ma=1.1-4) and Knudsen number of cavity (Kn=10-0.0033), in which the

corresponding Reynolds number is in the range of 0.181- 1997.6. Results show that velocity

slips and temperature jumps along the solid walls increase with increasing Knudsen number at

the same Mach number. The additional second vortex occur at the right bottom wall in all

Kn=0.01 and 0.0033 case. The Kn=0.0033 and M=4 has the third vortex at the left bottom

corner. Results show that vortex center move toward left and down as Mach number

increasing at the same Kn=0.01 and 0.0033. But the vortex center move toward the opposite

way for Kn=10, 1 and 0.1.

List of Tables

Table of Contents

List of Figures

Nomenclature

λ mean free path

ρ density

σ the differential cross section

ω viscosity temperature exponent

Ω : space domain

ε_{rot} rotational energy

ε_{v} vibrational energy

ζ_{rot} rotational degree of freedom

ζ_{v} vibrational degree of freedom

$\triangle t$ time-step

σ_T the total cross section

c the total velocity

c' random velocity

c_o mean velocity

c_r relative speed

d molecular diameter

D the throat diameter of the twin-jet interaction

d_{ref} reference diameter

E energy

k the Boltzmann constant

Kn Knudsen number

Kn_Q : local Knudsen numbers based on flow property Q

L characteristic length;

m molecule mass

M_∞ free-stream mach number

n number density

Re Reynolds number

T_o stagnation temperature

T_∞ free-stream temperature

T_{ref} reference temperature

T_{rot} rotational temperature

T_{tot} total temperature

T_{tr} translational temperature

T_{v} vibrational temperature

T_w wall temperature

Chapter 1

Introduction

1.1. Motivation and Background

1.1.1 Importance of Driven Cavity Flows

The driven cavity flow is one of the fundamental fluid flow problems that was often used as the benchmark test problem in computational fluid dynamics. The rationale behind this should be attributed to its simple geometry but having singular points at the corners, which may cause difficulties in numerical simulations. Although they have been thoroughly studied in the literature, most of them were focused on incompressible or continuum compressible regime [Karniadakis, 2001]. Very few researches have been done in the rarefied and near continuum regimes, where the understanding may become important in micro- and nano-scale gas flows that are often encountered in MEMS and NEMS related devices. Further, it may serve as the benchmarking problem for extending a numerical scheme into flow in these regimes, where standard Navier-Stokes equation fails to describe the flow accurately. Thus, an accurate numerical solution of a driven cavity flow in the rarefied and near-continuum regime is strongly required.

1.1.2 Classification of Rarefaction

Knudsen number ($Kn=\lambda/L$) is a standard parameter that is usually used to indicate the degree of rarefaction. Note that the mean free path λ is the average distance traveled by molecules before collision and L is the flow characteristic length. In general, flows are divided into four regimes as follows traditionally: $Kn <0.01$ (continuum), $0.01<Kn<0.1$ (slip flow), $0.1<Kn<3$ (Transitional flow) and $Kn>3$ (Free molecular flow). Fig. 1.1 (KC Tseng's thesis) is a sketch adopted from Bird [Bird's book, 1994] illustrating the various flow regions and their corresponding solution methods in a dilute gas. In this figure, the local Kn number is defined with L as the scale length of the macroscopic gradient; that is, $L = \dfrac{\rho}{d\rho/dx}$. Firstly, the lower bar indicates the continuum formulation. When the local Kn number approaches zero, the flow reaches inviscid limit and can be solved by Euler equation. As local Kn increases, molecular nature of the gas becomes dominated. Hence, the Navier-Stoke equation based computational fluid dynamics (CFD) techniques are often used until the Kn approach 0.01. When the Kn larger than 0.01, continuum assumption begins to break down and the particle-based method is necessary. Secondly, the top bar in this figure indicates the validity of the molecular modeling. It is well known that Boltzmann equation is more appropriate for all flow regimes; however it is rarely used to numerically solve the practical problems because of two major difficulties. They include higher dimensionality (up to seven) of the Boltzmann equation and the difficulties of correctly modeling the integral collision term. As the distance between the molecules increases, collisions between the molecules become less
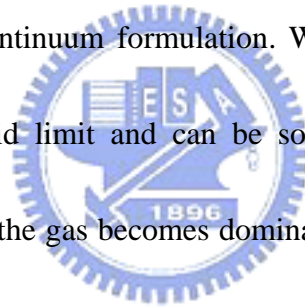
and thus neglected, and the flow can be solved by neglecting the collision term of the

collisionless Boltzmann equation.

1.1.3 Direct Simulation Monto Carlo Method

An alternative method, known as Direct Simulation Monte Carlo (DSMC), was proposed

by Bird to solve the Boltzmann equation using direct simulation of particle collision kinetics,

and the associated monograph was published in 1994 [Bird's book].   Later on, both Nanbu

[1986] and Wagner [1992] were able to demonstrate mathematically that the DSMC method is

equivalent to solving the Boltzmann equation as the simulated number of particles becomes

large.   The DSMC method is a particle method for the simulation of gas flows.   The gas is

modeled at the microscopic level using simulated particles, which each represents a large

number of physical molecules or atoms.   The physics of the gas are modeled through the

motion of particles and collisions between them. Mass, momentum and energy transports

between particles are considered at the particle level.   The method is statistical in nature and

depends heavily upon pseudo-random number sequences for simulation.   Physical events

such as collisions are handled probabilistically using largely phenomenological models, which

are designed to reproduce real fluid behavior when examined at the macroscopic level.   This

method has become a widely used computational tool for the simulation of gas flows in the

Low Kn flow regime, in which molecular effects become important.

The DSMC method becomes very time-consuming as the flow approaches continuum regime since the sampling cell size has to be much smaller than the local mean free path for the solution to be accurate. Several remedies in speeding up the DSMC computation include: 1) parallel computing [Robinson, 1996-1998]; 2) variable time-step scheme for steady flows [Kannenberg, 2000], and 3) sub-cells within each sampling cell [Bird's book, 1994]. Details of the "parallel computing" and "variable time-step scheme" can be found in those references cited in the above and are not described here for brevity. Only "sub-cells" concept is described here since it was rarely discussed in detail in the literature. In Bird's original implementation [see Bird's book, 1994], number of sub-cells in each sample cell is pre-determined and related sub-cell data are stored in the memory throughout the simulation, which is very costly. This strategy, which enables nearest-neighbor collisions to be enforced, greatly reduces the computational load by increasing the sampling cell size whilst maintaining the same accuracy as compared to that using smaller sampling cell size. Unfortunately, storage of the sub-cell data is memory intensive and inflexible in adjusting the number of sub-cells in each sampling cell during runtime, which may become important in reducing the merit of collision (ratio of mean collision distance to characteristic cell size). Recently, Bird [DS2V code by Bird] has proposed an idea of "transient sub-cells", which could overcome the above-mentioned shortcomings. However, this idea has been only implemented on structured grids. No report could be found on unstructured grids.

1.2. Literature Survey

The driven cavity flow is a fluid flow problem that has been very well studied in the continuum limit by using different numerical methods. Ghia, *et al.* [1982] used the vorticity-stream function of the 2D incompressible Navier-Stoke equation to study the laminar incompressible flow in a square cavity whose top wall moves with a uniform velocity. The Reynolds number in their study is varied from Re=100 to Re=10,000. They presented the velocity along vertical and horizontal line through geometry center of cavity and the primary vortex position. Erturk, *et al.* [2005] also utilized the 2D steady incompressible Navier-Stoke equation with a fine grid. The flow solutions are computed for Re=1000 to Re=21000 with a maximum absolute residuals of the governing equations that were less than 10^{-10}. Until very recently, Stergios, *et al.* [2005] solved the flow of a rarefied gas in a rectangular enclosure due to the motion of the upper wall over whose range of the Knudsen number. Their numerical method is base on the 2D linearized BGK kinetic equation with Maxwell diffuse-specular boundary conditions. They presented the simulation data over the whole range of the Knudsen number and various aspect ratio (height/width). However, simulation results by Stergios, *et al.* [2005] were only good for low speed rarefied gas flows since the linearized BGK Boltzmann equation was used. In addition, no data were validated by comparing with experiments or solution from direct Boltzmann equation, such as DSMC

method.

1.3.   Specific Objectives of the Thesis

The objectives of the thesis are briefly summarized as follows:

1. To verify the implementation of transient sub-cell technique in a parallelized DSMC code (PDSC) [Wu, *et al*].

2. To simulate driven cavity flows, including M=1.1-4 of the speed of top driven plate, and Kn=10-0.0033, based on the average number density and wall temperature.

3. To discuss the effects of Knudsen Number and Mach number of the driven plate on the flow fields.

The organization of the thesis is stated as follows. Chapter 1 describes the Introduction, Chapter 2 describes the Numerical Method, Chapter 3 describes the verification of implementation of transient sub-cells, and followed by the Results and Discussion, and finally Chapter 4 describes the conclusion and recommendation of future work..
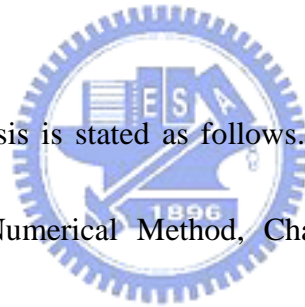
Chapter 2

Numerical Method

2.1.   The Boltzmann Equation

The Boltzmann equation is one of the most important transport equations in non-equilibrium statistical mechanics, which deals with systems far from thermodynamics equilibrium. There are some assumptions made in the derivation of the Boltzmann equation which defines limits of applicability. They are summarized as follows:

1.   Molecular chaos is assumed which is valid when the intermolecular forces are short range. It allows the representation of the two particles distribution function as a product of the two single particle distribution functions.

2.   Distribution functions do not change before particle collision. This implies that the encounter is of short time duration in comparison to the mean free collision time.

3.   All collisions are binary collisions.

4.   Particles are uninfluenced by intermolecular potentials external to an interaction.

According to these assumptions, the Boltzmann equation is derived and shown as Eq. (2.1)

$$\frac{\partial(nf)}{\partial t} + u_i \frac{\partial(nf)}{\partial x_i} + F_i \frac{\partial(nf)}{\partial u_i} = \frac{\partial f}{\partial x_i}\Big|_c = \int_{-\infty}^{\infty} \int_0^{4\pi} n^2 (f'f_1' - ff_1) g\sigma d\Omega dU \qquad (2.1)$$

Meaning of particle phase-space distribution function f is the number of particles with center of mass located within a small volume d^3r near the point r, and velocity within a

7

range d^3u, at time t. F_i is an external force per unit mass and t is the time and u_i is the

molecular velocity. σ is the differential cross section and $d\Omega$ is an element of solid angle.

The prime denotes the post-collision quantities and the subscript 1 denotes the collision

partner. Meaning of each term in Eq. (2.1) is described in the following;

1. The first term on the left hand side of the equation represents the time variation of

   the distribution function of the particles (unsteady term).

2. The second term gives the spatial variation of the distribution function (flux term).

3. The third term describes the effect of a force on the particles (force term).

4. The term at right hand side of the equation is called the collision integral (collision

   term). It is the source of most of the difficulties in obtaining solutions of the

   Boltzmann equation.
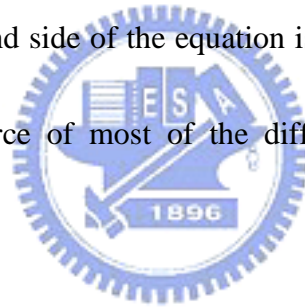
In general, it is very hard to solve the Boltzmann equation directly using numerical

method because the difficulties of correctly modeling the integral collision term. Instead, the

DSMC method was used to simulated problems involving rarefied gas dynamics, which is the

simulation tool used in the current thesis.

2.2. General Description of the Standard DSMC

According to the expected rarefaction caused by the rarefied gas flows, the direct

simulation Monte Carlo (DSMC) method, which is a particle-based method developed by

Bird during the 1960s, and was widely used as an efficient technique to simulate rarefied gas regime [Bird, 1976 and Bird, 1994]. In the DSMC method, a large number of particles are generated in the flow field to represent real physical molecules rather than a mathematical foundation and it has been proved that the DSMC method is equivalent to solving the Boltzmann equation [Nanbu, 1986 and Wagner, 1992]. The assumptions of molecular chaos and a dilute gas are shared by both the Boltzmann equation and the DSMC method [Bird, 1976 and Bird, 1994]. An important feature of DSMC is that the molecular motion and the intermolecular collisions are uncoupled over the time intervals that are much smaller than the mean collision time. Both the collision between molecules and the interaction between molecules and solid boundaries are computed on a probabilistic basis and, hence, this method makes extensive use of random numbers. In most practical applications, the number of simulated molecules is extremely small as compared to the number of real molecules. The general procedures of the DSMC method are described in the next section, and the consequences of the computational approximations can be found in Bird [Bird, 1976 and Bird, 1994].

In DSMC, there are three popular molecular collision models for real physical behavior and imitate the real particle collision. They include the Hard Sphere (HS), Variable Hard Sphere (VHS) and Variable Soft Sphere (VSS) molecular models [Bird, 1994]. No time counter (NTC) method is often used to determined the probability of collision within a

samping cell based on the acceptance-rejection method. This method can yield the exact collision rate in both simple gases and gas mixtures, and under either equilibrium or non-equilibrium conditions.

Fig. 2.2 is a general flowchart of the DSMC method. Important steps of the DSMC method include setting up the initial conditions, moving all the simulated particles, indexing (or sorting) all the particles, colliding between particles and sampling the molecules within cells to determine the macroscopic quantities.   The details of each step are described in the following:

● Initialization

The first step to use the DSMC method is to set up the geometry and flow conditions. A physical space is discredited into a network of cells and the boundary conditions at domain boundaries have to be assigned according to the flow conditions. An important rule of thumb of selecting the cell size is it should be much smaller than the local mean free path. At the same time the distance of the molecular movement per time step should be smaller than the cell dimension, which is similar to the CFL condition in CFD. After the data of geometry and flow conditions have been read in the code, the number of simulation particles each cell is calculated according to the initial number density and the cell volume. The initial particle velocities are normally assigned to each particle based on the Maxwell-Boltzmann distribution according to the initial velocities and temperature. The position of each particle is

then randomly allocated within the cell.

- Molecular Movement

After initialization process, the molecule begins move one by one, and the molecule moves in a straight line over the time step. If the particle collides with a solid surface, then it has to reflected back based on the boundary conditions at the surface. If the particle passes through a inflow/outflow boundary, then it has to be removed from the simulation immediately. After the particle reaches its final destination, the cell with which the particle affiliated is recorded.

- Indexing

Relation between particles and cells are reordered according to the order of the increasing particle number in each cell, which is used for collision step.
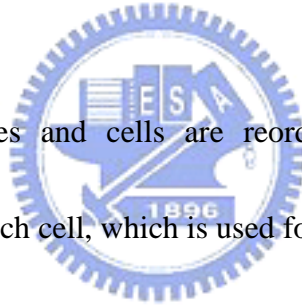
- Gas Phase Collision

The other most important phase of the DSMC method is the gas phase collision. The DSMC method uses the no time counter (NTC) method to determine the correct collision rate in the collision cell. Number of collision pairs within a cell of volume V_c over a time interval Δt is calculated by the following equation:

$$\frac{1}{2} N \overline{N} F_N (\sigma_T c_r)_{max} \Delta t / V_c \qquad (2.2)$$

where N and $\overline{N}$ are fluctuating and average number of simulated particles, respectively. F_N is the particle weight, which is the number of real particles that a simulated particle

11

represents. σ_T and c_r are the cross section and the relative speed, respectively. The

collision probability for each pair of particle chosen can be expressed as

$$(\sigma_T c_r)/(\sigma_T c_r)_{max} \qquad (2.3)$$

Collision is accepted if the above value for the pair is greater than a random fraction. Each

cell is treated independently and the collision partners for interactions are chosen randomly,

regardless of their positions within the cell. Collision procedures are summarized as

follows:

1. Number of collision pairs is calculated according to the NTC method, Eq. (2.2), in
   each cell.

2. The first particle is chosen randomly from the list of particles within a collision cell.

3. The other collision partner is also chosen randomly within the same cell.

4. The collision is accepted if the computed probability, Eq. (2.3), is greater than a
   random number.

5. If the collision pair is accepted, then the post-collision velocities are calculated
   using the mechanics of elastic collision. If the collision pair is not to collide, then
   proceed to choose the next collision pair.

6. If the collision pair is polyatomic gas, the translational and internal energy can be
   redistributed by the Larsen-Borgnakke model [1975], which assumes the state is in
   equilibrium.

The collision process will be finished until all the collision pairs are handled for all cells

and then progress to the next step.

- Sampling

After the particle movement and collision process complete, the particle has updated

positions and velocities. Macroscopic flow properties in each cell are assumed to be

constant over the cell volume and are sampled from the microscopic properties of all the

particles within the cell. Macroscopic properties, including number density, velocities and

temperatures, are calculated following the equations as shown below:

$$\rho = nm \tag{2.4a}$$

$$c_o = \bar{c} = \overline{c_o} + \overline{c'} \tag{2.4b}$$

$$\frac{3}{2}kT_{tr} = \frac{1}{2}m(\overline{u'^2} + \overline{v'^2} + \overline{w'^2}) \tag{2.4c}$$

$$T_{rot} = \frac{2}{k}(\varepsilon_{rot}/\zeta_r) \tag{2.4d}$$

$$T_v = \frac{2}{k}(\varepsilon_v/\zeta_v) \tag{2.4e}$$

$$T_{tot} = (3T_{tr} + \zeta_{rot}T_{rot} + \zeta_v T_v)/(3 + \zeta_{rot} + \zeta_v) \tag{2.4f}$$

where n, m are the number density and molecule mass, receptively. c, c_o, and c' are the total

velocity, mean velocity, and random velocity, respectively. In addition, T_{tr}, T_{rot}, T_v and T_{tot} are

translational, rotational, vibration and total temperature, respectively. ε_{rot} and ε_v are the

rotational and vibration energy, respectively. ζ_{rot} and ζ_v are the number of degree of

freedom of rotation and vibration, respectively. If the simulated particle is monatomic gas, the

13

translational temperature is regarded simply as the total temperature. Vibration effect can be neglect if the temperature of the flow is low enough.

The flow will be monitored if steady state is reached. If the flow is still in the transient phase, then sampling of the properties should be reset until the flow reaches steady state. As the flow reaches physically steady state, time averaging in each cell is used to obtain macroscopic properties in each cell. As a rule of thumb, sampling of particles starts when the number of molecules in the calculation domain becomes approximately constant.

2.3. General Description of the PDSC

In the past few years, we have developed a parallelized direct simulation Monte Carlo code, named PDSC, which is portable on distributed memory machines. Important features of the PDSC code can be found in the references [Wu *et al.*'s JCP paper, 2006; JCP paper submitted in June 2007; JFM paper under preparation, 2007] and only several of them are briefly described in the following.

1) *2D/2D-axisymmetric/3-D unstructured-grid topology*: PDSC can accept either 2D/2D-axisymmetric (triangular, quadrilateral or hybrid triangular-quadrilateral) or 3D (tetrahedral, hexahedral or hybrid tetrahedral-hexahedral) mesh [Wu et al.'s JCP paper, 2006]. Computational cost of particle tracking for the unstructured mesh is generally higher than that for the structured mesh. However, the use of the unstructured mesh, which provides excellent flexibility of handling boundary conditions with complicated geometry and of parallel computing using dynamic domain decomposition based on load balancing, is highly justified.

2) *Parallel computing using dynamic domain decomposition*: Load balancing of PDSC is achieved by repeatedly repartitioning the computational domain using a multi-level graph-partitioning tool, PMETIS [Wu and Tseng, 2005], by taking advantage of the unstructured mesh topology employed in the code. A decision policy for repartition with a concept of Stop-At-Rise (SAR) [Wu and Tseng, 2005] or constant period of time (fixed number of time steps) can be used to decide when to repartition the domain. Capability of repartitioning of the domain at constant or variable time interval is also provided in PDSC. Resulting parallel performance is excellent if the problem size is comparably large. Details can be found in Wu and Tseng [Wu and Tseng, 2005].

3) *Spatial variable time-step scheme*: PDSC employs a spatial variable time-step scheme (or equivalently a variable cell-weighting scheme), based on particle flux (mass, momentum, energy) conservation when particles pass interface between cells. This strategy can greatly reduce both the number of iterations towards the steady state, and the required number of simulated particles for an acceptable statistical uncertainty. Past experience shows this scheme is very effective when coupled with an adaptive mesh refinement technique [Wu et al.'s CPC paper, 2004].

4) *Unsteady flow simulation*: An unsteady sampling routine is implemented in PDSC, allowing the simulation of time-dependent flow problems in the near continuum range [JCP paper submitted in June 2007]. A post-processing procedure called DSMC Rapid Ensemble Averaging Method (DREAM) is developed to improve the statistical scatter in the results while minimizing both memory and simulation time. In addition, a temporal variable time-step (TVTS) scheme is also developed to speed up the unsteady flow simulation using PDSC. More details can be found in [JCP paper submitted in June 2007].

5) *Transient Sub-cells*: Recently, transient sub-cells are implemented in PDSC directly on the unstructured grid, in which the nearest-neighbor collision can be enforced, whilst maintaining minimal computational overhead [JFM paper under preparation, 2007].   Details of the idea and implementation are described next.

2.4.   Transient Sub-Cells for PDSC [JFM paper under preparation, 2007]

The implementation of sub-cells in DSMC allows the maintenance of good collision quality within the simulation, even for grids which are "under-resolved" (that is, if the sampling cells are bigger than the recommended setting of 1/3~ 1/2 times the local mean free path).   Running simulations with under-resolved sampling cells which employ sub-cells results in a reduction in the computational and memory requirements of the simulation, albeit at the cost of a reduction in the possible sampling resolution of the macroscopic properties, but without sacrificing simulation accuracy.
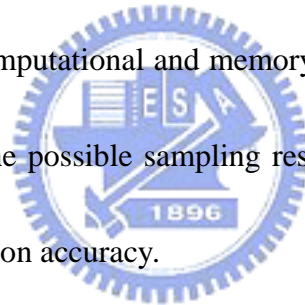
In PDSC, unstructured grids are used, requiring an adaptation of the transient sub-cells scheme, which was originally promoted by Bird [DS2V code by Bird]. In PDSC, the sampling cells are divided into sub-cells during the collision routine. Because the sub-cells only exist in one sampling cell at a time, and only during the collision routine, they can be considered "transient sub-cells" which will have negligible computer memory overhead. In every case, these sub-cells are quadrilateral in 2D or hexahedral in 3D which reduces the complexity of sub-dividing the sampling cell and greatly facilitates particle indexing. The size of the sub-cells is indirectly controlled by the user, who inputs the desired averaged number of

particles per sub-cell, *P*. The program then determines the dimensions of the sub-cell array based on the number of particles with the cell, N_{parts}. Briefly, the total number of sub-cells are computed by the rule for the 2-D case

$$\sqrt{N_{parts}/P} \times \sqrt{N_{parts}/P} \tag{2.21}$$

Fig. 2.4 shows the way in which both rectangular and triangular sampling cells are divided into sub-cells. As can be seen, in the unstructured case, there may be sub-cells which are entirely outside the boundary of the sampling cell, however this has no affect on the collision routine. In both cases, the concept is easily extended to three-dimensional sampling cells.
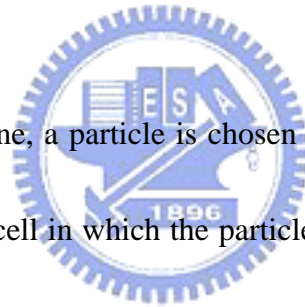
During the collision routine, a particle is chosen at random from some point within the whole sampling cell. The sub-cell in which the particle lies is then determined and if another particle is in the same sub-cell then these particles are chosen for collision. If the first particle is alone within the sub-cell, then adjacent sub-cells are scanned for a collision partner. These sub-cell routines ensure nearest neighbor collisions, even within under-resolved sampling cells, with minimal computational and memory overhead.

Bird has also shown that preventing particles from colliding again their last collision partner, reduces the error in some variables such as heat transfer and shear stress by up to 5% [ref-Bird manual of DS2V code]. The basis of this is that collisions between particles which just collided with each other is unphysical, since the particle must be moving away from each

other after the first collision. A minor modification was made to PDSC to prevent particles

colliding with their last collision partner. This involved the creation of an array in which the

last collision partner for every particle is stored and if the two particles are subsequently

chosen for collision without having collided with any other particle, the collision is rejected.
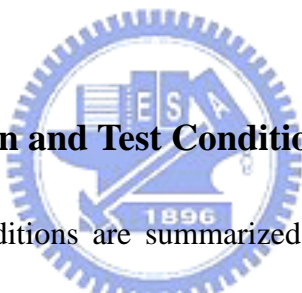
Chapter 3

Results and Discussion

3.1   Benchmark of Transient Sub-cell Method

Although this thesis is concerned with supersonic square driven cavity flows in rarefied

regime, a subsonic flow case with M=0.5 and Kn=0.01 is used as the benchmark case. The

rationale is that a subsonic flow represents a more stringent test problem than a supersonic

flow for the DSMC method in terms of statistical uncertainties.

3.1.1 Problem Description and Test Conditions

Flow and simulation conditions are summarized in Table I. Fig. 3.1 sketches the 2D

square driven cavity flow. PDSC simulations are conducted, respectively, using a coarse mesh

(100×100 cells, 100 particles per cell) with transient sub-cells and a finer mesh (400×400

cells, 25 particles per cell) without transient sub-cells. Results using the finer mesh are

considered to be a benchmark solution since the simulation conditions satisfy all requirements

for a good DSMC computation. Since the overhead of indexing the particles using transient

sub-cells is minimal (at most 15% as compared to that without using transient sub-cells if less

than 100 particles per cell), resulting computational time using transient sub-cells is about

only 1/4 of that without transient sub-cells, considering the similar accuracy of DSMC

simulations, which is shown next. If 100 particles per cell is used in the case without transient

sub-cells, more benefit of computational time can gained by using transient sub-cells.

3.1.2 Simulation Results of Benchmark

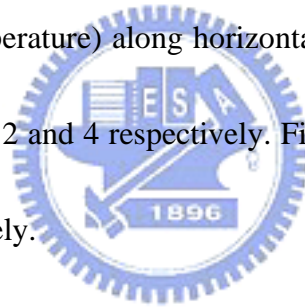Fig. 3.5 (a)-(d) (a)-(d) present the profiles of various properties ((a) u-velocity, (b)

v-velocity, (c)number density and (d)temperature) along the central vertical line (x/L=0.5). In

these figures, $\mathbf{u}_p$ and $\mathbf{L}$ represents the top plate speed and length (also width) of the driven

cavity, respectively. Results show that simulation data with and without transient sub-cells are

in good agreement considering the inherent statistical uncertainties of the DSMC method.

Statistical uncertainties with transient sub-cells are even lower than those without transient

sub-cells, especially for the $\mathbf{v}$ velocity, which is generally low as compared to the $\mathbf{u}$ velocity

along the x/L=0.5 line. It clearly demonstrates that with transient sub-cells accuracy of DSMC

simulation can be well preserved using cell size even close to local mean path. Similar trends

can be found in Fig. 3.6 (a)-(d), in which the profiles of various properties are presented along

the central horizontal line (y/L=0.5). In the simulation, desired averaged number of particles

per sub-cell, P, is set to be 1. Not unexpectedly, the merit of collision (=mean collision

distance/local mean free path), which represents the quality of collisions in a DSMC

simulation, is generally much smaller by using transient sub-cells than that without using

transient sub-cells, as illustrated in Fig. 3.11 and Fig. 3.12. Bird [???] has argued that the

merit of collision in the range of 0.1~0.2 represents a good DSMC simulation.   Result show

that the simulation used coarse mesh with transient sub-cell approximate that used finer mesh

without transient sub-cell. Therefore, the simulation with transient sub-cell keeping minimal

computational overhead and memory requirement simultaneously, but still has simulation

accuracy.

3.2   Simulation Results of Driven Cavity Flows

According to previous section, we have found the transient sub-cell method can greatly

reduce the computational cost and still has good quality of solution. In this section, we have

used this technique in PDSC to simulate steady supersonic square driven cavity flows in a

systematic way. Thus, we can understand more about the effects of rarefaction and

compressibility in such conditions.
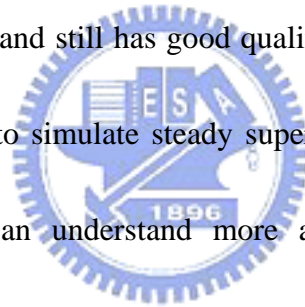
3.2.1   Problem Description and Test Conditions

Fig. 3.1 shows the sketch of the 2D square (L/H=1) driven cavity flow with moving top

plate. Flow and simulation conditions are summarized in Table II and Table III.   Argon is

used as the working gas, while the initial temperatures inside the cavity and wall temperatures

are set as 300K.   Mach number and Knudsen number (based on wall temperature and width

of the cavity) is in the range of 1.1-4 and 10-0.0033. Uniform mesh distribution is used

throughout the present study for all cases.

3.2.2   Effects of Knudsen Number

In this section, we were observed effects of Knudsen number in the same Mach number (Ma=1.1-4). We were showed general simulation results include density, velocity in the x-direction, velocity in the y-direction, temperature, Mach number, and streamline. We were showed property distributions across cavity centroid for x/L = 0.5, y/L = 0 to 1 and y/L = 0.5, x/L = 0 to 1. We showed property distributions near the solid walls. Finally, we were observed the recirculation center position in different cases.

3.2.2.1   General Simulation Results

Fig. 3.23 shows that number density contour for Ma=4, and Knudsen number 10, 1, 0.1, 0.01 and 0.0033 respectively. Driven plate takes particles to the right-hand upper corner. An ultra high-density region appears at the very right-hand upper corner due to the high-speed moving plate at the top of the cavity. Therefore the particles are larger than initial value. In addition, there are low densities at the left-hand upper corner. In the other series, fixed M=1.1 and M=2 are showed in Fig. 3.13 and Fig. 3.18.

Fig. 3.24 show that temperature contour for Ma=4, and Knudsen number 10, 1, 0.1, 0.01 and 0.0033 respectively. We normalize temperature to divide the initial temperature 300K.

There are two ultra temperatures region in the cavity. One of them is the right-hand upper corner which temperature increased as a result of density increased; the other one is left-hand upper corner which temperature increased due to high vertical speed. Finally, the temperature increase more seriously as Knudsen number decreased. In the other series, fixed M=1.1 and M=2 are showed in Fig. 3.14 and Fig. 3.19.

Fig. 3.25 show that Mach contour for Ma=4, and Knudsen number 10, 1, 0.1, 0.01 and 0.0033 respectively. In the other series, fixed M=1.1 and M=2 are showed in Fig. 3.15 and Fig. 3.20.

Fig. 3.26 show that u-velocity contour for Ma=4, and Knudsen number 10, 1, 0.1, 0.01 and 0.0033 respectively. The maximum u-velocity values are 0.3, 0.35, 0.55, 0.8, and 0.9 with Knudsen number 10, 1, 0.1, 0.01 and 0.0033, respectively. Because of rarefaction effect caused slip phenomenon and the slip velocity along the solid walls increase with Knudsen number at the same Mach number. We normalize u-velocity to divide the upper plate velocity. The velocity more and more decrease when Knudsen number increase. In the other series, fixed M=1.1 and M=2 are showed in Fig. 3.16 and Fig. 3.21.

Fig. 3.27 show that v-velocity contour for Ma=4, and Knudsen number 10, 1, 0.1, 0.01 and 0.0033 respectively. We normalize v-velocity to divide the upper plate velocity. An ultra high-speed region appears at the left-hand and right-hand upper region. In the other series, fixed M=1.1 and M=2 are showed in Fig. 3.17 and Fig. 3.22.

As mentioned above, we can be briefly summarized as follows:

1. The slip velocity more and more decrease when Knudsen number increase.

2. An ultra high-density region appears at the very right-hand upper corner due to the high-speed moving plate at the upper of the cavity

3. There are two ultra temperatures region in the right and left corner in cavity.

3.2.2.2   Property Distributions Across Cavity Centroid

Fig. 3.65 (a)-(d) present the profiles of various properties ((a) u-velocity, (b) v-velocity, (c)number density and (d)temperature) along vertical line through geometry center(x/L=0.5) for Ma=4, and Knudsen number 10, 1, 0.1, 0.01 and 0.0033 respectively. In the other series, fixed M=1.1 and M=2 are showed in Fig. 3.53 and Fig. 3.59.
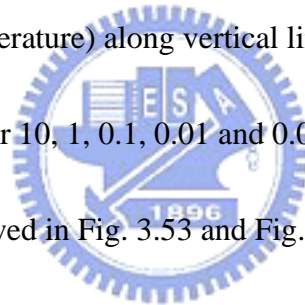
Fig. 3.66 (a)-(d) present the profiles of various properties ((a) u-velocity, (b) v-velocity, (c)number density and (d)temperature) along horizontal line through geometry center(y/L=0.5) for Ma=4, and Knudsen number 10, 1, 0.1, 0.01 and 0.0033 respectively. In the other series, fixed M=1.1 and M=2 are showed in Fig. 3.54 and Fig. 3.60.

3.2.2.3   Property Distributions Near Solid Walls

Usually, the simulation data save in the cell center for DSMC technique. Thus, observation cell center data properties are average and correct. The positions are show in Table IV. Fig. 3.67

24

(a)-(d) present the profiles of various properties ((a) u-velocity, (b) v-velocity, (c)number density and (d)temperature) along horizontal line near top wall(y/L=1) for Ma=4, and Knudsen number 10, 1, 0.1, 0.01 and 0.0033 respectively. In the other series, fixed M=1.1 and M=2 are showed in Fig. 3.55 and Fig. 3.61.

Fig. 3.68 (a)-(d) present the profiles of various properties ((a) u-velocity, (b) v-velocity, (c)number density and (d)temperature) along horizontal line near bottom wall(y/L=0) for Ma=4, and Knudsen number 10, 1, 0.1, 0.01 and 0.0033 respectively. In the other series, fixed M=1.1 and M=2 are showed in Fig. 3.56 and Fig. 3.62.

Fig. 3.69 (a)-(d) present the profiles of various properties ((a) u-velocity, (b) v-velocity, (c)number density and (d)temperature) along vertical line near left wall(x/L=0) for Ma=4, and Knudsen number 10, 1, 0.1, 0.01 and 0.0033 respectively. In the other series, fixed M=1.1 and M=2 are showed in Fig. 3.57 and Fig. 3.63.

Fig. 3.70 (a)-(d) present the profiles of various properties ((a) u-velocity, (b) v-velocity, (c)number density and (d)temperature) along vertical line near right wall(x/L=1) for Ma=4, and Knudsen number 10, 1, 0.1, 0.01 and 0.0033 respectively. In the other series, fixed M=1.1 and M=2 are showed in Fig. 3.58 and Fig. 3.64.

3.2.2.4   Recirculation Center Position

Fig. 3.100 shows the streamline of M=1.1 and Knudsen number 10, 1, 0.1, 0.01 and

0.0033 respectively. There are only one vortex for Kn=10, 1 and 0.1, but it has the additional

second vortex at the right bottom corner for Kn=0.01 and 0.0033. Fig. 3.101 shows the

streamline of M=2 and Knudsen number 10, 1, 0.1, 0.01 and 0.0033 respectively. Identically,

it has the additional second vortex at the right bottom corner. Besides, the second vortex

appear for Kn=10. Fig. 3.102 shows the streamline of M=4 and Knudsen number 10, 1, 0.1,

0.01 and 0.0033 respectively. It has second vortex in all case besides Kn=0.1.

Fig. 3.103 shows the relative horizontal distance (x/L) of the vortex center for various

values of Knudsen number and Mach number. Result show that the vertex center position has

no obvious regular in x-direction. Fig. 3.103 shows the relative vertical distance (y/L) of the

vortex center for various values of Knudsen number and Mach number. It shows that the

vortex center move down as decreasing Knudsen number for M=2 and 4; but it has no regular

for M=1.1.
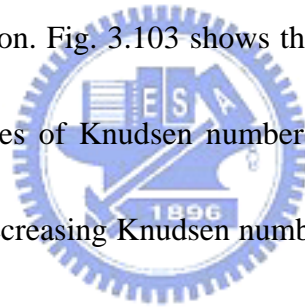
3.2.3   Effects of Mach Number of the Driven Plate

In this section, we were observed effects of Mach number in the same Knudsen number

(Kn=10-0.0033). We were showed general simulation results include density, velocity in the

x-direction, velocity in the y-direction, temperature, Mach number, and streamline. We were

showed property distributions across cavity centroid for x =0.5m, y= 0 to 1m and y=0.5m,

x=0 to 1m. We showed property distributions near the solid walls. Finally, we were observed

the recirculation center position in different cases.

3.2.3.1 General Simulation Results

3.2.3.1.1 High Kn Regime (Kn=10, 1, 0.1)

Fig. 3.28 shows that number density contour for Kn=10, and Mach number 1.1, 2 and 4

respectively. Driven plate takes particles to the right-hand upper corner. An ultra high-density

region appears at the very right-hand upper corner due to the high-speed moving plate at the

top of the cavity. In addition, there is low density at the left-hand upper corner. The max

number density reaches 2.2, 4.2 and 7.5 times the initial value as M = 1.1, 2 and 4

respectively. In the other series, fixed Kn=1 and Kn=0.1 are showed in Fig. 3.33 and Fig.

3.38.
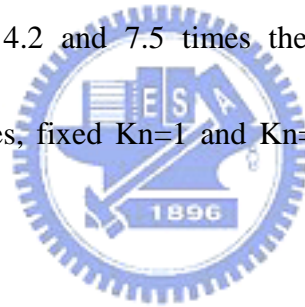
Fig. 3.29 shows that temperature contour for Kn=1, and Mach number 1.1, 2 and 4

respectively. We normalize temperature to divide the initial temperature 300K. Temperature

near the top plate increases with increasing driven plate velocity. Besides, the temperature

increase more seriously as Mach number increased. In the other series, fixed Kn=1 and

Kn=0.1 are showed in Fig. 3.34 and Fig. 3.39.

Fig. 3.30 shows that Mach number contour for Kn=0.1, and Mach number 1.1, 2 and 4

respectively. The velocity near the top plate is lower compared with the top plate velocity; it

is just about 0.3 times the velocity of driven plate. In the other series, fixed Kn=1 and

Kn=0.1are showed in Fig. 3.35 and Fig. 3.40.

Fig. 3.31 shows that u-velocity contour for Kn=0.01, and Mach number 1.1, 2 and 4 respectively. We normalize temperature to divide the initial driven plate velocity. The maximum u-velocity values are all about 0.3. Because of rarefaction effect caused slip phenomenon and the velocity remain the 0.3 times the top plate velocity. In the other series, fixed Kn=1 and Kn=0.1 are showed in Fig. 3.36 and Fig. 3.41.

Fig. 3.32 shows that v-velocity contour for Kn=0.0033, and Mach number 1.1, 2 and 4 respectively. We normalize v-velocity to divide the upper plate velocity. An ultra high-speed region appears at the left-hand and right-hand upper region. In the other series, fixed Kn=1 and Kn=0.1 are showed in Fig. 3.37 and Fig. 3.42.
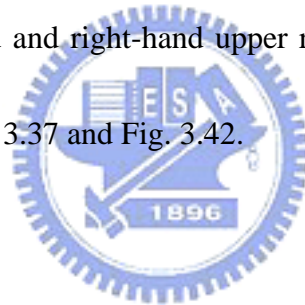
3.2.3.1.2 Low Kn Regime (Kn=0.01, 0.0033)

Fig. 3.42 shows that number density contour for Kn=0.01, and Mach number 1.1, 2 and 4 respectively. In this regime, the region of influence is about all domain. An ultra high-density region appears at the very right-hand upper corner. the number density of sides of the cavity is larger than inside of the cavity, besides it near the top plate. The max number density reaches 3, 7 and 15 times the initial value as M = 1.1, 2 and 4 respectively. When increasing Mach number, the phenomenon is acuter. In the other series, fixed Kn=0.0033 is showed in Fig. 3.48.

Fig. 3.43 shows that temperature contour for Kn=0.01, and Mach number 1.1, 2 and 4 respectively. We normalize temperature to divide the initial temperature 300K. Temperature near the top plate increases with increasing driven plate velocity. Besides, the temperature increase more seriously as Mach number increased. In the other series, fixed Kn=0.0033 is showed in Fig. 3.49.

Fig. 3.44 shows that Mach number contour for Kn=0.01, and Mach number 1.1, 2 and 4 respectively. Compare the velocity near the top plate with the top plate is much lower, it is 0.8 times the velocity of driven plate. In the other series, fixed Kn=0.0033 is showed in Fig. 3.50.
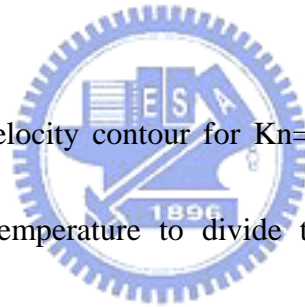
Fig. 3.45 shows that u-velocity contour for Kn=0.01, and Mach number 1.1, 2 and 4 respectively. We normalize temperature to divide the initial driven plate velocity. The maximum u-velocity values are all about 0.8. Because of rarefaction effect caused slip phenomenon and the velocity reduces 20   of the top plate velocity. In the other series, fixed Kn=0.0033 is showed in Fig. 3.51.

Fig. 3.46 shows that v-velocity contour for Kn=0.01, and Mach number 1.1, 2 and 4 respectively. We normalize v-velocity to divide the upper plate velocity. An ultra high-speed region appears at the left-hand and right-hand upper region. In the other series, fixed Kn=0.0033 is showed in Fig. 3.52.

3.2.3.2 Property Distributions Across Cavity Centroid

3.2.3.2.1 High Kn Regime (Kn=10, 1, 0.1)

Fig. 3.75 (a)-(d) present the profiles of various properties ((a) u-velocity, (b) v-velocity, (c)number density and (d)temperature) along vertical line through geometry center(x/L=0.5) for Kn = 10, and Mach number 1.1, 2 and 4 respectively.

Fig. 3.76 (a)-(d) present the profiles of various properties ((a) u-velocity, (b) v-velocity, (c)number density and (d)temperature) along horizontal line through geometry center(y/L=0.5) for Kn = 10, and Mach number 1.1, 2 and 4 respectively.

3.2.3.2.2 Low Kn Regime (Kn=0.01, 0.0033)

Fig. 3.88 (a)-(d) present the profiles of various properties ((a) u-velocity, (b) v-velocity, (c)number density and (d)temperature) along vertical line through geometry center(x/L=0.5) for Kn = 0.01, and Mach number 1.1, 2 and 4 respectively.

Fig. 3.89 (a)-(d) present the profiles of various properties ((a) u-velocity, (b) v-velocity, (c)number density and (d)temperature) along horizontal line through geometry center(y/L=0.5) for Kn = 0.01, and Mach number 1.1, 2 and 4 respectively.

3.2.3.3   Property Distributions Near Solid Walls

3.2.3.3.1 High Kn Regime (Kn=10, 1, 0.1)

Usually, the simulation data save in the cell center for DSMC technique. Thus, observation cell center data properties are average and correct. The positions are show in Table IV. Fig. 3.72 (a)-(d) present the profiles of various properties ((a) u-velocity, (b) v-velocity, (c)number density and (d)temperature) along horizontal line near top wall (y/L=1) for Kn = 10, and Mach number 1.1, 2 and 4 respectively. Fig. 3.76 and Fig. 3.82 change the Mach number as 1 and 0.1, respectively.

Fig. 3.73 (a)-(d) present the profiles of various properties ((a) u-velocity, (b) v-velocity, (c)number density and (d)temperature) along horizontal line near bottom plate (y/L=0) for Kn = 10, and Mach number 1.1, 2 and 4 respectively. Fig. 3.77 and Fig. 3.83 change the Mach number as 1.1 and 2, respectively.

Fig. 3.74 (a)-(d) present the profiles of various properties ((a) u-velocity, (b) v-velocity, (c)number density and (d)temperature) along vertical line near left wall(x/L=0) for Kn = 10, and Mach number 1.1, 2 and 4 respectively. Fig. 3.77 and Fig. 3.83 change the Mach number as 1.1 and 2, respectively.

Fig. 3.75 (a)-(d) present the profiles of various properties ((a) u-velocity, (b) v-velocity, (c)number density and (d)temperature) along vertical line near right wall(x/L=1) for Kn = 10, and Mach number 1.1, 2 and 4 respectively. Fig. 3.77 and Fig. 3.83 change the Mach number

as 1.1 and 2, respectively.

3.2.3.3.2 Low Kn Regime (Kn=0.01, 0.0033)

Fig. 3.89 (a)-(d) present the profiles of various properties ((a) u-velocity, (b) v-velocity, (c)number density and (d)temperature) along horizontal line near top wall (y/L=1) for Kn = 0.01, and Mach number 1.1, 2 and 4 respectively. Fig. 3.76 and Fig. 3.82 change the Mach number as 1 and 0.1, respectively.

Fig. 3.90 (a)-(d) present the profiles of various properties ((a) u-velocity, (b) v-velocity, (c)number density and (d)temperature) along horizontal line near bottom wall(y/L=0) for Kn = 0.01, and Mach number 1.1, 2 and 4 respectively. Fig. 3.77 and Fig. 3.83 change the Mach number as 1.1 and 2, respectively.

Fig. 3.91 (a)-(d) present the profiles of various properties ((a) u-velocity, (b) v-velocity, (c)number density and (d)temperature) along vertical line near left wall(x/L=0) for Kn = 0.01, and Mach number 1.1, 2 and 4 respectively. Fig. 3.77 and Fig. 3.83 change the Mach number as 1.1 and 2, respectively.

Fig. 3.92 (a)-(d) present the profiles of various properties ((a) u-velocity, (b) v-velocity, (c)number density and (d)temperature) along vertical line near right wall(x/L=1) for Kn = 0.01, and Mach number 1.1, 2 and 4 respectively. Fig. 3.77 and Fig. 3.83 change the Mach number as 1.1 and 2, respectively.

3.2.3.4 Recirculation Center Position

Fig. 3.105 shows the streamline of Kn=10 and Mach number 1.1, 2 and 4 respectively. There are second vortex occur as M=2 and 4. Fig. 3.106 shows the streamline of Kn=1 and Mach number 1.1, 2 and 4 respectively. There is second vortex occur as M=4. Fig. 3.107 shows the streamline of Kn=0. 1 and Mach number 1.1, 2 and 4 respectively. There are no additional second vortex. Fig. 3.108 shows the streamline of Kn=0.01 and Mach number 1.1, 2 and 4 respectively. There are more and more obvious second vortex as Mach number increasing. Fig. 3.109 shows the streamline of Kn=0.0033 and Mach number 1.1, 2 and 4 respectively. The second vortex all occurs in this case. The third vortex appear at the left bottom corner for M=4.
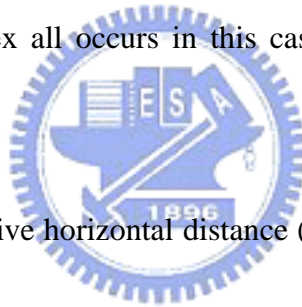
Fig. 3.110 shows the relative horizontal distance (x/L) of vortex center for various value of Mach number and Knudsen number. Results show that vortex center move toward left as Mach number increasing for Kn=0.01 and 0.0033. But the vortex center move toward the opposite way (right) for Kn=10, 1 and 0.1. Fig. 3.110 shows the relative vertical distance (y/L) of vortex center for various value of Mach number and Knudsen number. It show that vortex center moves down as Mach number increasing for Kn=0.01 and 0.0033. But the vortex center move toward the opposite way (toward the top wall) for Kn=10, 1 and 0.1.

Chapter 4

Conclusions and Recommendation of Future Work

4.1. Summary

The current study carries out the simulations of top driven supersonic (M=1.1-4) cavity flow at various Knudsen numbers using a parallelized DSMC code (PDSC) with transient sub-cells. Important conclusions are summarized as follows:

1. Use of transient sub-cells on unstructured grids is very beneficial considering the great reduction of both the memory and computational speed without losing the solution accuracy. Overhead of employing transient sub-cells is minimal for particles per cell less than approximately 100 based on our experience.

2. Velocity slips and temperature jumps increase at the solid walls with increasing rarefaction at the same Mach number.

3. The additional section vortex occur at the right bottom in Kn=0.01 and 0.0033 with various moving wall. The third vortex appears at the left bottom corner for Kn=0.0033 and M=4.

4. Results show that vortex center move toward left and down as Mach number increasing for Kn=0.01 and 0.0033. But the vortex center move toward the opposite way for Kn=10, 1 and 0.1.

4.2. Recommendation of Future Work

Based on this study, future work is suggested as follows:

1. To simulate the flows in detail by changing the ratio of height to width of the cavity;

2. To simulate the flows in detail by changing the wall temperatures and to focus on the discussion of heat transfer along the solid walls;

3. To simulate the driven cavity flow in subsonic region;

4. To simulate the driven cavity flow with oscillatory top moving plate.

5. To simulate the driven cavity flows with gas mixture and discuss the effects of moving plate speed and oscillation to the mixing of different species within the cavity.

References

[1]   , G. A., <u>Molecular Gas Dynamics</u>, Clarendon Press, Oxford, UK, 1976.

[2]   Bird, G..A., "Monte Carlo Simulation in an Engineering Context", Progr. Astro. Aero., 74, pp.239-255, 1981.

[3]   Bird, G..A., "Definition of Mean Free Path for Real Gases", Phys. Fluids, 26, pp.3222-3223, 1983.

[4]   Bird, G. A., <u>Molecular Gas Dynamics and the Direct Simulation of Gas Flows</u>, Oxford University Press, New York, 1994.

[5]   Borgnakke, C. and Larsen, P. S., "Statistical Collision Model for Monto Carlo Simulation of Polyatomic Gas Mixture", Journal of Computational Physics, 18, pp. 405-420, 1975.

[6]   Cercignani, C. and Cortese, S., "Validation of a Monte Carlo simulation of the plate Couette flow of a rarefied gas", J. Stat. Phys. 75, 817, 1994.

[7]   Cercignani, C, <u>The Boltzmann Equation and Its Application</u> (Springer, New York, 1998)

[8]   Cave, H. M., Krumdieck, S.P., and Jermy, M.C., "Development of a model for high precursor conversion efficiency pulsed-pressure chemical vapor deposition (PP-CVD) processing", Chem. Eeg. J., 2007 (in press).

[9]   Cave, H. M., Tseng, K.-C., Wu, J.-S., Jermy, M. C., Huang, J.-C. and Krumdieck, S. P., "Implementation of Unsteady Sampling Procedures for the Parallel Direct Simulation Monto Carlo Method", J. of Computational Physics, 2007 (submitted)

[10] Ghia, U., Ghia, K.N., and Shin, C.T., "High –Re solutions for incompressible flow using the Navier-Stokes equations and a multigrid method". J. of Computational Physics, 48, pp.387-411, 1982.

[11] Hou, S., Zou, Q., Chen, S., and Doolen, G., "Simulation of cavity flow by the lattice Boltzmann method", J. Comput. Phys. 118, 329, 1995.

[12] Kannenberg, K. and Boyd, I. D.,"Strategies for Efficient Particel Resolution in the Direct Simulation Monte Carlo Method", Journal of Computational Physics, 157, pp. 727-745, 2000.

[13] Karniadakis, G.E., and Beskok, A., <u>Micro Flows. Fundamentals and Simulation</u> (Springer, New York, 2001)

[14] Nanbu, K., "Theoretical Basis on the Direct Monto Carlo Method", Rarefied Gas Dynamics, 1, Boffi, V. and Cercignani, C. (editor), Teubner, Stuttgart, 1986.

[15] Naris, S., and Valougeorgis, D., "The driven cavity flow over the whole range of the Knudsen number", Physics of Fluids, 17, 2005.

[16] Robinson, C. D., and Harvey, J. k., " A parallel DSMC Implementation on Unstructured Meshes with Adaptive Domain Decomposition", Proceeding of 20th International Symposium on Rarefied Gas Dynamics, pp. 227-232, Shen, C. (editor), Peking University Press, 1996.

[17] Robinson, C. D., and Harvey, J. k., "Adaptive Domain Decomposition for Unstructured Meshes

Applied to the Direct Simulation Monte Carlo Method", Parallel Computational Fluid Dynamics: Algorithm and Results using Advanced Computers, pp. 469-476, 1997.

[18] Robinson, C. D., <u>Particle Simulations on Parallel Computers with Dynamic Load Balancing, Imperial College of Science</u>, Technology and Medicine, UK, Ph.D. Thesis, 1998.

[19] Tseng, K.-C., Cave, H. M., Wu, J.-S., Huang, J.-C., Lian, Y.-Y., Jermy, M. C. and Krumdieck, S. P., "Implementation of Transient Sub-Cells on Unstructured Grids for the Parallel Direct Simulation Monto Carlo Method", Journal of Computational Physics, 2007 (submitted)

[20] Wagner, W., "A convergence proof for Bird's Direct simulation Monte Carlo method for the Boltzmann equation", Journal State Physics, 66(3/4), pp. 1011-1044, 1992.

[21] Wu, J.-S., and Tseng, K.-C., "Parallel DSMC Method Using Dynamic Domain Decomposition", International Journal for Numerical Methods in Engineering, Vol. 63, pp. 37-76, 2005.

[22] Wu, J.-S., Lee, W.-S., Lee, Fred and Wong, S.-C., "Pressure Boundary Treatment In Micromechanical Devices Using Direct Simulation Monto Carlo Method", JSME International Journal, Series B, 44(3), pp. 439-450, 2001.

[23] Wu, J.-S., and Hsu Y.-L., "Derivation of Variable Soft Sphere Model Parameters in Direct-Simulation Monte Carlo Method Using Quantum Chemistry Computation", Japanese Journal of Applied Physics, 42, pp. 7574-7575, 2003.

[24] Wu, J.-S., Tseng, K.-C., and Wu, F.-Y., " Parallel Three Dimensional Simulation Monte Carlo Method Using Adaptive Mesh and Variable Time Step", Computer Physics Communications", Vol. 162, No. 3, pp. 166-187, 2004.

[25] Wu, J.-S., Lian, Y.-Y., Cheng, G., Koomullil, R. P., and Tseng, K.-C., "Development and Verification of a Coupled DSMC-NS Scheme Using Unstructured Mesh", Journal of Computational Physics, Vol. 219, No. 2, pp. 579-607, 2006.

Tables

Table I   The condition of benchmark cases.

	Knudsen number	Mach number	Mesh	Particle per cell
With sub-cell	0.01	0.5	100 x 100	100
Without sub-cell	0.01	0.5	400 x 400	25
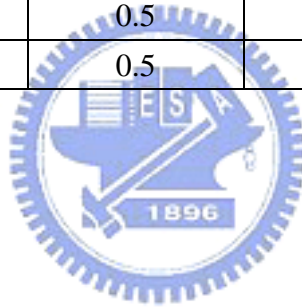
Table II   The mesh information

Knudsen number	Mach number	Mesh	Grid size of the each cell	Particles per cell
10	4	40 x 40	0.025	25
10	2	40 x 40	0.025	25
10	1.1	40 x 40	0.025	25
1	4	40 x 40	0.025	25
1	2	40 x 40	0.025	25
1	1.1	40 x 40	0.025	25
0.1	4	40 x 40	0.025	25
0.1	2	40 x 40	0.025	25
0.1	1.1	40 x 40	0.025	25
0.01	4	100 x 100	0.01	100
0.01	2	100 x 100	0.01	100
0.01	1.1	100 x 100	0.01	100
0.0033	4	300 x 300	3.33e-3	100
0.0033	2	300 x 300	3.33e-3	100
0.0033	1.1	300 x 300	3.33e-3	100

Table III Simulation condition

Knudsen number	Mach number	Driven plate velocity	Initial wall and gas temperature	Number Density
10	4	1288	300	1.29438E+17
10	2	644	300	1.29438E+17
10	1.1	354.2	300	1.29438E+17
1	4	1288	300	1.29438E+18
1	2	644	300	1.29438E+18
1	1.1	354.2	300	1.29438E+18
0.1	4	1288	300	1.29438E+19
0.1	2	644	300	1.29438E+19
0.1	1.1	354.2	300	1.29438E+19
0.01	4	1288	300	1.29438E+20
0.01	2	644	300	1.29438E+20
0.01	1.1	354.2	300	1.29438E+20
0.0033	4	1288	300	3.88314E+20
0.0033	2	644	300	3.88314E+20
0.0033	1.1	354.2	300	3.88314E+20

Table IV Position of properties distribution across

Knudsen number	Near top wall	Near bottom wall	Near left wall	Near right wall
10	y/L=0.9875	y/L=0.0125	x/L=0.0125	x/L=0.9875
1	y/L=0.9875	y/L=0.0125	x/L=0.0125	x/L=0.9875
0.1	y/L=0.9875	y/L=0.0125	x/L=0.0125	x/L=0.9875
0.01	y/L=0.995	y/L=0.005	x/L=0.995	x/L=0.995
0.0033	y/L=0.9967	y/L=0.0033	x/L=0.0033	x/L=0.9967

Figures
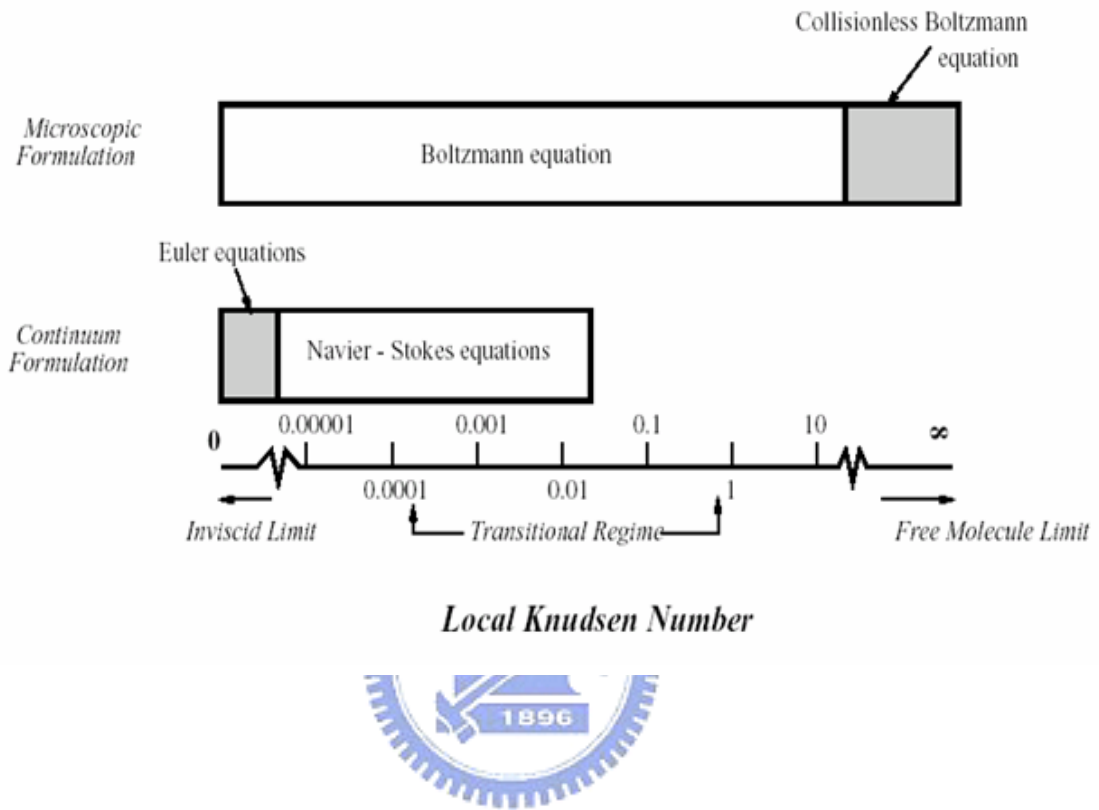
Fig. 1.1   Classifications of Gas Flows
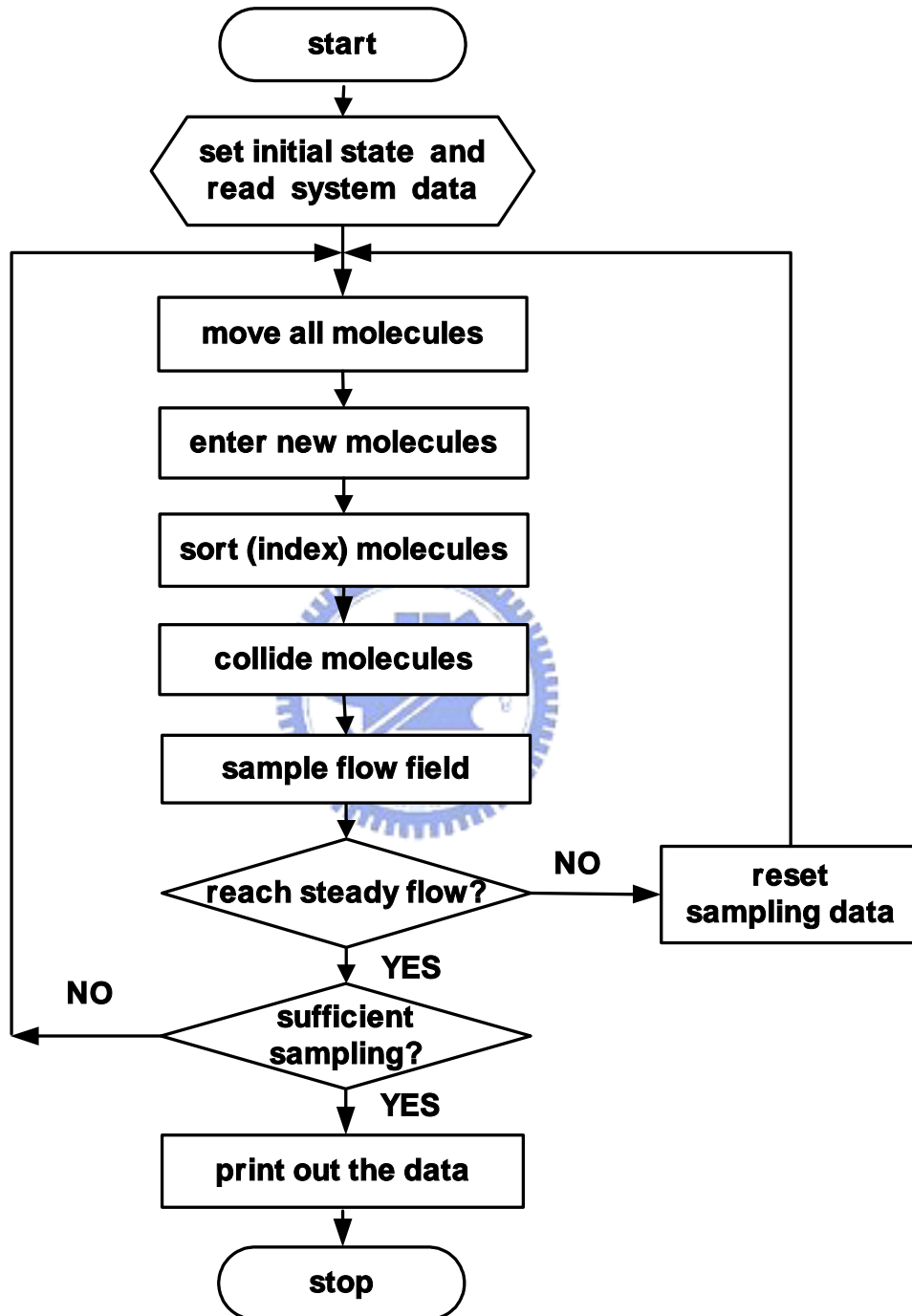
Fig. 2.1 Flow chart of the DSMC method.
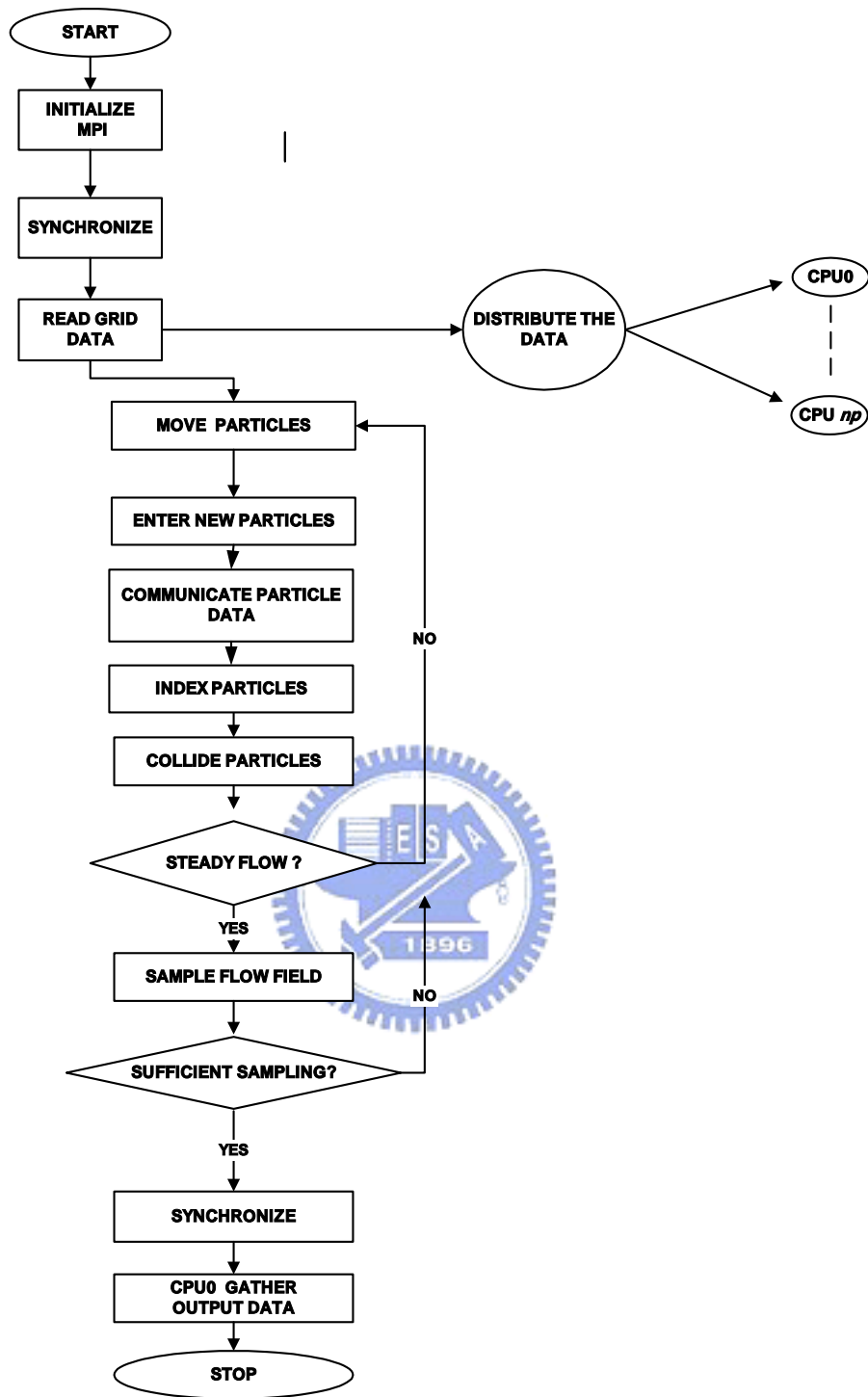
Fig. 2.2 Simplified flow chart of the parallel DSMC method for np processors.
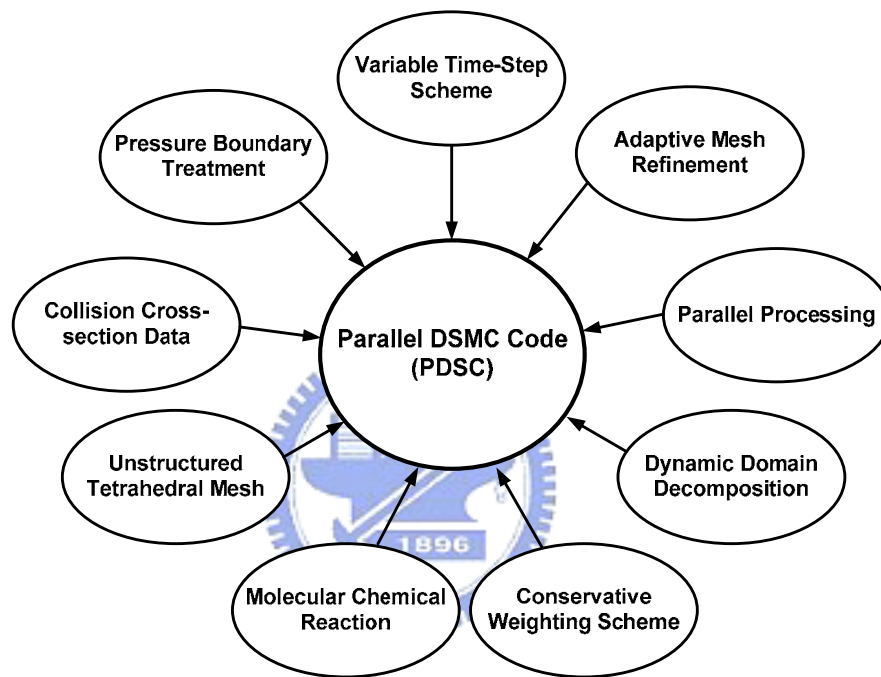
Fig. 2.3   The additional schemes in the parallel DSMC code.
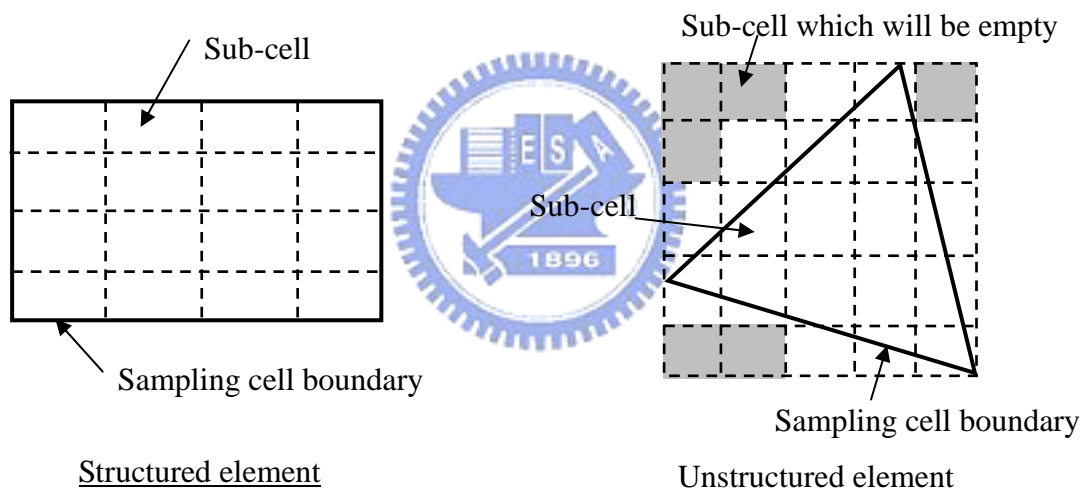
Fig. 2.6 Division of structured and unstructured elements into sub-cells
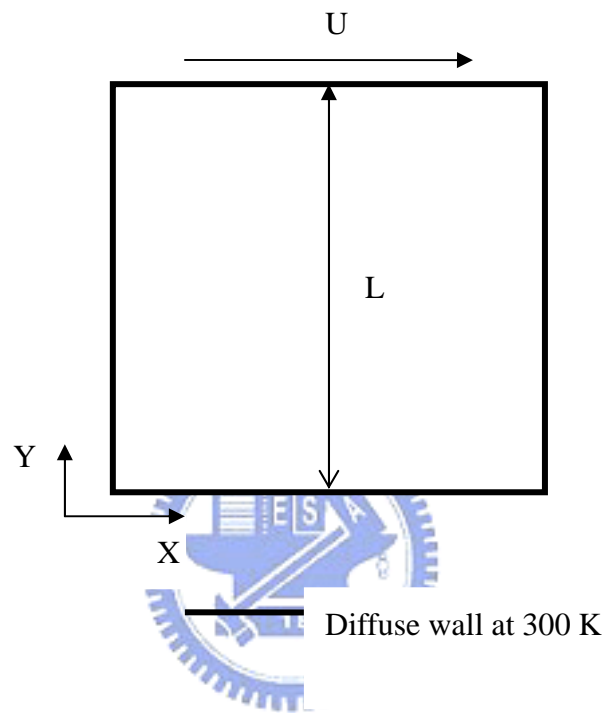
Fig. 3.1 The 2D square (L/H) driven cavity flow with moving top plate
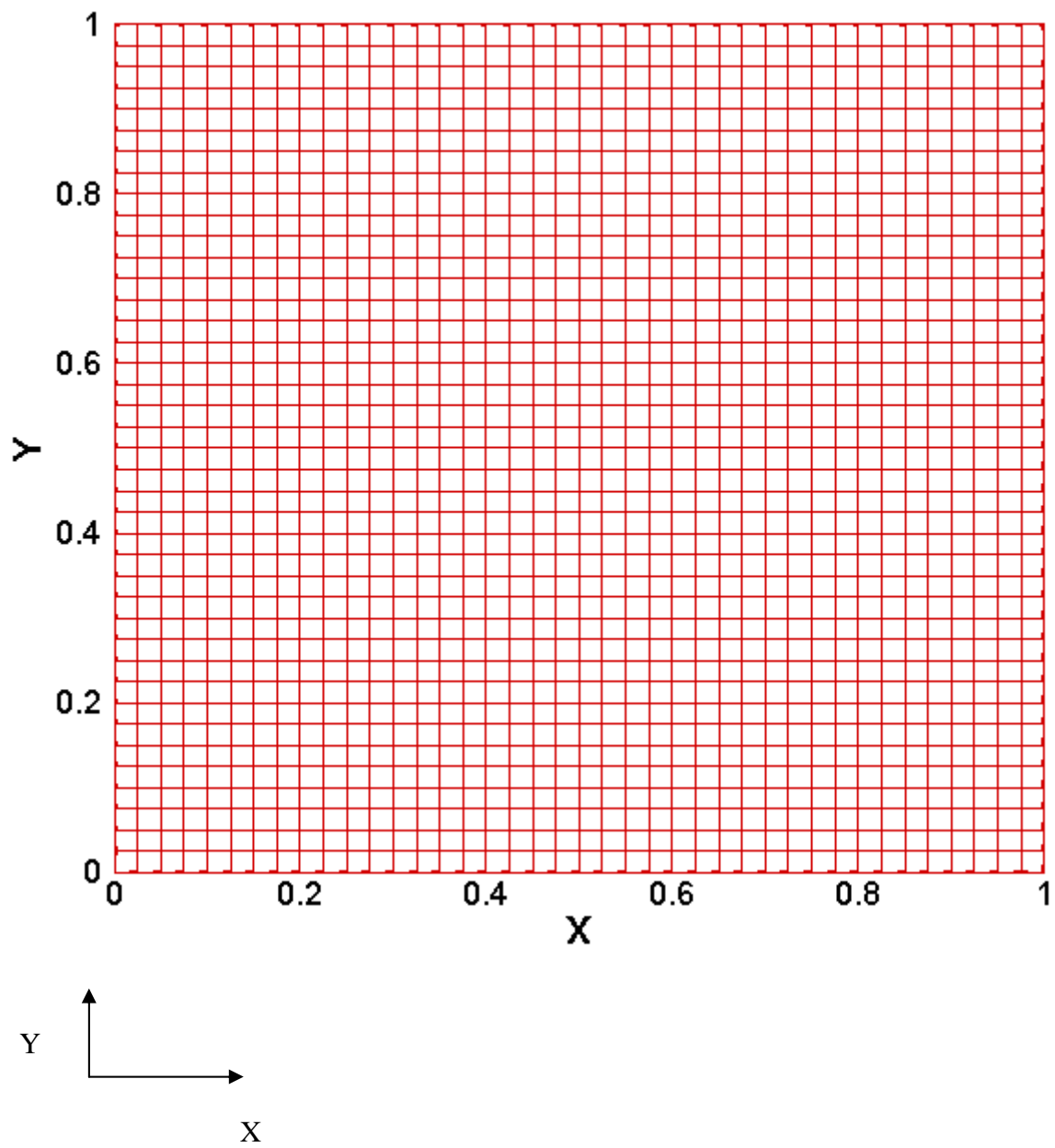
Fig. 3.2   The mesh for Knudsen number 10, 1, 0.1(40×40)
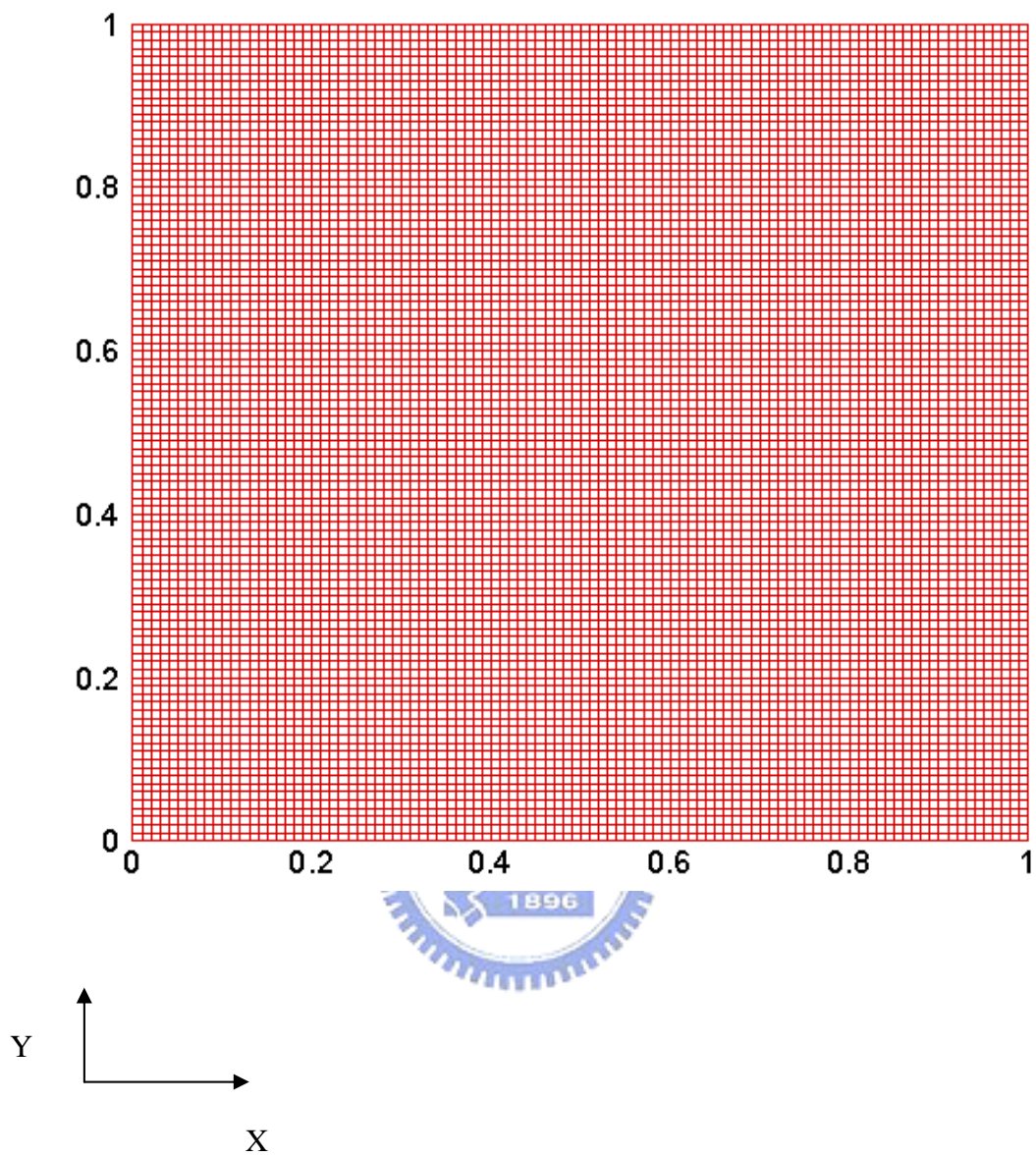
Fig. 3.3   The mesh for Knudsen number 10, 1, 0.1(100×100).
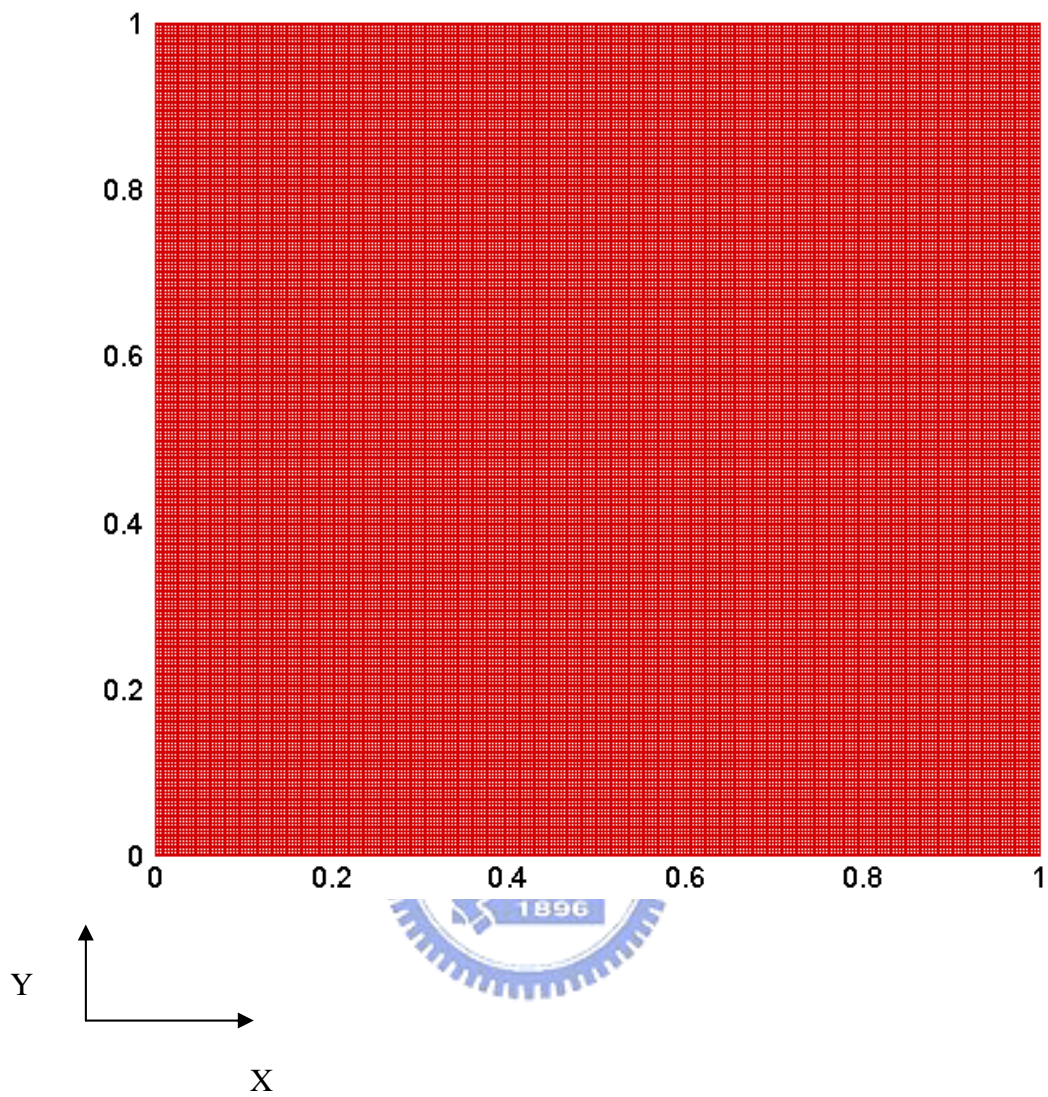
Fig. 3.4   The mesh for Knudsen number 0.0033(300×300)
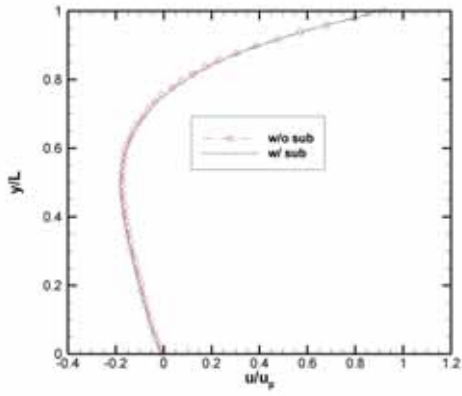
(a)
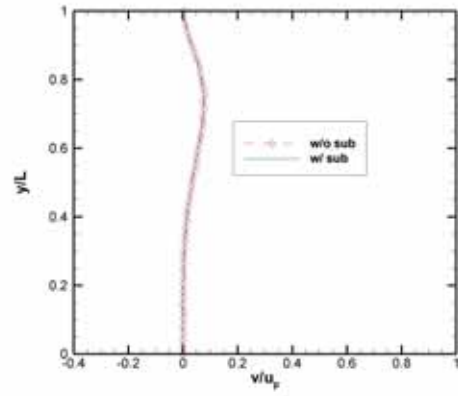
(c)
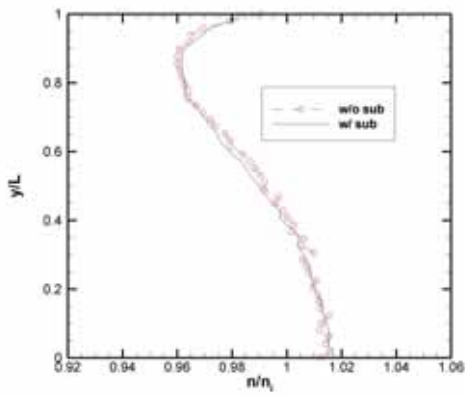
(b)
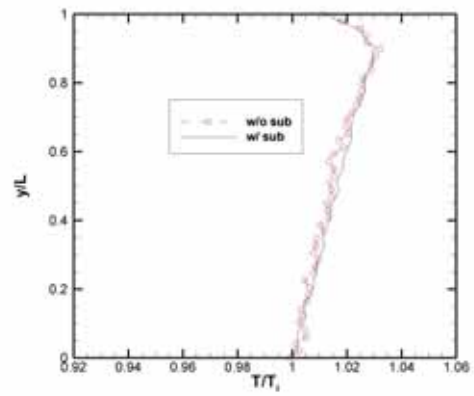
(d)

Fig. 3.4 Properties distribution along vertical line through geometry center (x/L=0.5)

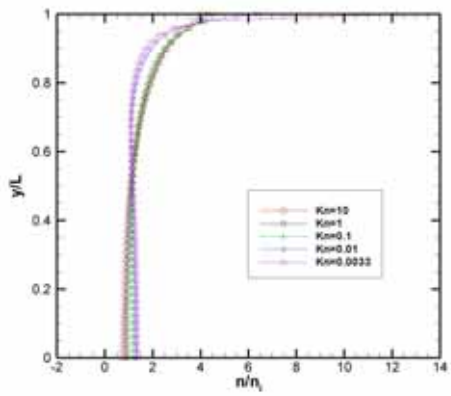(a) u velocity: (b) v velocity: (c) number density: (d) temperature.
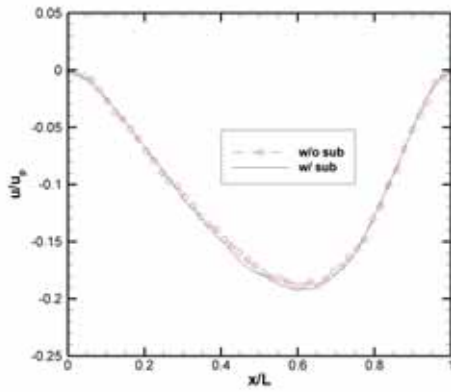
(a)
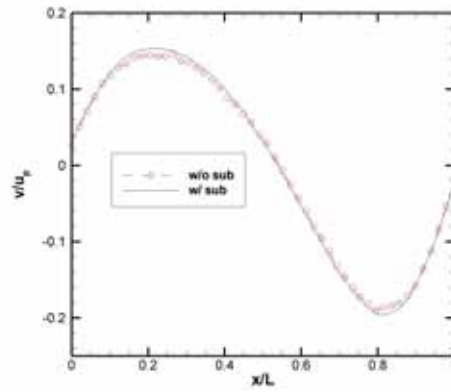
(c)
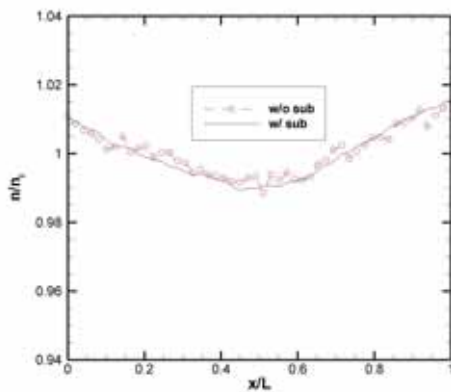
(b)
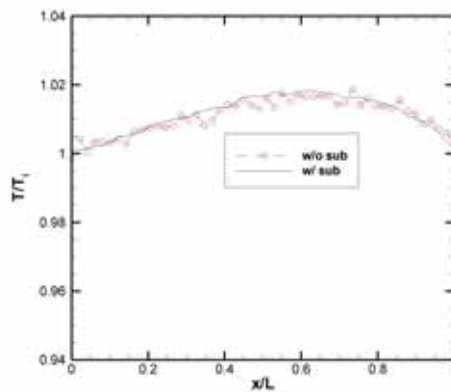
(d)

Fig. 3.5   Properties distribution along horizontal line through geometry center (y/L=0.5)

(a) u velocity: (b) v velocity: (c) number density: (d) temperature.
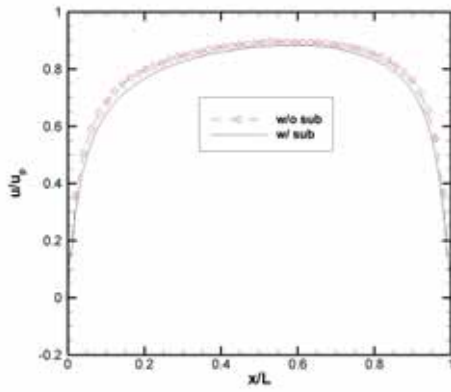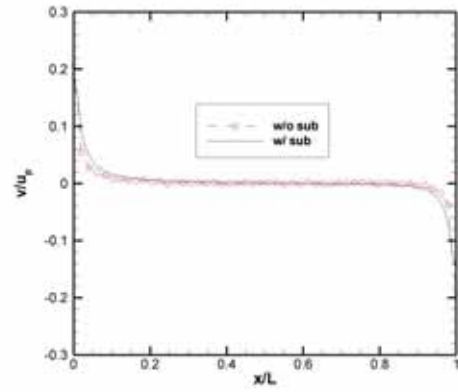
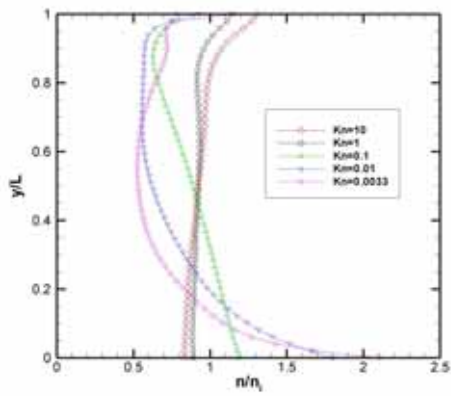(a)   (c)
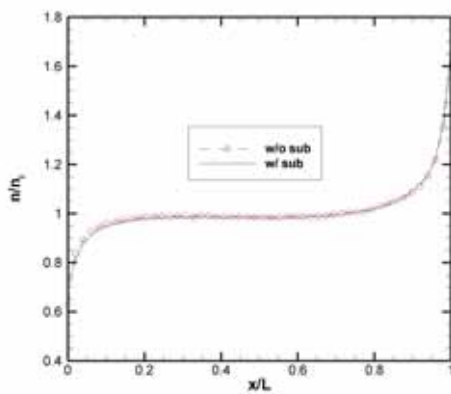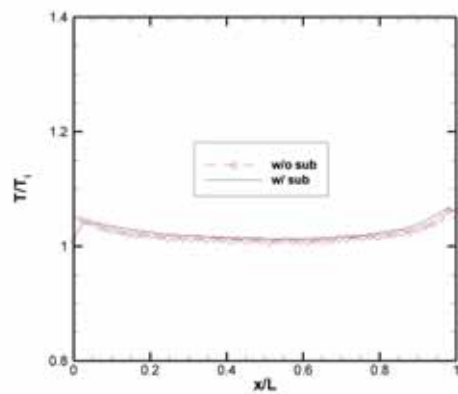
(b)   (d)

Fig. 3.6   Properties   distribution   along   horizontal   line   near   top   wall(y/L=1)

(a) u velocity: (b) v velocity: (c) number density: (d) temperature.

53
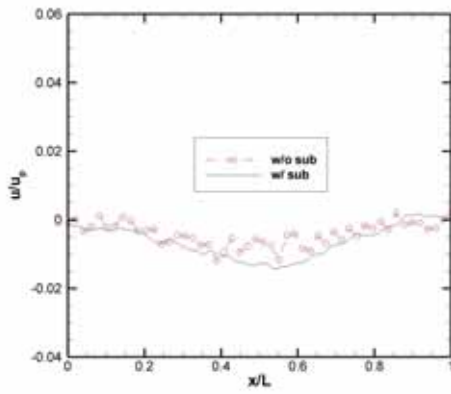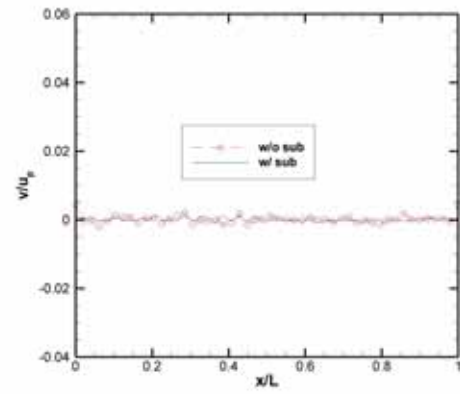
(a)   (c)
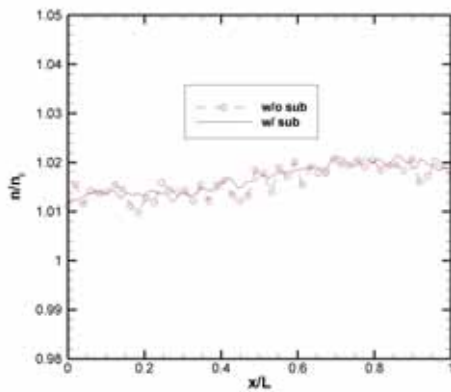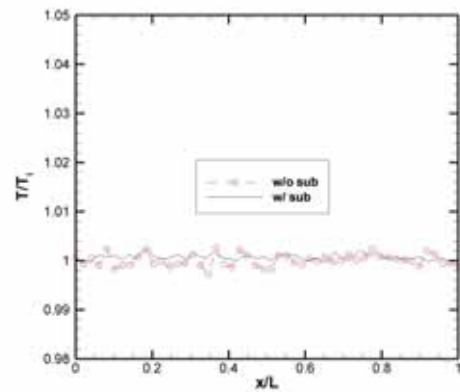
(b)   (d)

Fig. 3.7   Properties   distribution   along   horizontal   line   near   bottom   wall(y/L=0)

(a) u velocity: (b) v velocity: (c) number density: (d) temperature.
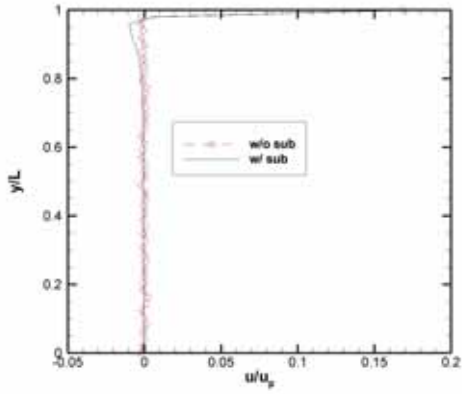
(a)
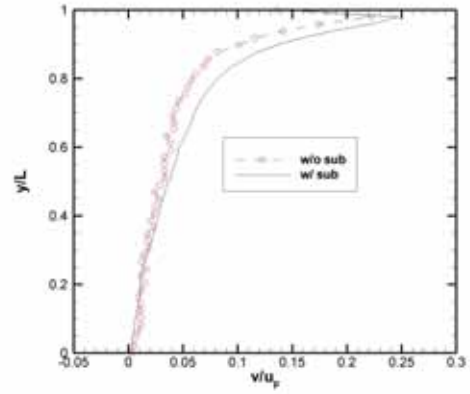
(c)
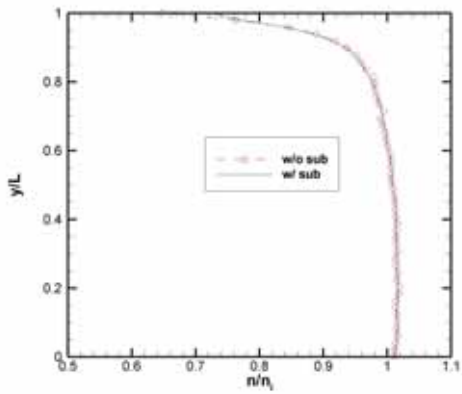
(b)
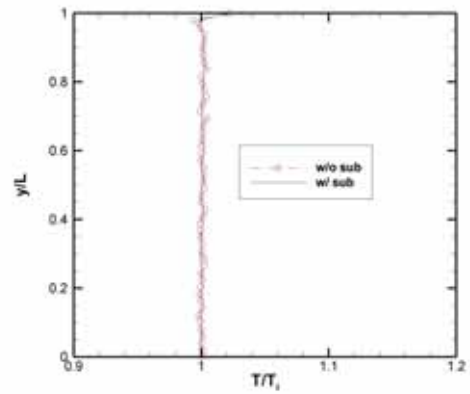
(d)

Fig. 3.8 Properties distribution along vertical line near left wall(x/L=0) (a) u velocity: (b) v velocity: (c) number density: (d) temperature.
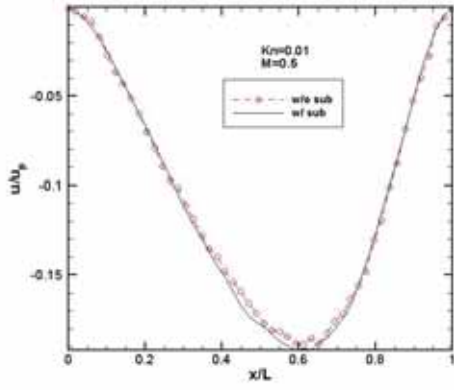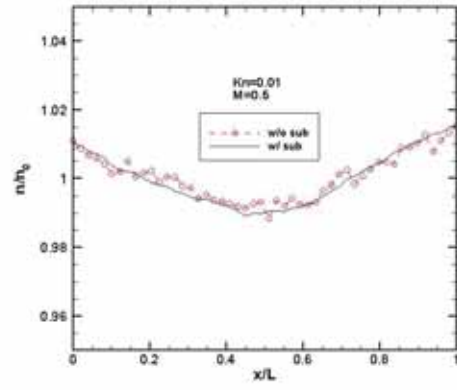
(a)   (c)
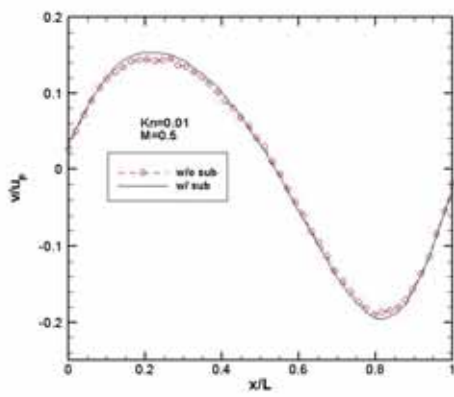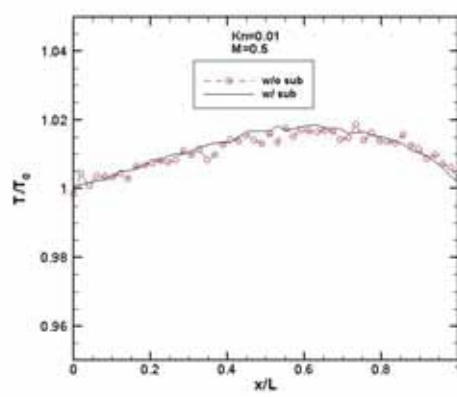

(b)   (d)

Fig. 3.9 Properties distribution along vertical line near right wall(x/L=1)

(a) u velocity: (b) v velocity: (c) number density: (d) temperature.
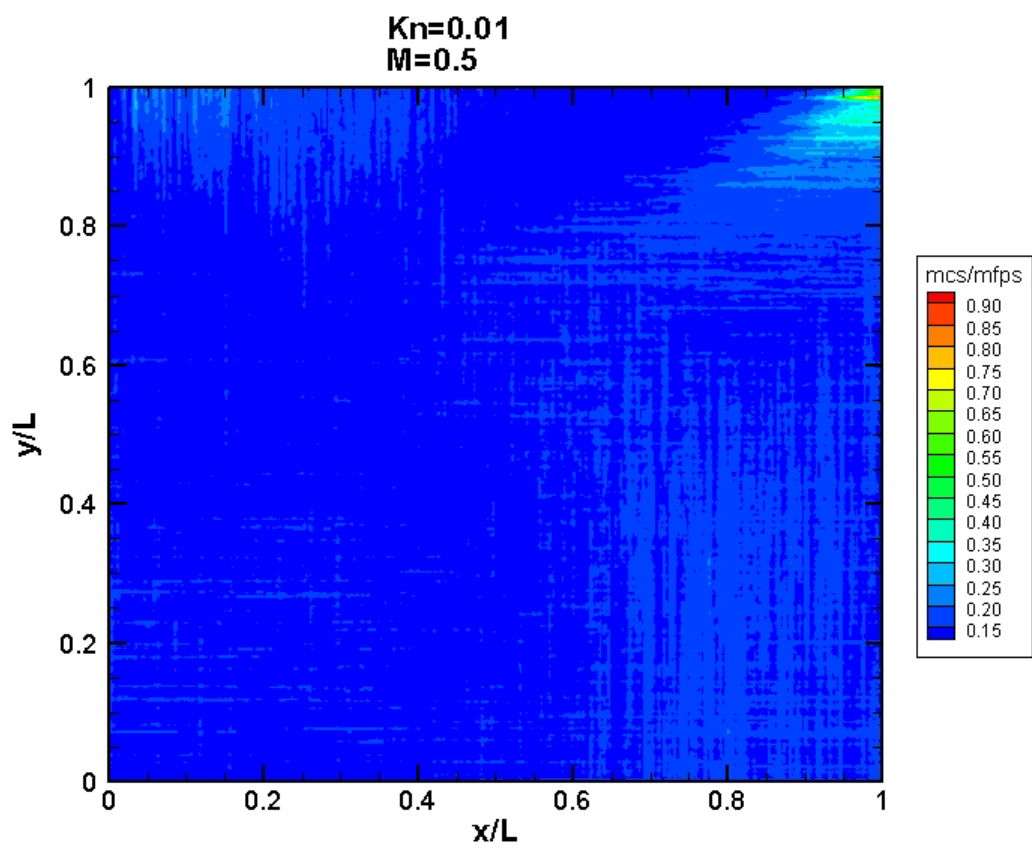
Fig. 3.10   The merit of collision without sub-cells case
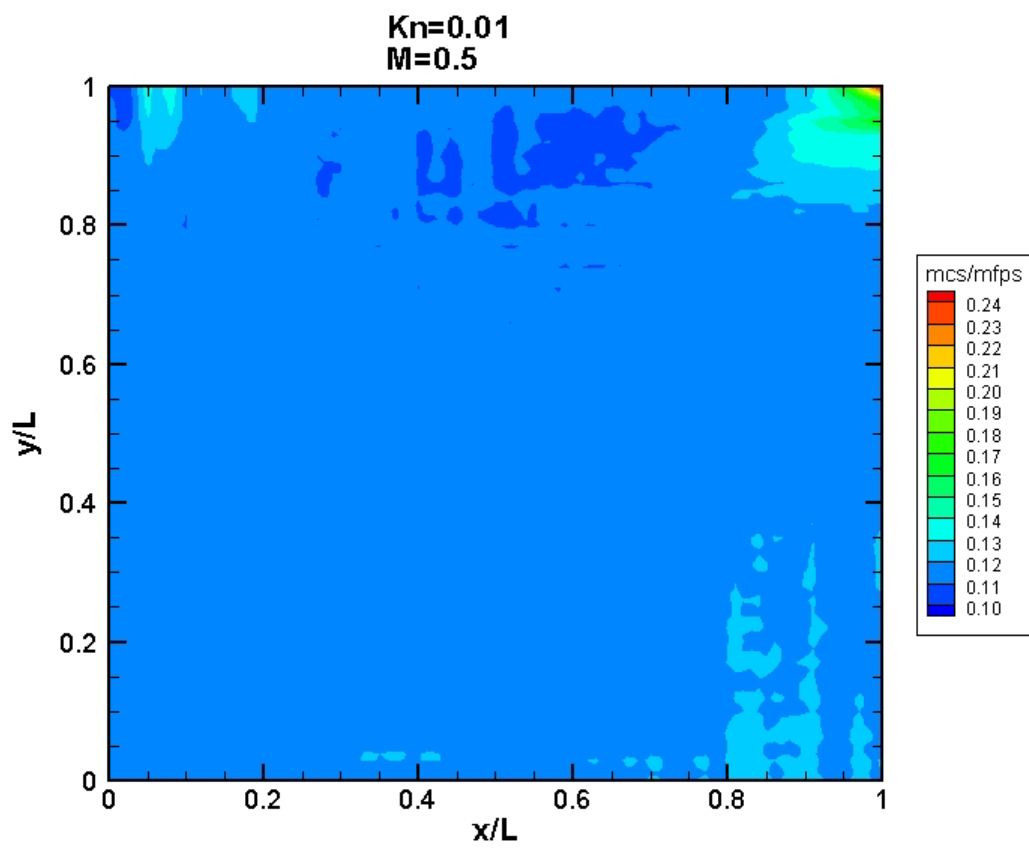
Fig. 3.11   The merit of collision with sub-cells case
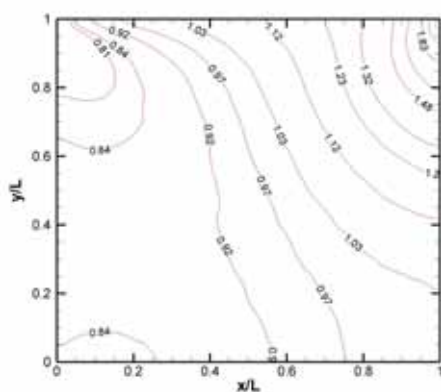
(a)
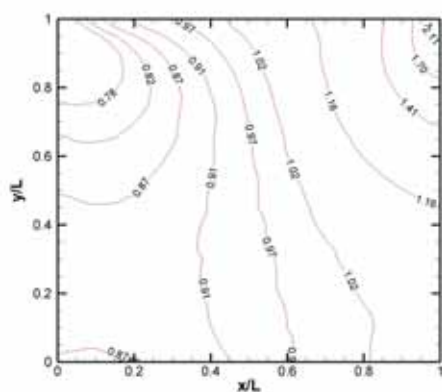
(b)
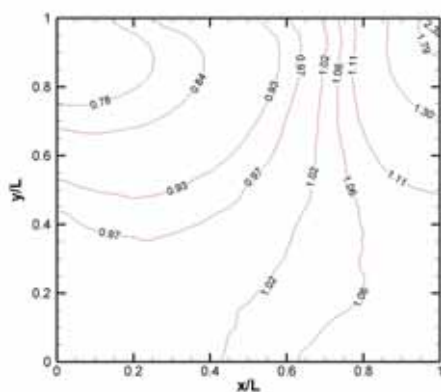
(c)
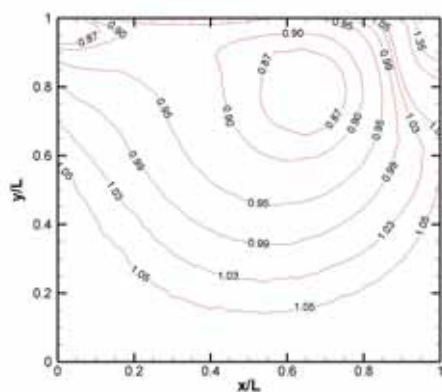
(d)
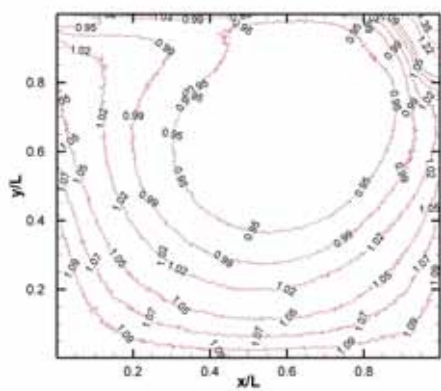
(e)

Fig. 3.12 Contour of number density for M = 1.1, (a) Kn = 10; (b) Kn = 1; (c) Kn = 0.1;
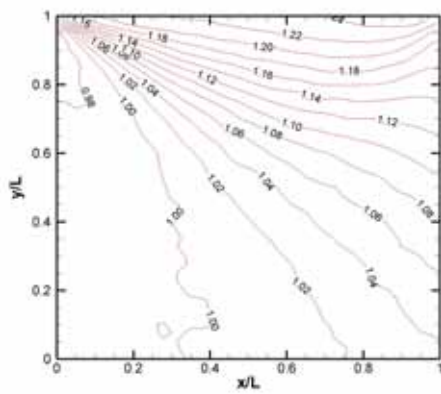
(d) Kn = 0.01; (e) Kn = 0.0033.

(a)
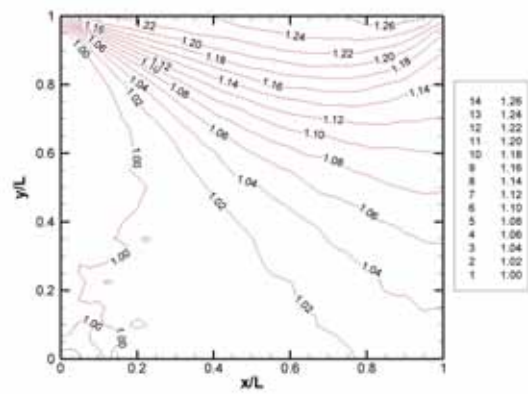
(b)
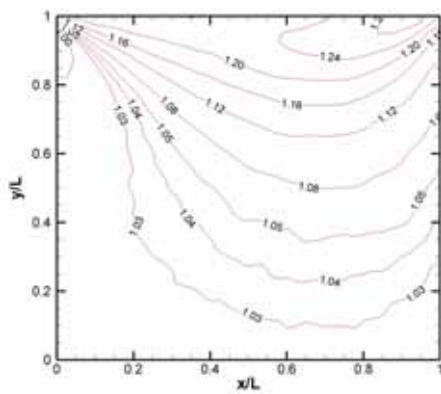
(c)
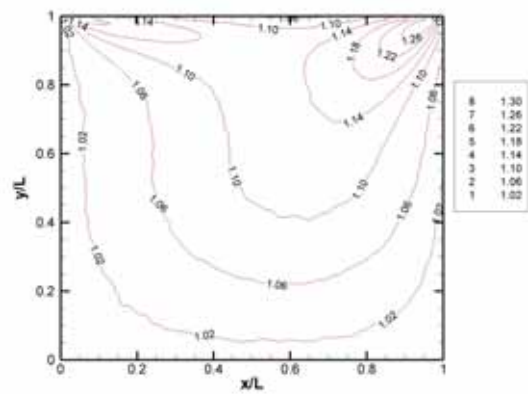
(d)
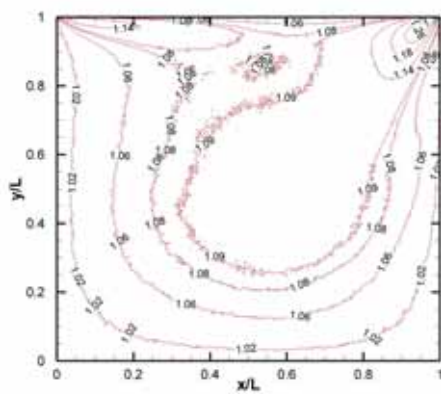
(e)

Fig. 3.13   Contour of temperature for M = 1.1, (a) Kn = 10; (b) Kn = 1; (c) Kn = 0.1; (d)
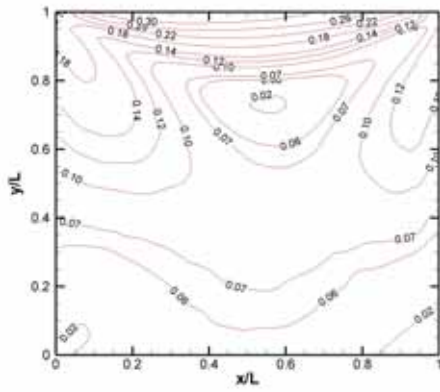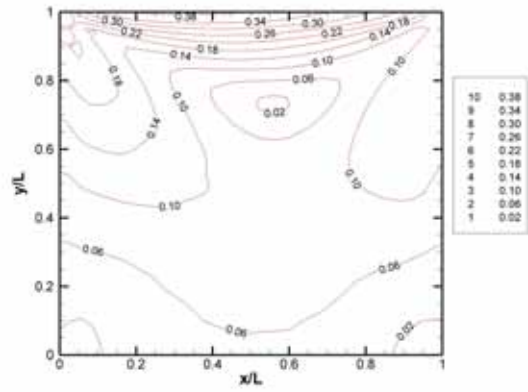
Kn = 0.01; (e) Kn = 0.0033.

(a)   (b)
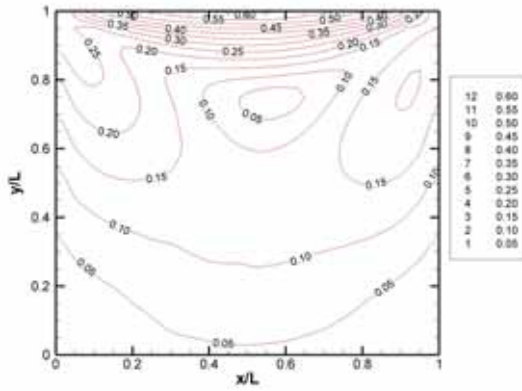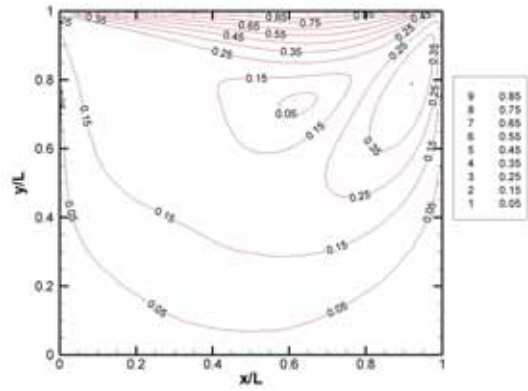
(c)   (d)
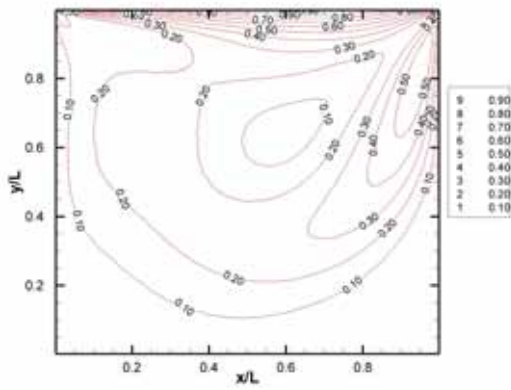
(e)

Fig. 3.14   Contour of Mach number for M = 1.1, (a) Kn = 10; (b) Kn = 1; (c) Kn = 0.1; (d)

Kn = 0.01; (e) Kn = 0.0033.

61
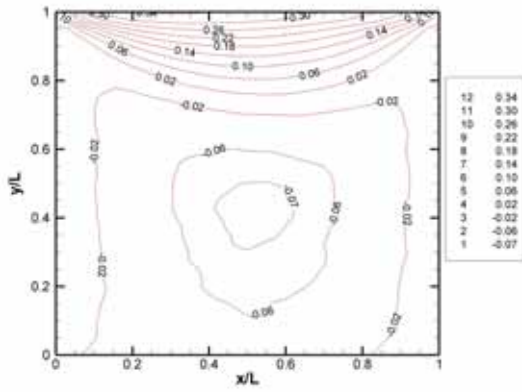
(a)
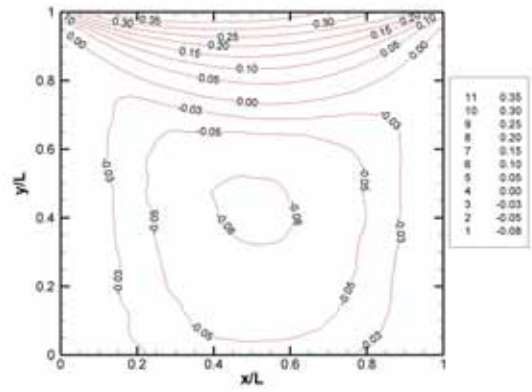
(b)
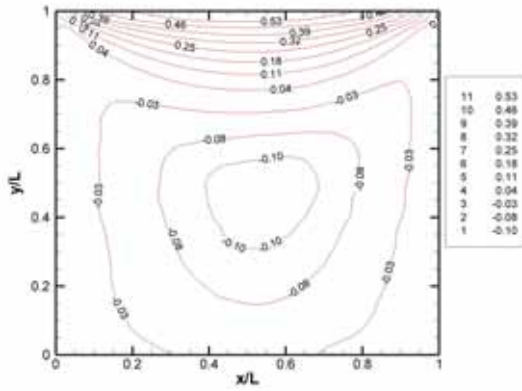
(c)
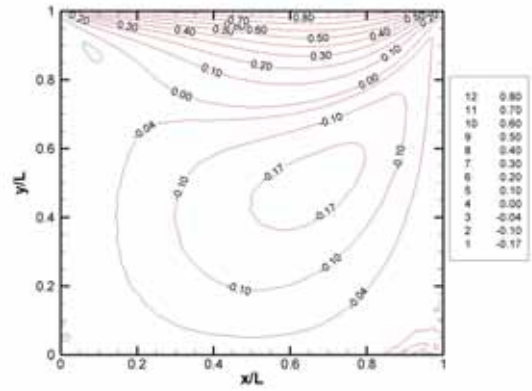
(d)
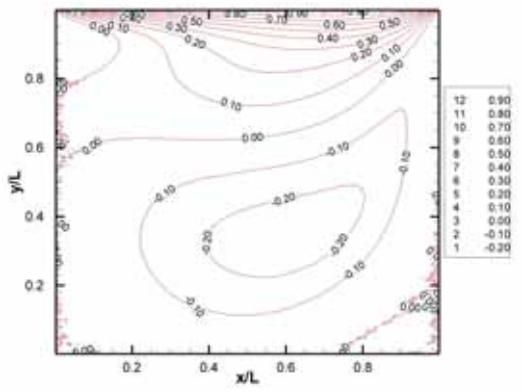
(e)

Fig. 3.15   Contour of u-velocity for M = 1.1, (a) Kn = 10; (b) Kn = 1; (c) Kn = 0.1;

(d) Kn = 0.01; (e) Kn = 0.0033.

(a)

(b)

(c)

(d)

(e)
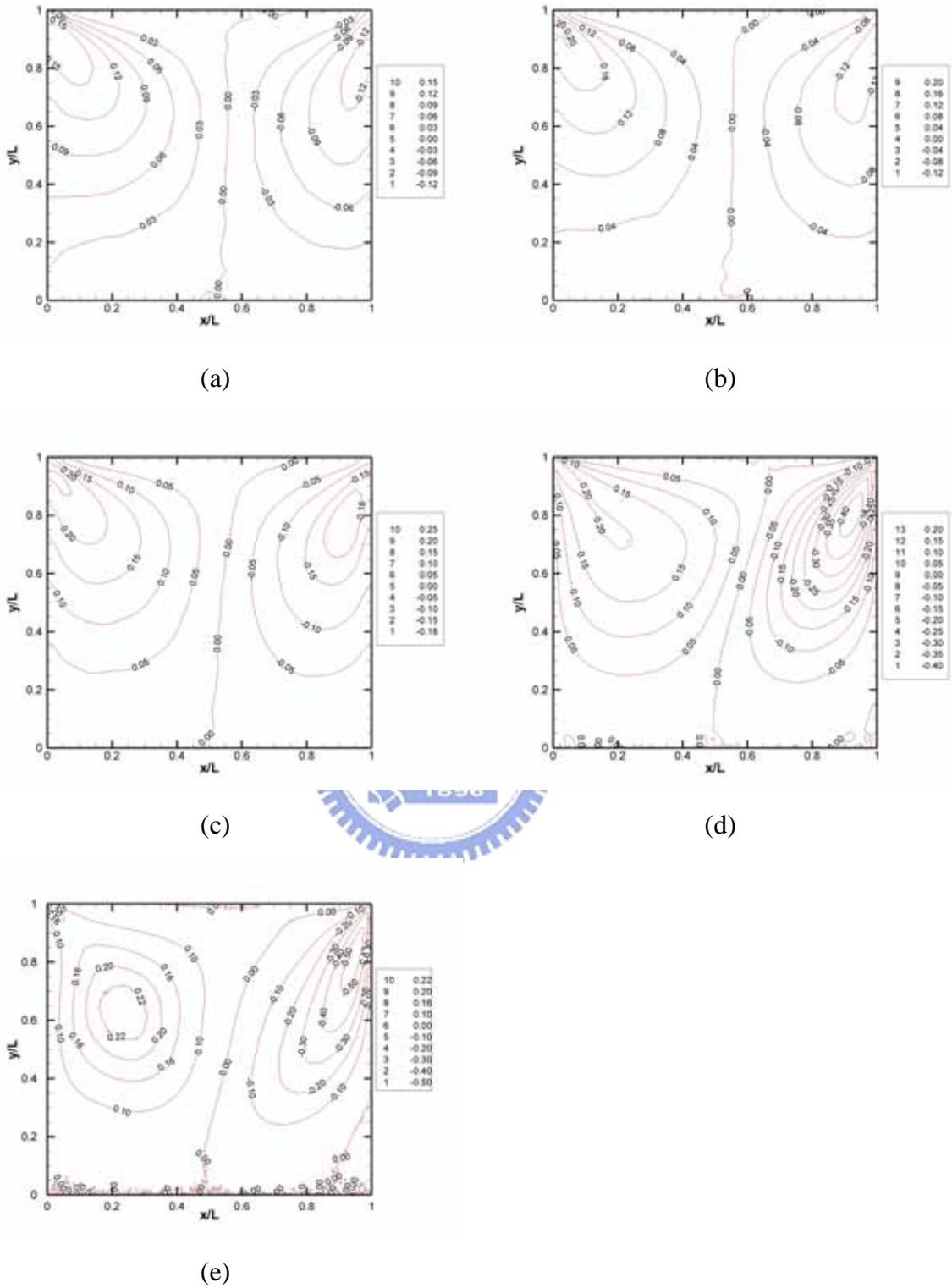
Fig. 3.16 Contour of v-velocity for M = 1.1, (a) Kn = 10; (b) Kn = 1; (c) Kn = 0.1; (d) Kn = 0.01; (e) Kn = 0.0033.
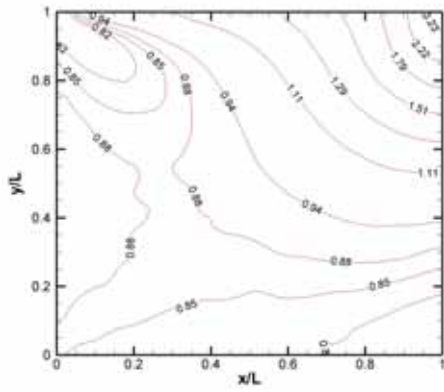
(a)
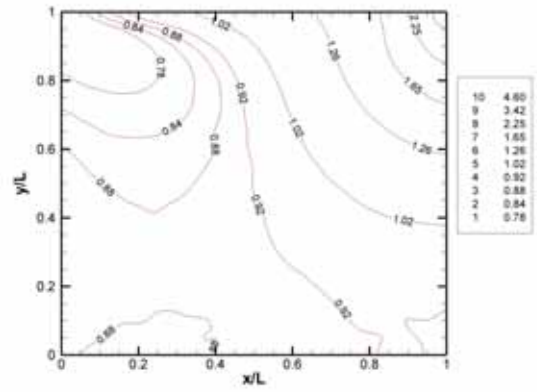
(b)
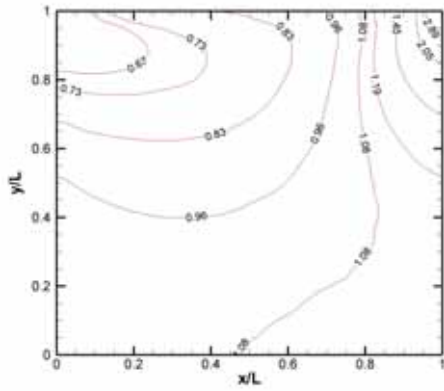
(c)
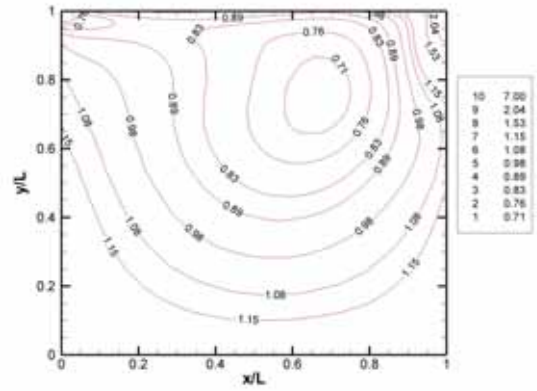
(d)
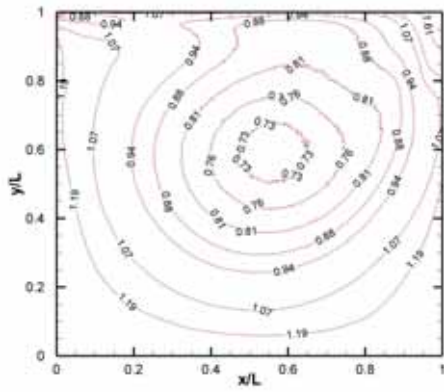
(e)

Fig. 3.17 Contour of number density for M = 2, (a) Kn = 10; (b) Kn = 1; (c) Kn = 0.1;
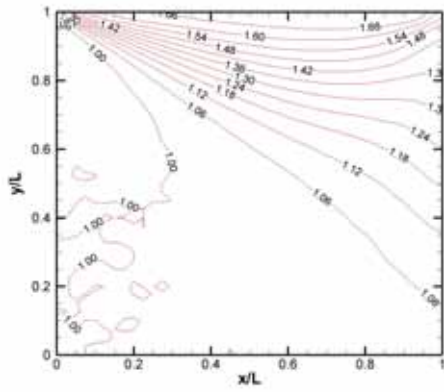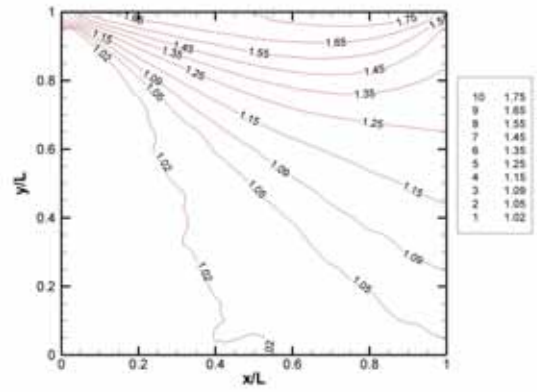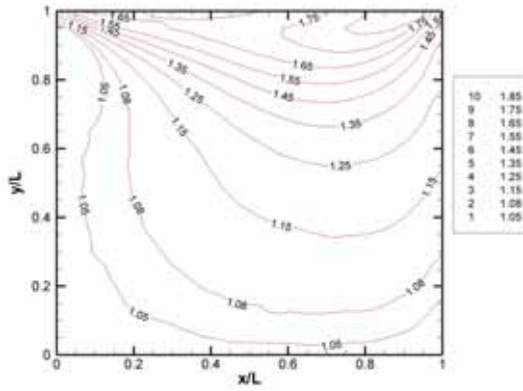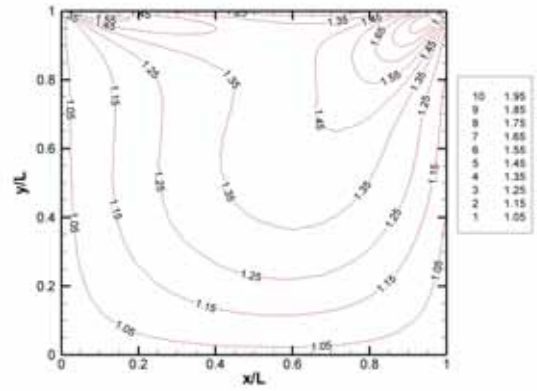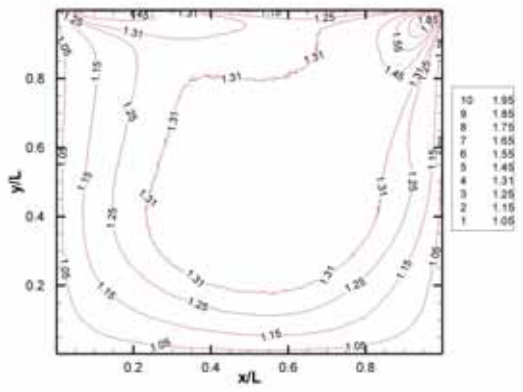
(d) Kn = 0.01; (e) Kn = 0.0033.

Fig. 3.18 Contour of temperature for M = 2, (a) Kn = 10; (b) Kn = 1; (c) Kn = 0.1; (d) Kn = 0.01; (e) Kn = 0.0033.
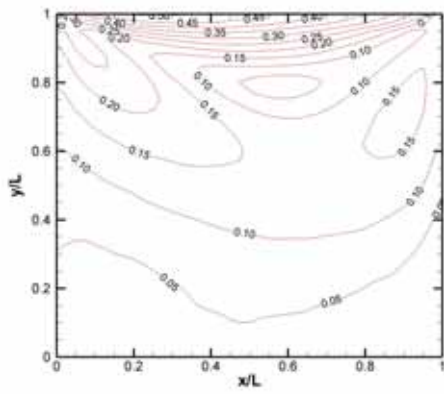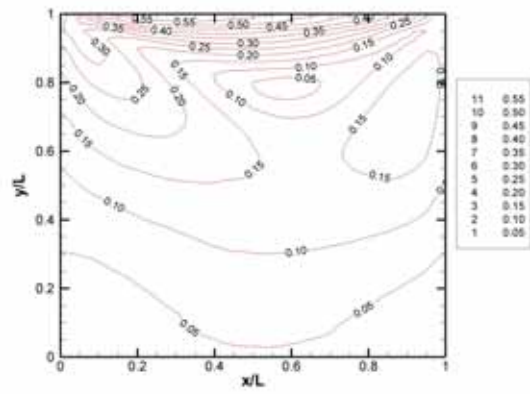
(a)   (b)
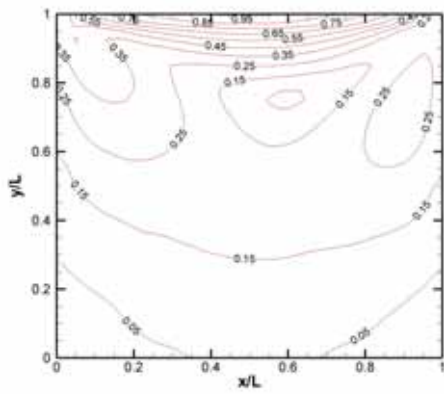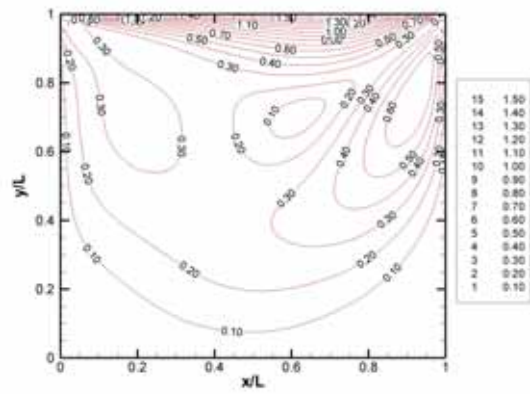
(c)   (d)
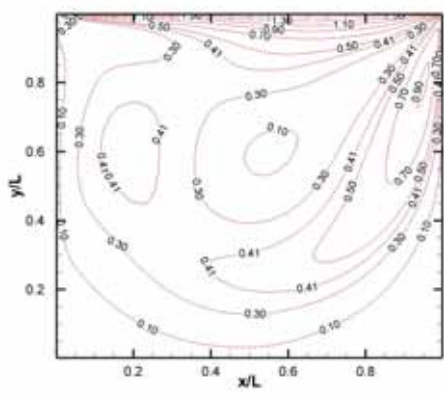
(e)

Fig. 3.19   Contour of Mach number for M = 2, (a) Kn = 10; (b) Kn = 1; (c) Kn = 0.1;
(d) Kn = 0.01; (e) Kn = 0.0033.
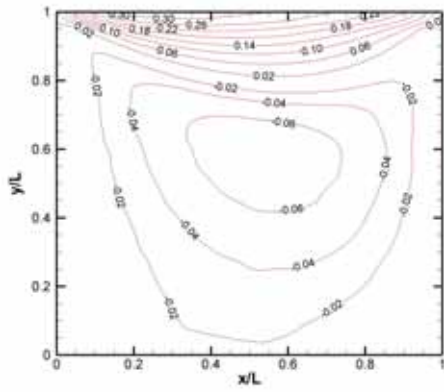
(a)
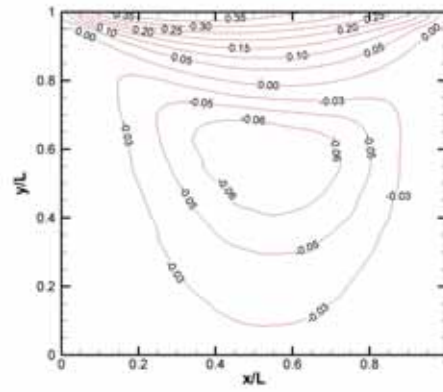
(b)
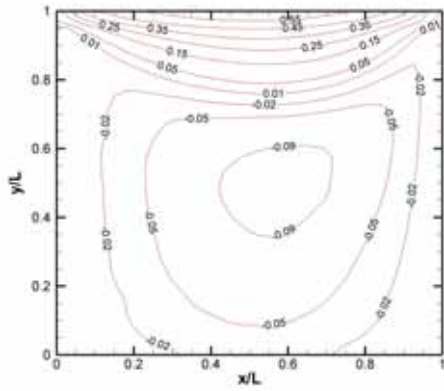
(c)
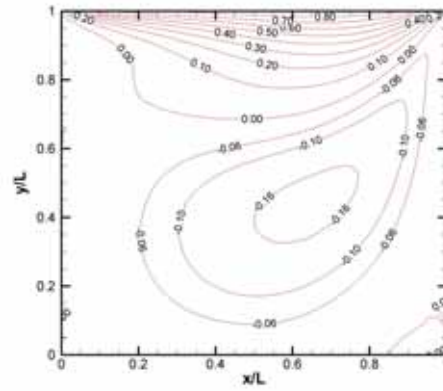
(d)
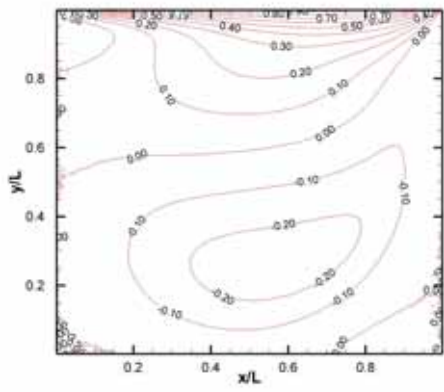
(e)

Fig. 3.20   Contour of u-velocity for M = 2, (a) Kn = 10; (b) Kn = 1; (c) Kn = 0.1;
(d) Kn = 0.01; (e) Kn = 0.0033.
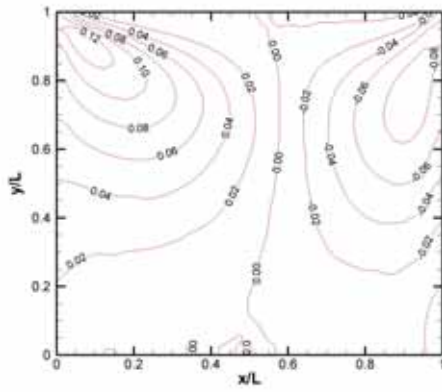
(a)
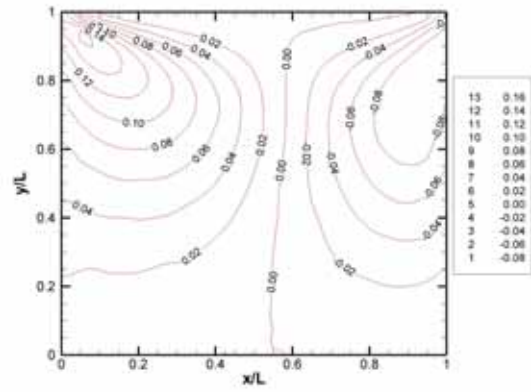
(b)
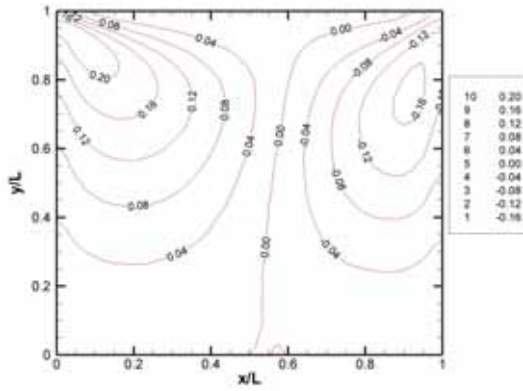
(c)
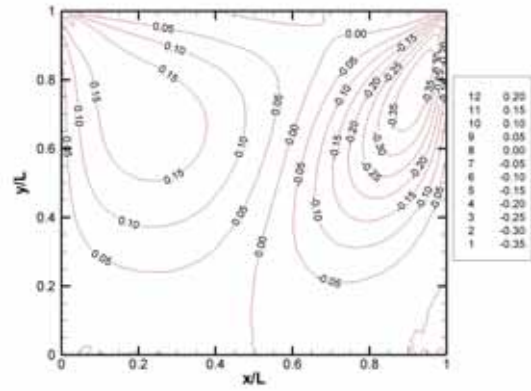
(d)
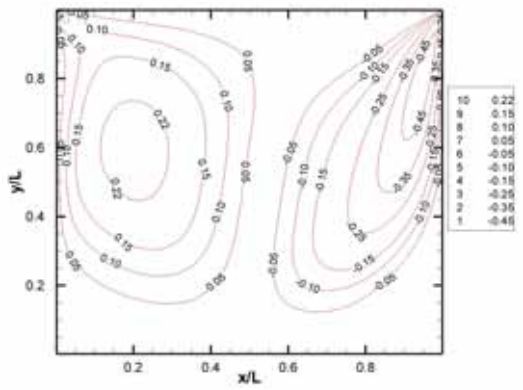
(e)

Fig. 3.21 Contour of v-velocity for M = 2, (a) Kn = 10; (b) Kn = 1; (c) Kn = 0.1; (d) Kn = 0.01; (e) Kn = 0.0033.
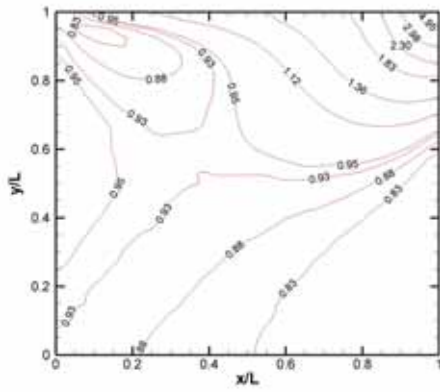
(a)
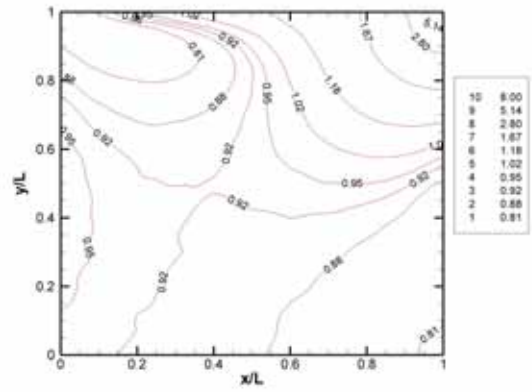
(b)
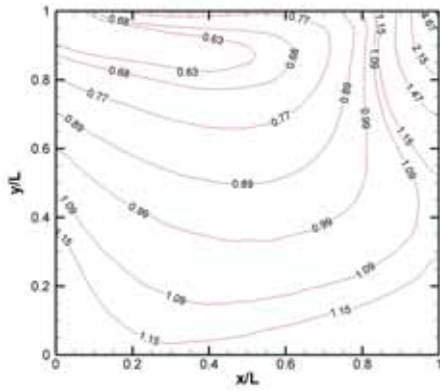
(c)
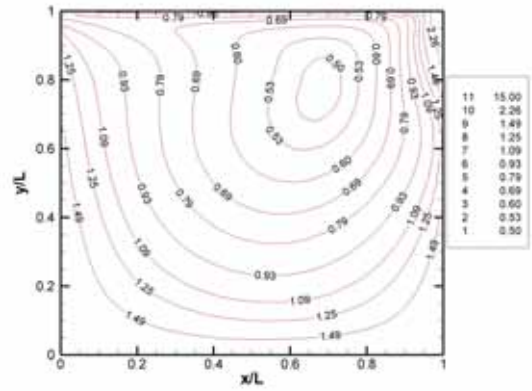
(d)
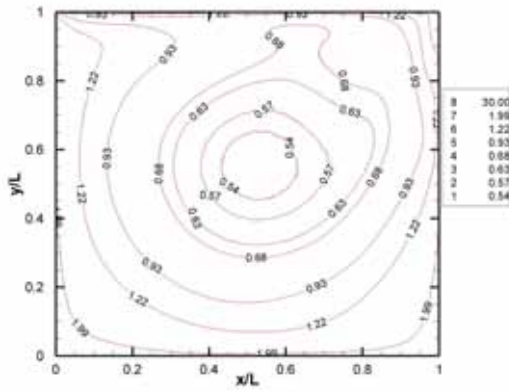
(e)

Fig. 3.22 Contour of number density for M = 4, (a) Kn = 10; (b) Kn = 1; (c) Kn = 0.1; (d) Kn = 0.01; (e) Kn = 0.0033.
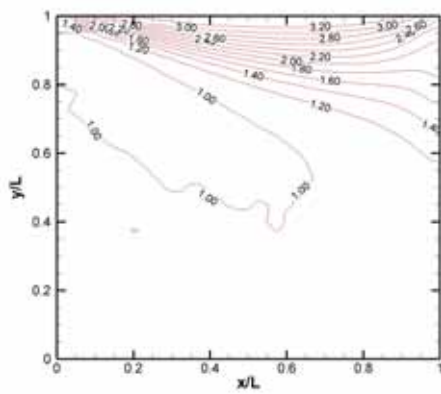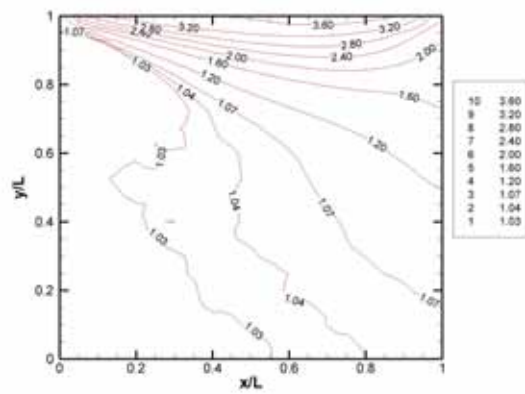
(a)   (b)
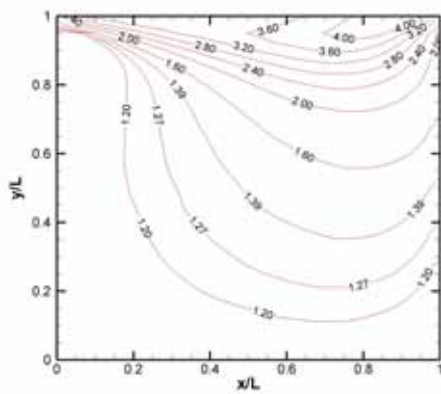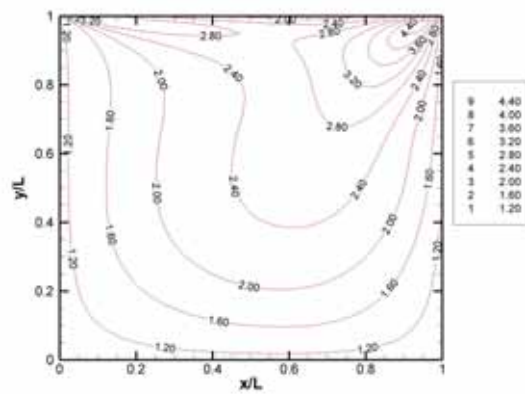

(c)   (d)
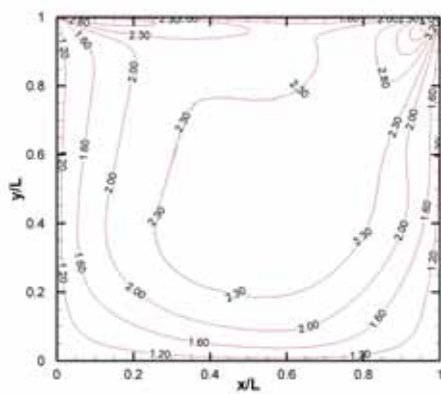
(e)

Fig. 3.23   Contour of temperature for M = 4, (a) Kn = 10; (b) Kn = 1; (c) Kn = 0.1;   (d)

Kn = 0.01; (e) Kn = 0.0033.

70
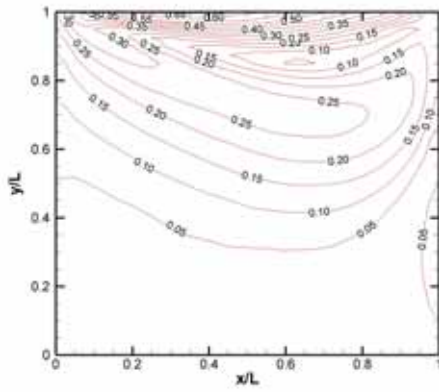
(a)
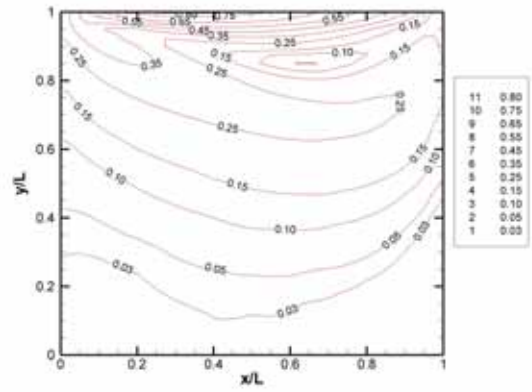
(b)
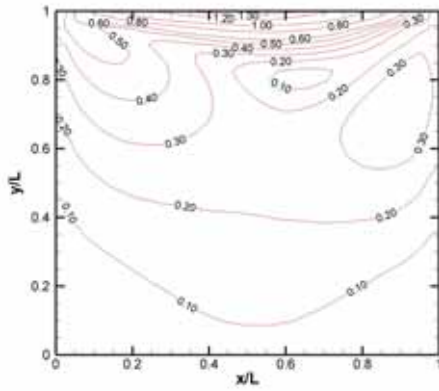
(c)
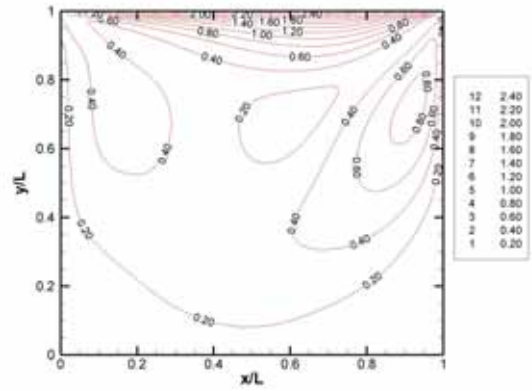
(d)
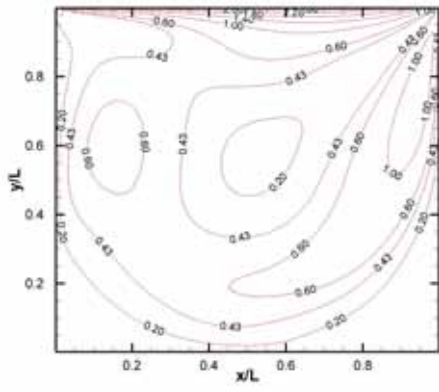
(e)

Fig. 3.24   Contour of Mach number for M = 4, (a) Kn = 10; (b) Kn = 1; (c) Kn = 0.1;   (d)

Kn = 0.01; (e) Kn = 0.0033.

(a)   (b)

(c)   (d)

(e)
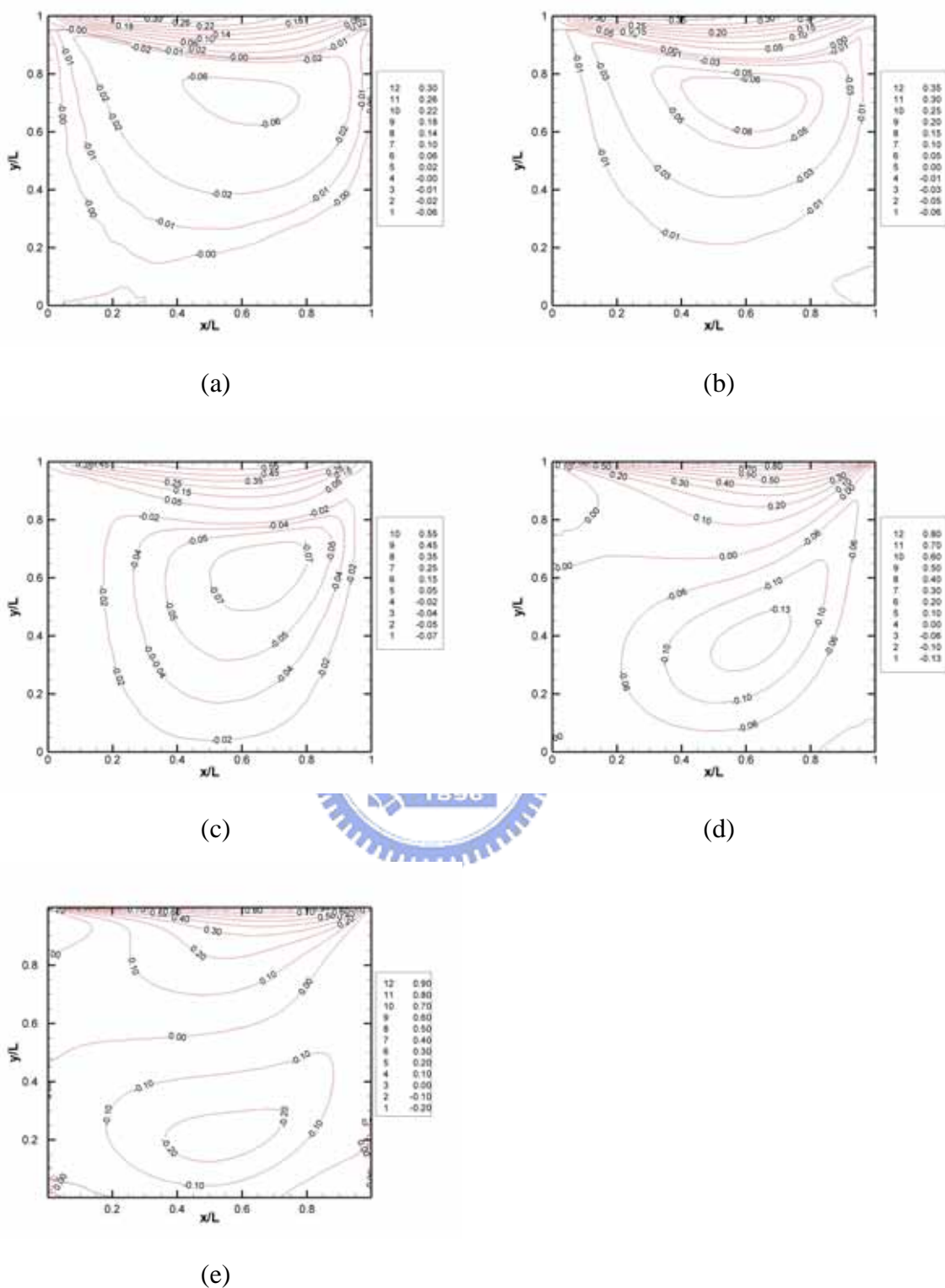
Fig. 3.25   Contour of u-velocity for M = 4, (a) Kn = 10; (b) Kn = 1; (c) Kn = 0.1;

(d) Kn = 0.01; (e) Kn = 0.0033.

72
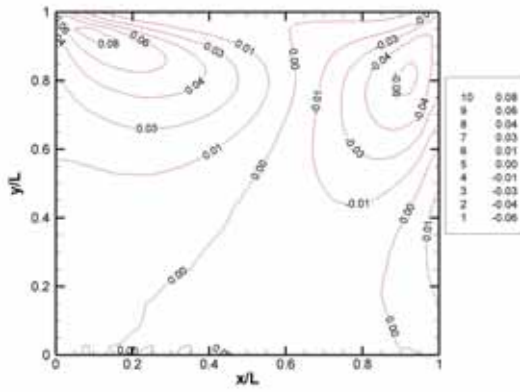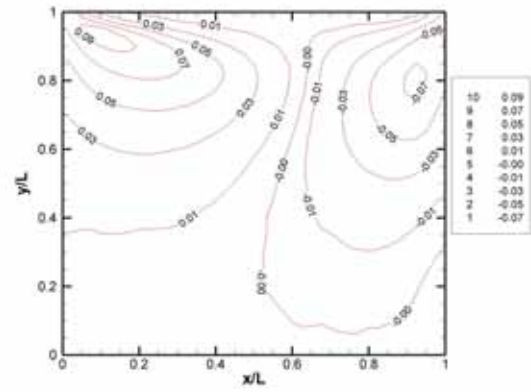
(a)   (b)
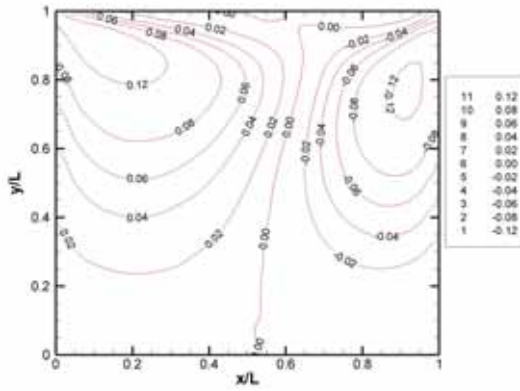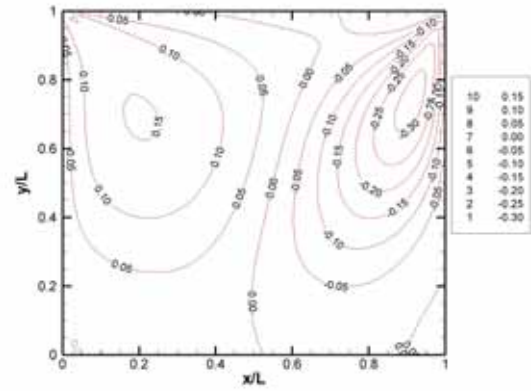
(c)   (d)
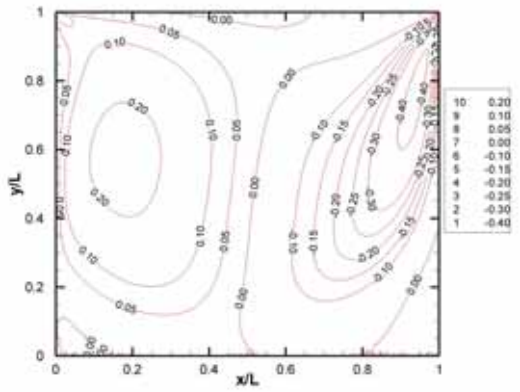
(e)

Fig. 3.26   Contour of v-velocity for M = 4, (a) Kn = 10; (b) Kn = 1; (c) Kn = 0.1;

(d) Kn = 0.01; (e) Kn = 0.0033.

73
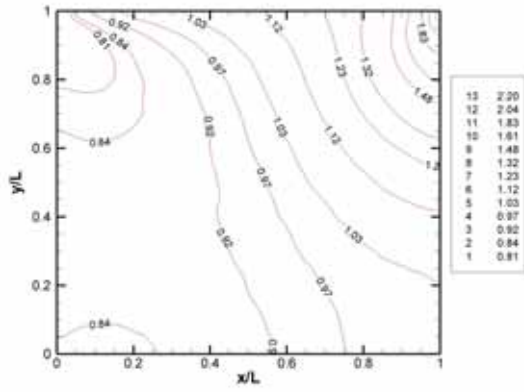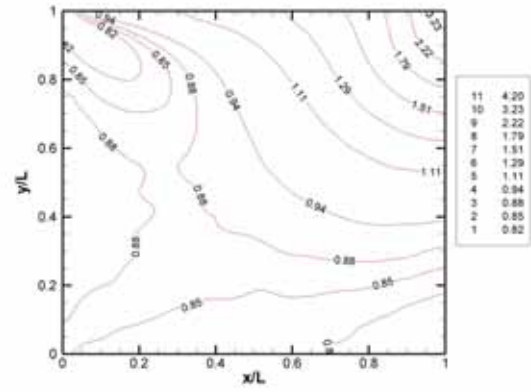
(a)   (b)
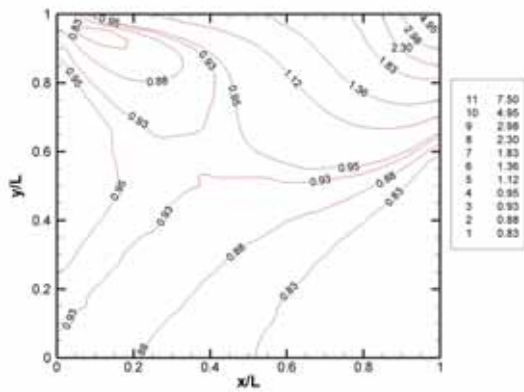

(c)

Fig. 3.27   Contour of number density for Kn = 10, (a) M = 1.1; (b) M = 2; (c) M = 4
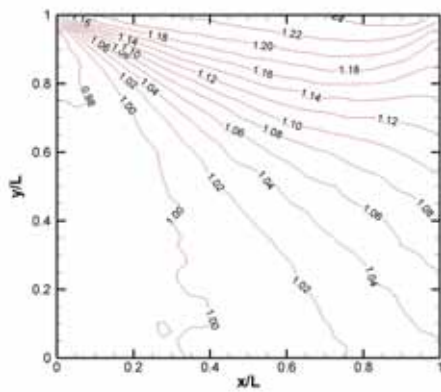
(a)
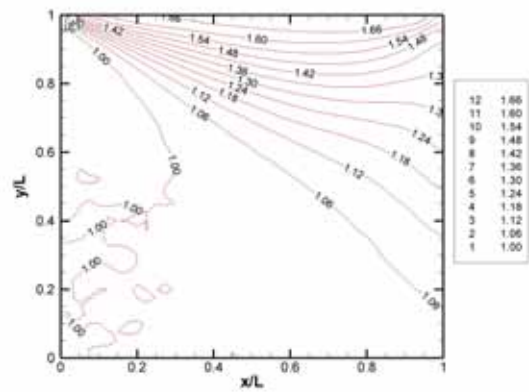
(b)
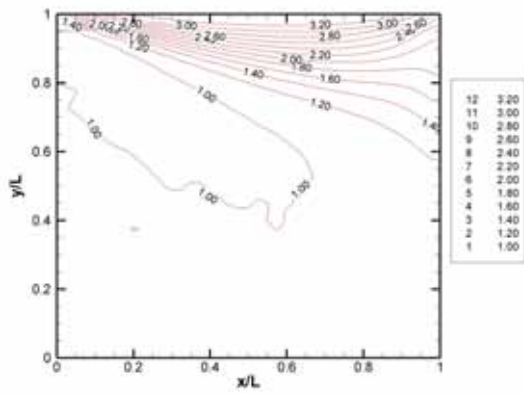
(c)

Fig. 3.28   Contour of temperature for Kn = 10, (a) M = 1.1; (b) M = 2; (c) M = 4
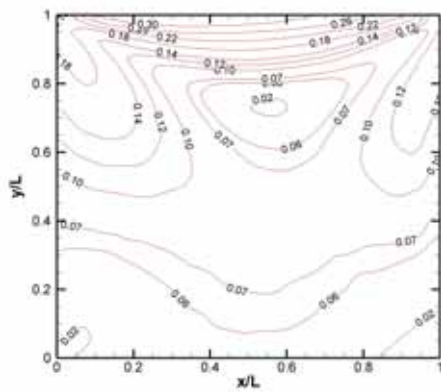
(a)
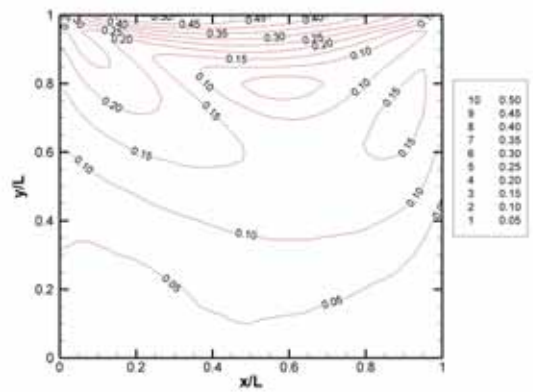
(b)
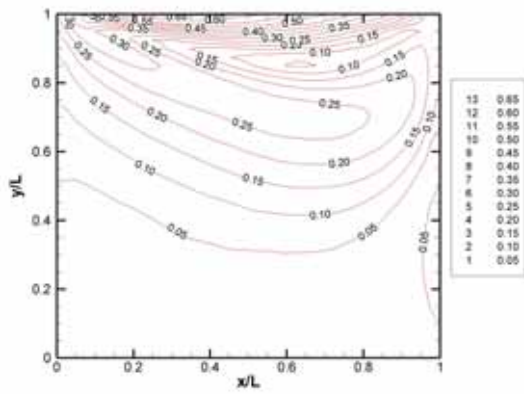
(c)

Fig. 3.29   Contour of Mach number for Kn = 10, (a) M = 1.1; (b) M = 2; (c) M = 4
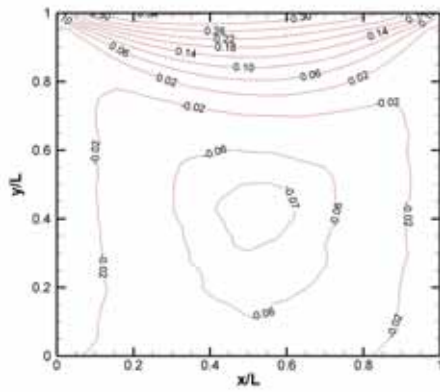
(a)
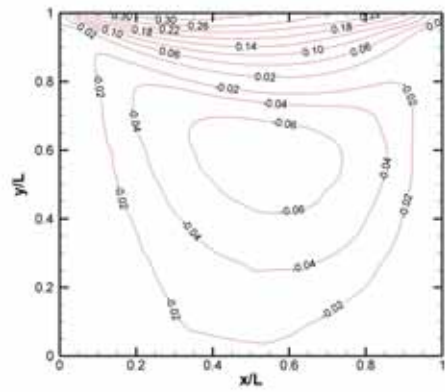
(b)
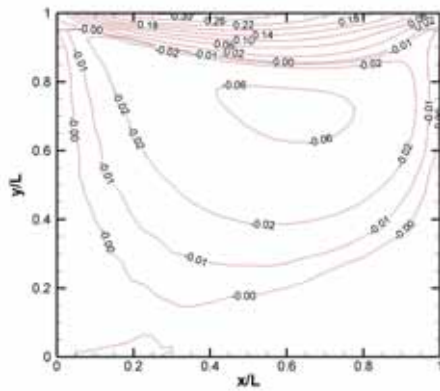
(c)

Fig. 3.30 Contour of u-velocity for Kn = 10, (a) M = 1.1; (b) M = 2; (c) M = 4
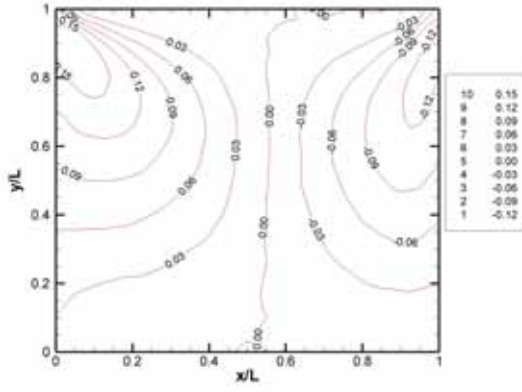
(a)
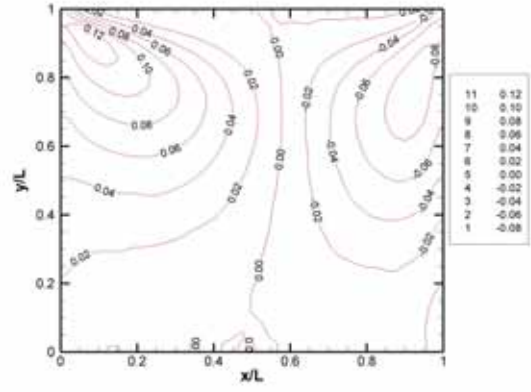
(b)
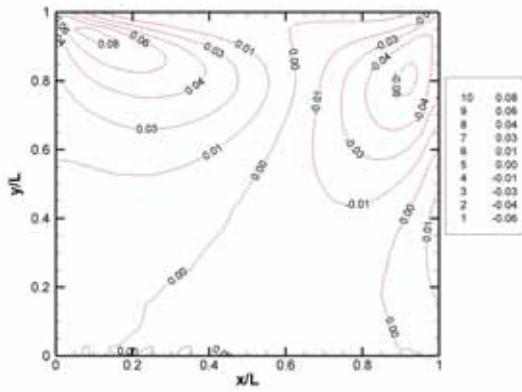
(c)

Fig. 3.31   Contour of v-velocity for Kn = 10, (a) M = 1.1; (b) M = 2; (c) M = 4
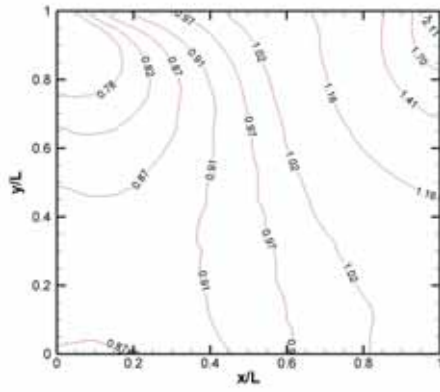
(a)
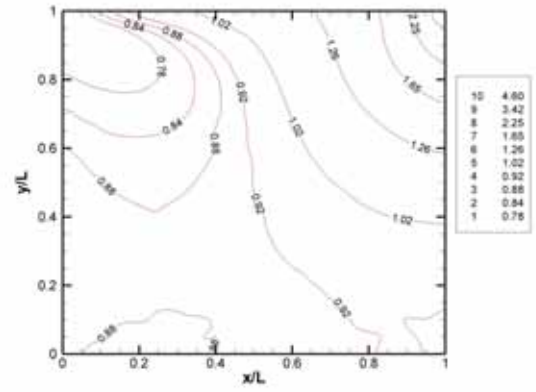
(b)
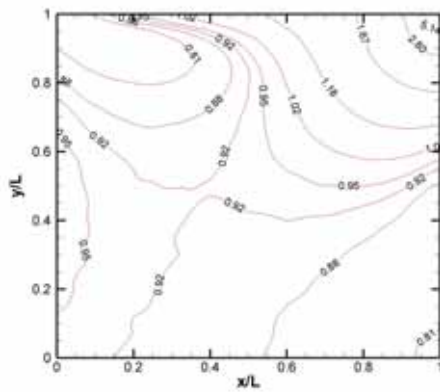
(c)

Fig. 3.32　　Contour of number density for Kn = 1, (a) M = 1.1; (b) M = 2; (c) M = 4
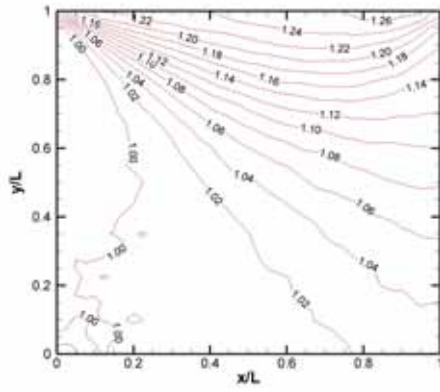
(a)
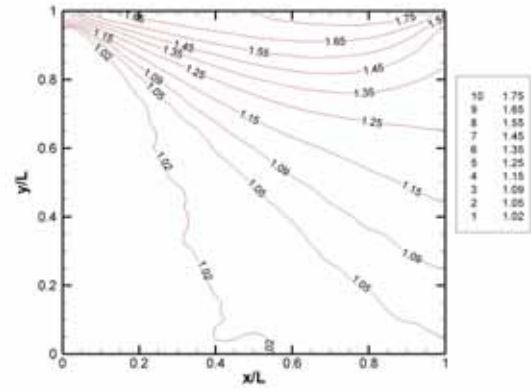
(b)
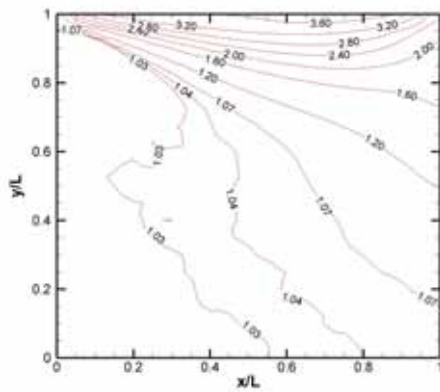
(c)

Fig. 3.33   Contour of temperature for Kn = 1, (a) M = 1.1; (b) M = 2; (c) M = 4
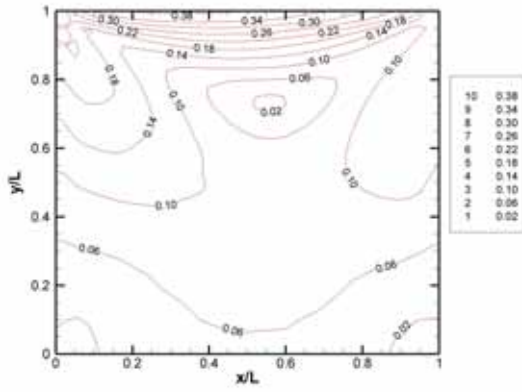
(a)
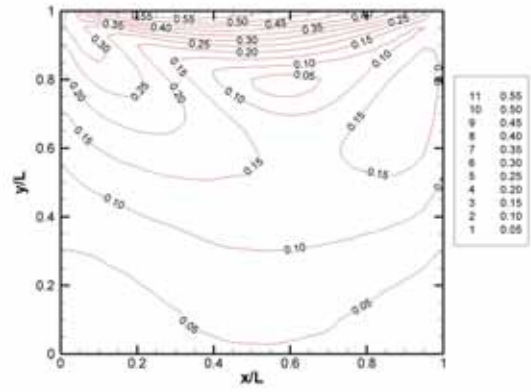
(b)
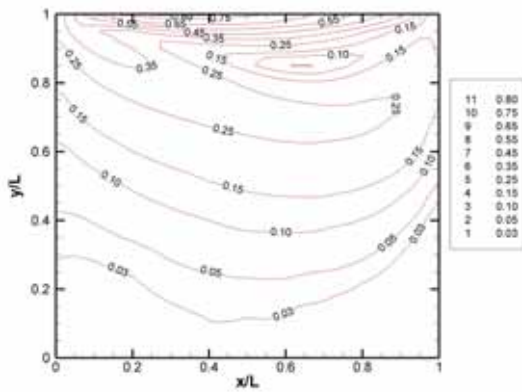
(c)

Fig. 3.34   Contour of Mach number for Kn = 1, (a) M = 1.1; (b) M = 2; (c) M = 4
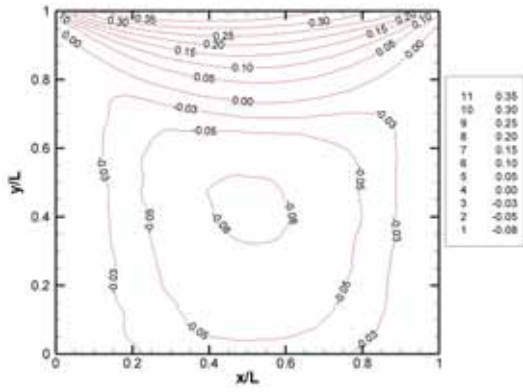
(a)
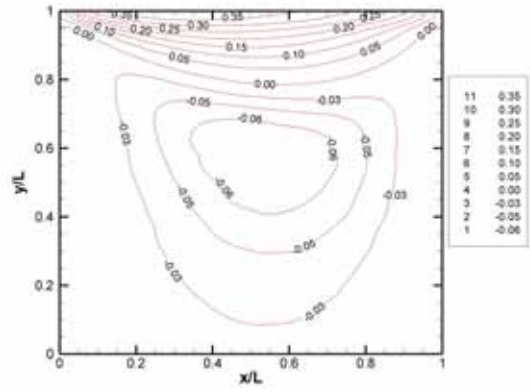
(b)
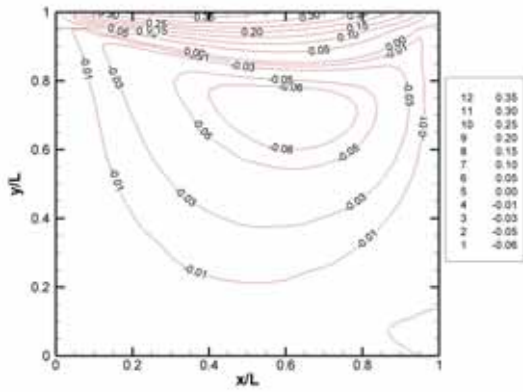
(c)

Fig. 3.35   Contour of u-velocity for Kn = 1, (a) M = 1.1; (b) M = 2; (c) M = 4
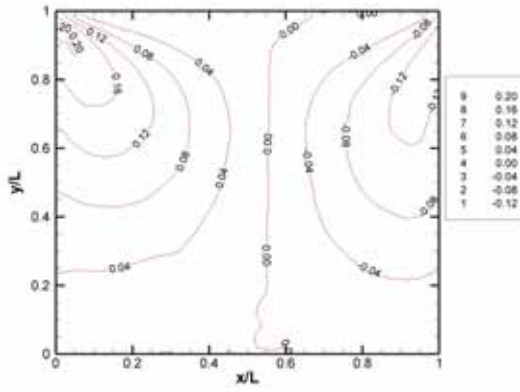
(a)
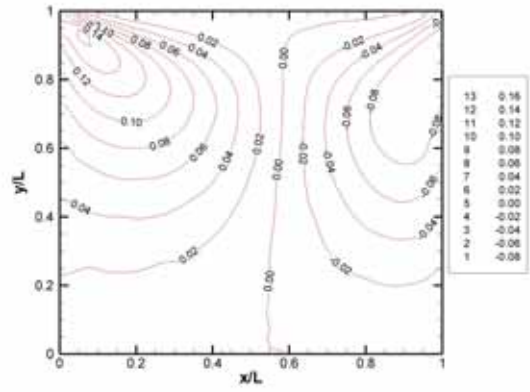
(b)
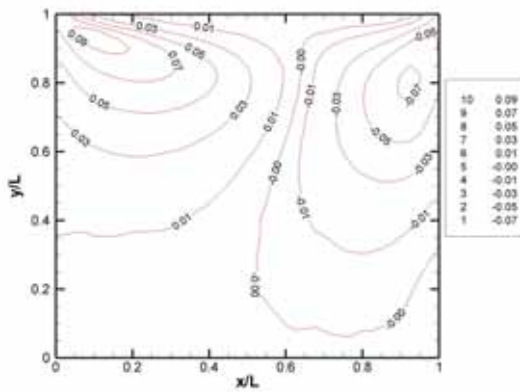
(c)

Fig. 3.36 Contour of v-velocity for Kn = 1, (a) M = 1.1; (b) M = 2; (c) M = 4
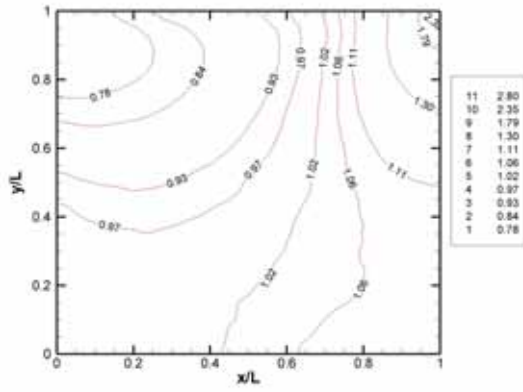
(a)
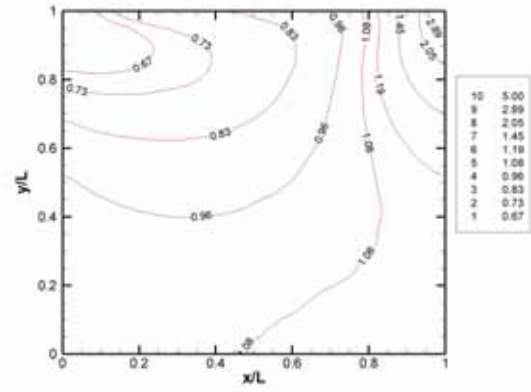
(b)
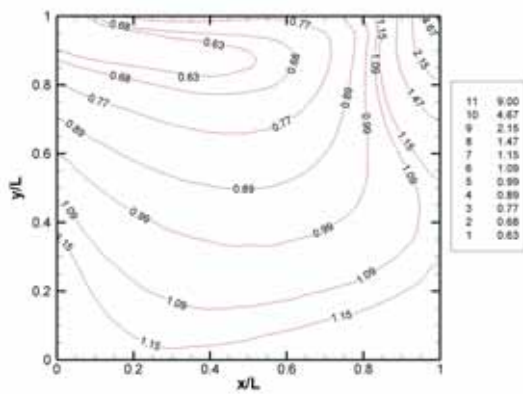
(c)

Fig. 3.37   Contour of number density for Kn = 0.1, (a) M = 1.1; (b) M = 2; (c) M = 4
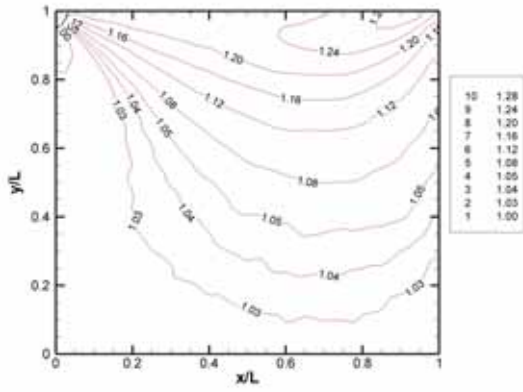
(a)
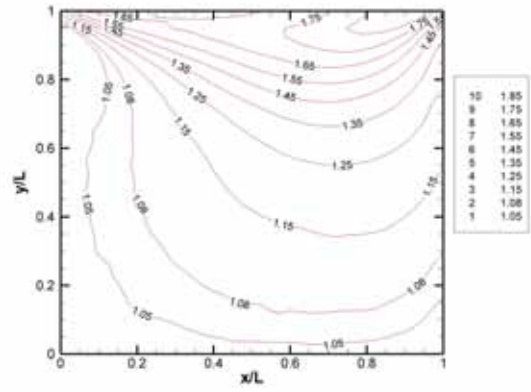
(b)
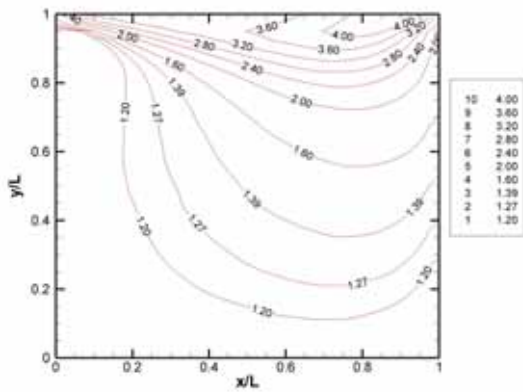
(c)

Fig. 3.38   Contour of temperature for Kn = 0.1, (a) M = 1.1; (b) M = 2; (c) M = 4
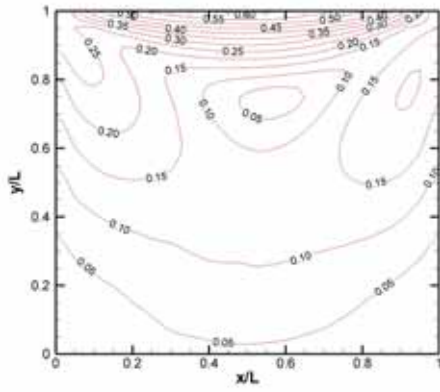
(a)
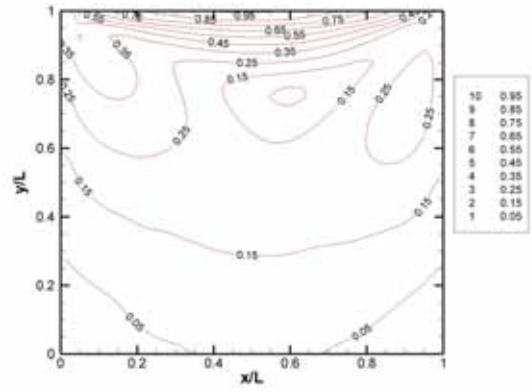
(b)
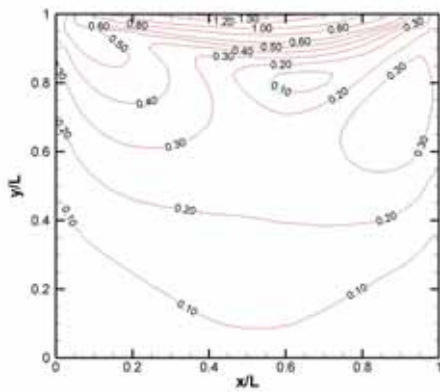
(c)

Fig. 3.39   Contour of Mach number for Kn = 0.1, (a) M = 1.1; (b) M = 2; (c) M = 4
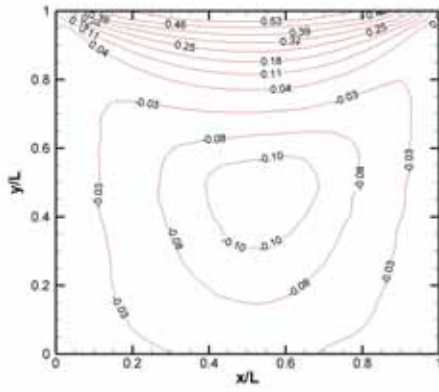
(a)
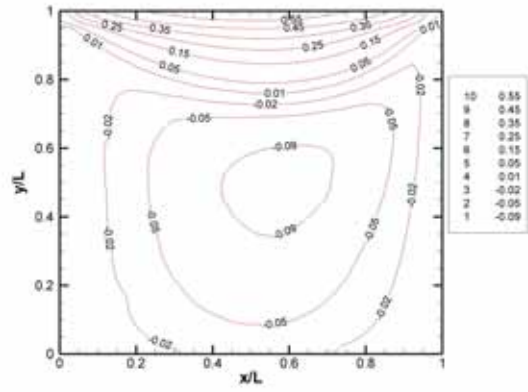
(b)
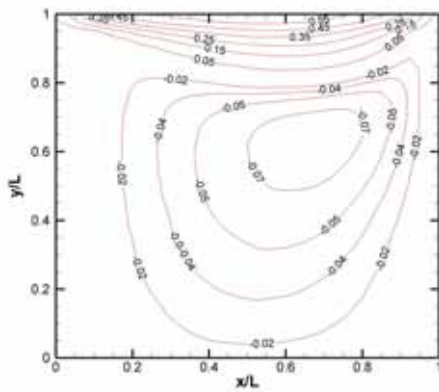
(c)

Fig. 3.40 Contour of u-velocity for Kn = 0.1, (a) M = 1.1; (b) M = 2; (c) M = 4
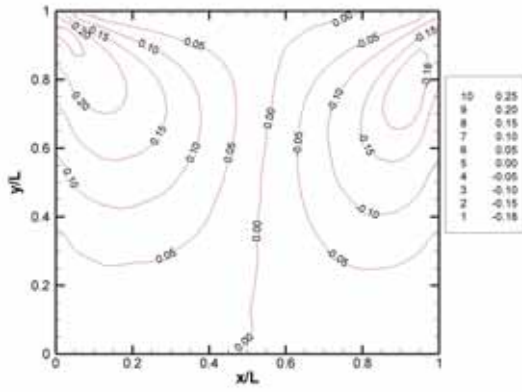
(a)
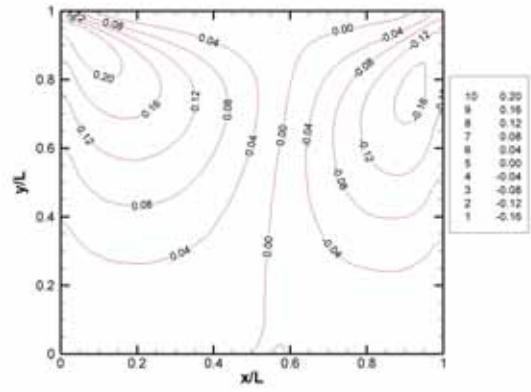
(b)
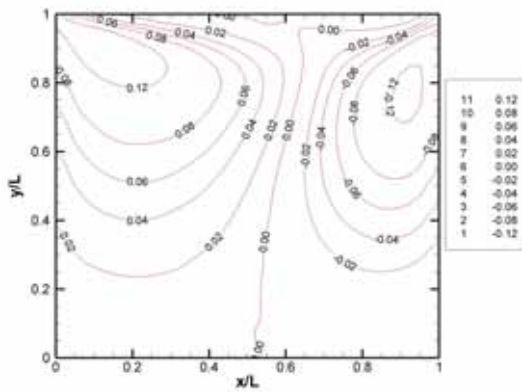
(c)

Fig. 3.41   Contour of v-velocity for Kn = 0.1, (a) M = 1.1; (b) M = 2; (c) M = 4
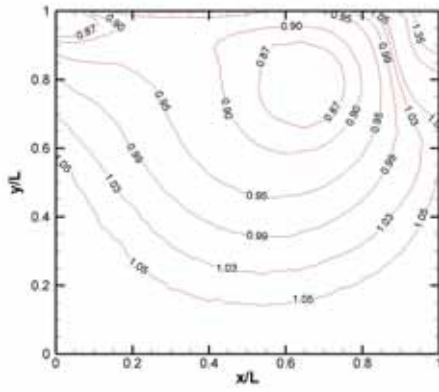
(a)
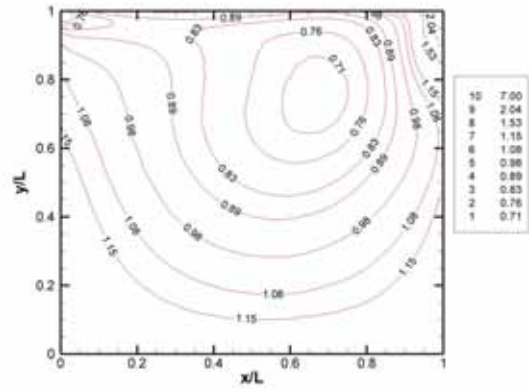
(b)
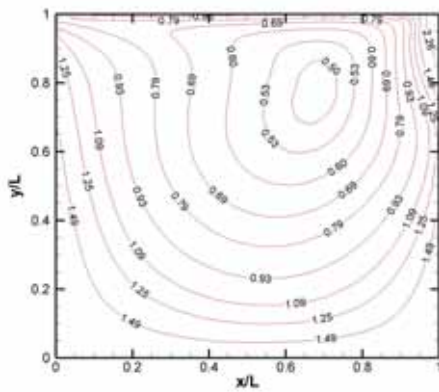
(c)

Fig. 3.42 Contour of number density for Kn = 0.01, (a) M = 1.1; (b) M = 2; (c) M = 4
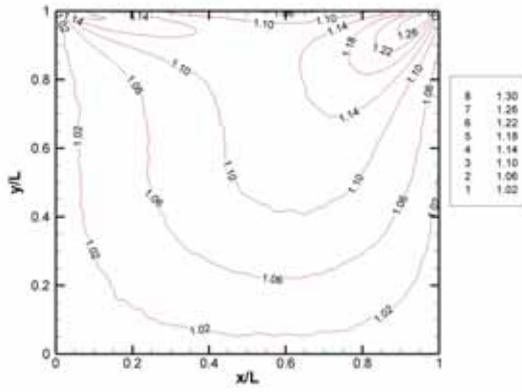
(a)
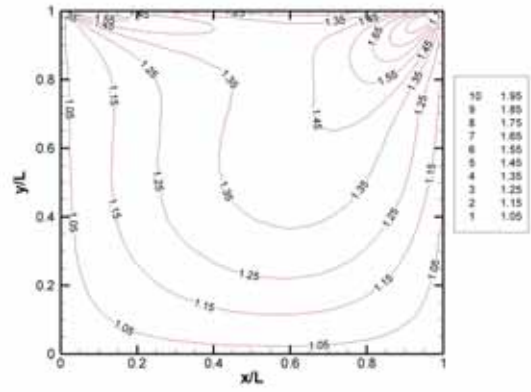
(b)
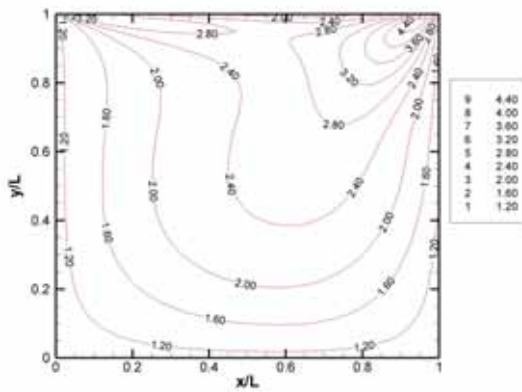
(c)

Fig. 3.43 Contour of temperature for Kn = 0.01, (a) M = 1.1; (b) M = 2; (c) M = 4
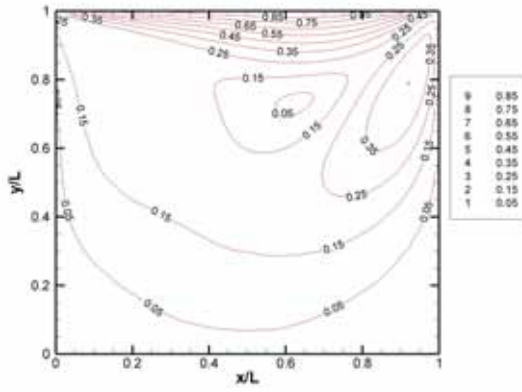
(a)
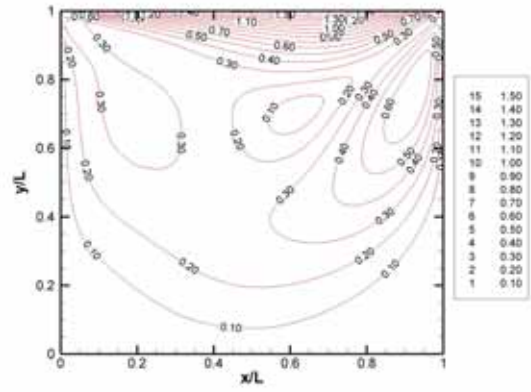
(b)
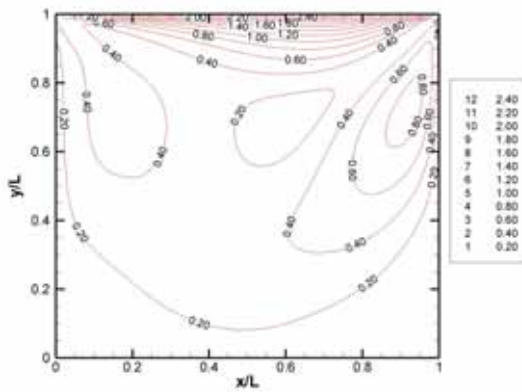
(c)

Fig. 3.44 Contour of Mach number for Kn = 0.01, (a) M = 1.1; (b) M = 2; (c) M = 4
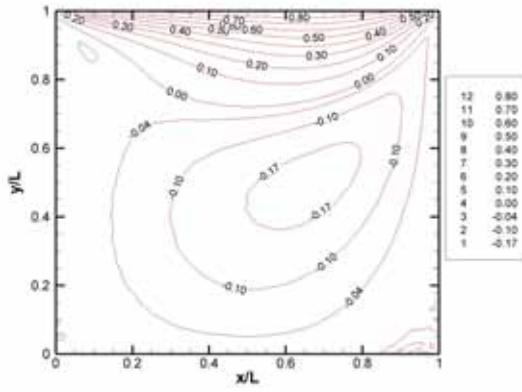
(a)
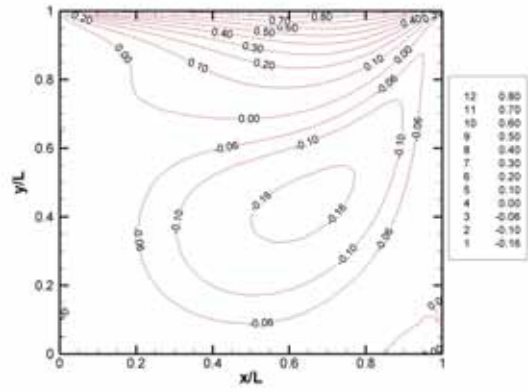
(b)
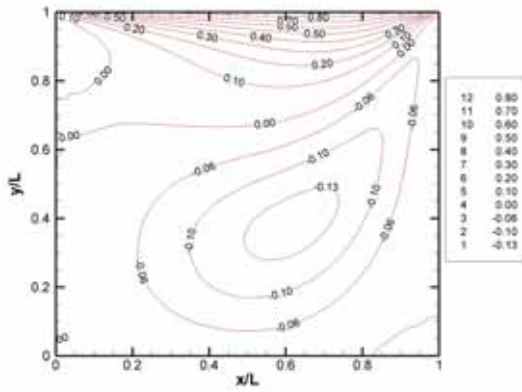
(c)

Fig. 3.45   Contour of u-velocity for Kn = 0.01, (a) M = 1.1; (b) M = 2; (c) M = 4
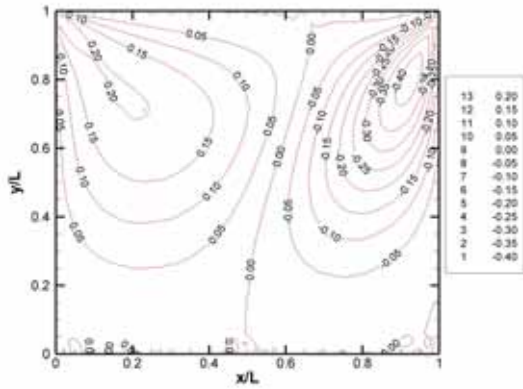
(a)
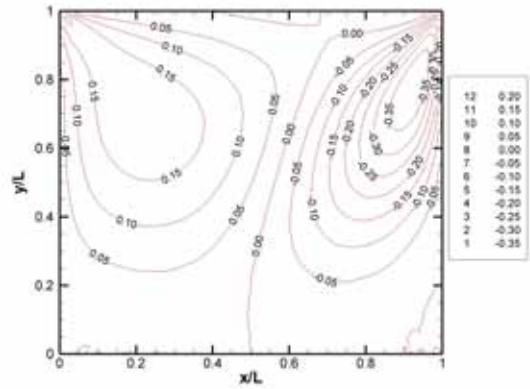
(b)
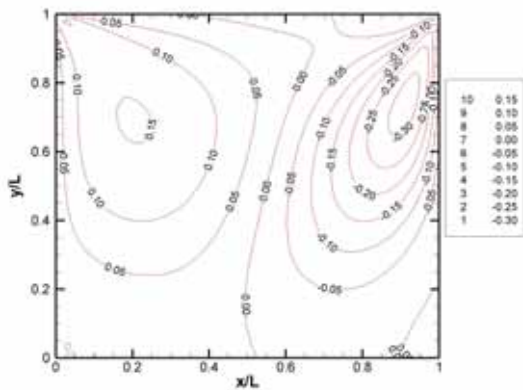
(c)

Fig. 3.46   Contour of v-velocity for Kn = 0.01, (a) M = 1.1; (b) M = 2; (c) M = 4
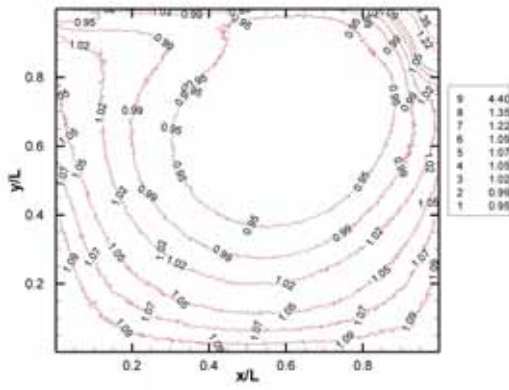
(a)
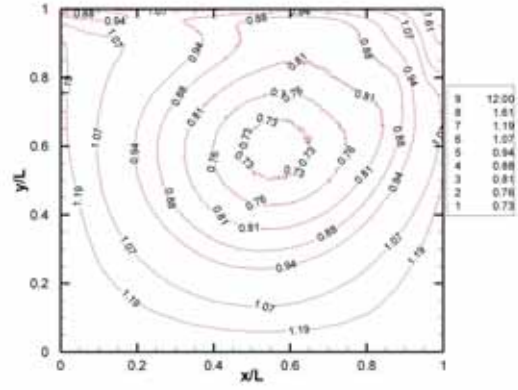
(b)
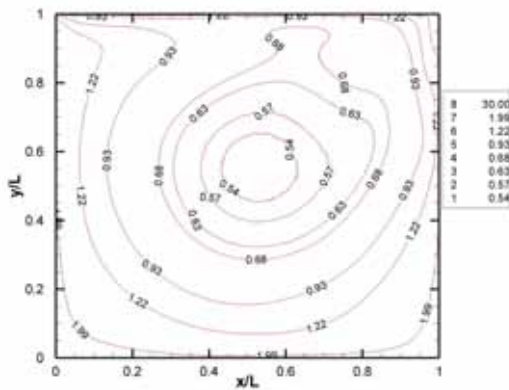
(c)

Fig. 3.47   Contour of number density for Kn = 0.0033, (a) M = 1.1; (b) M = 2; (c) M = 4
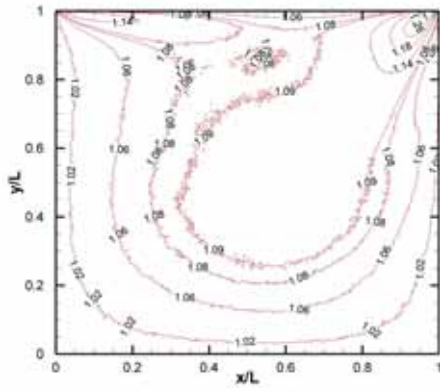
(a)
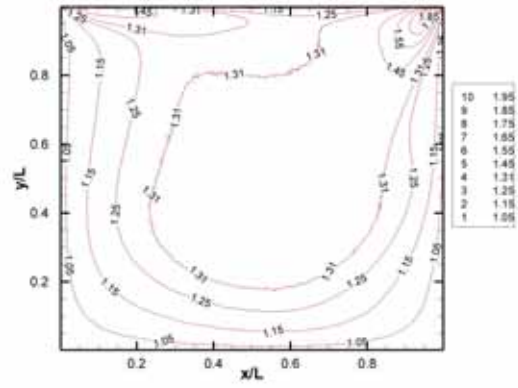
(b)
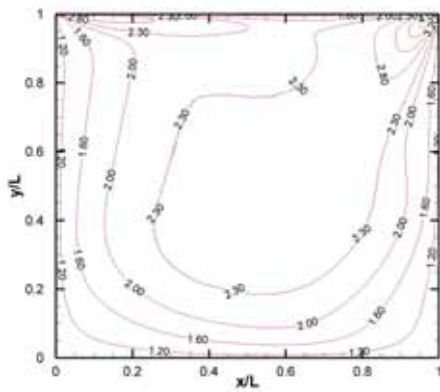
(c)

Fig. 3.48   Contour of temperature for Kn = 0.0033, (a) M = 1.1; (b) M = 2; (c) M = 4
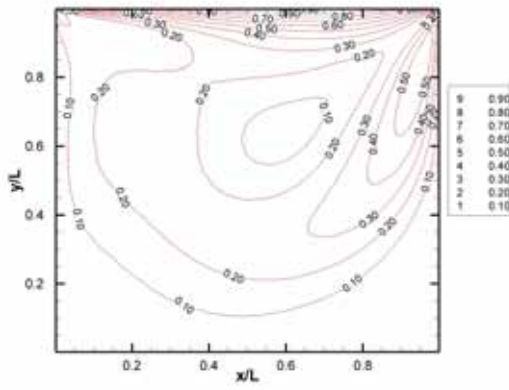
(a)
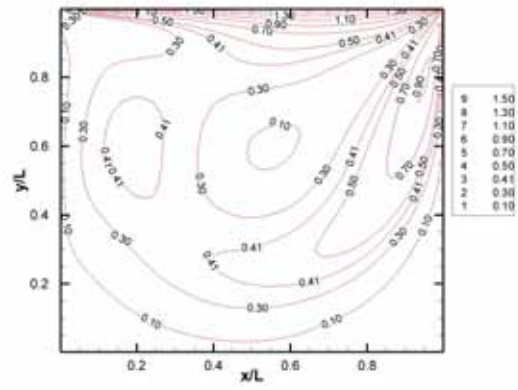
(b)
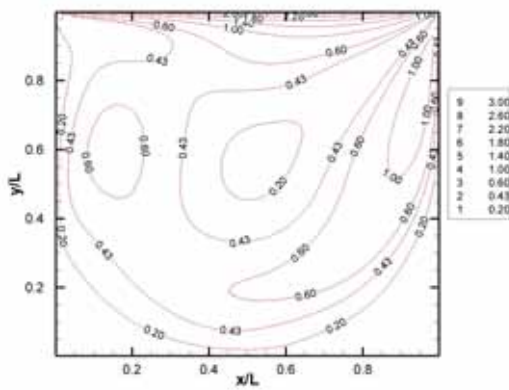
(c)

Fig. 3.49   Contour of Mach number for Kn = 0.0033, (a) M = 1.1; (b) M = 2; (c) M = 4
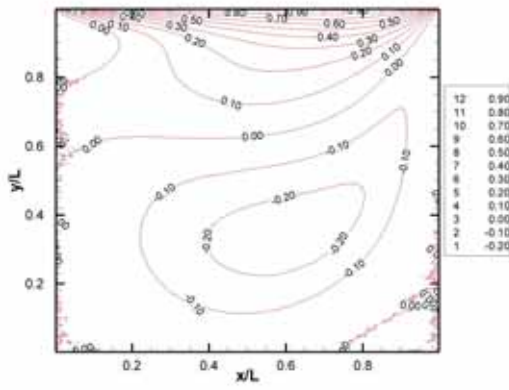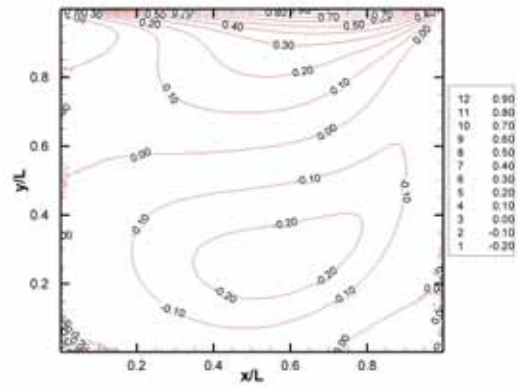
(a)   (b)
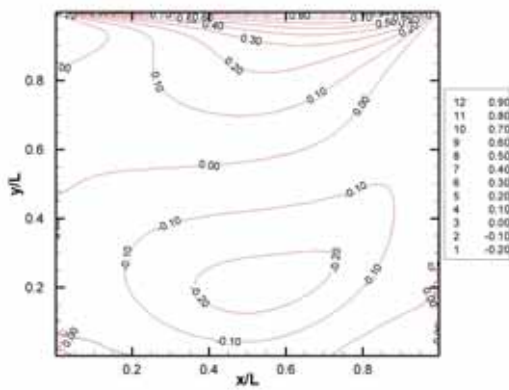
(c)

Fig. 3.50   Contour of u-velocity for Kn = 0.0033, (a) M = 1.1; (b) M = 2; (c) M = 4
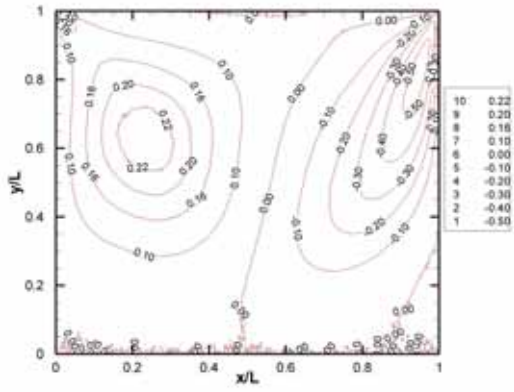
(a)
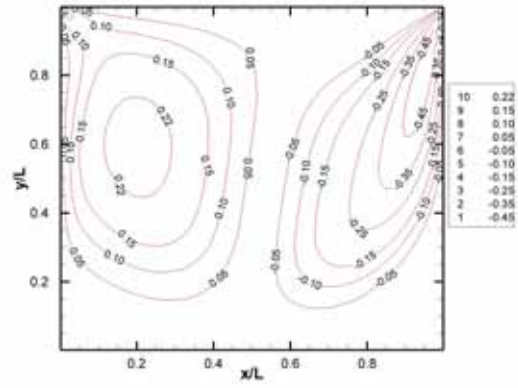
(b)
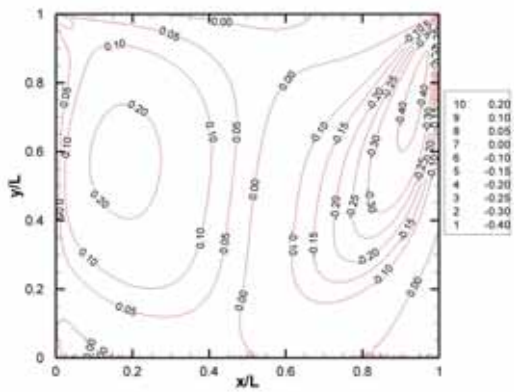
(c)

Fig. 3.51   Contour of v-velocity for Kn = 0.0033, (a) M = 1.1; (b) M = 2; (c) M = 4
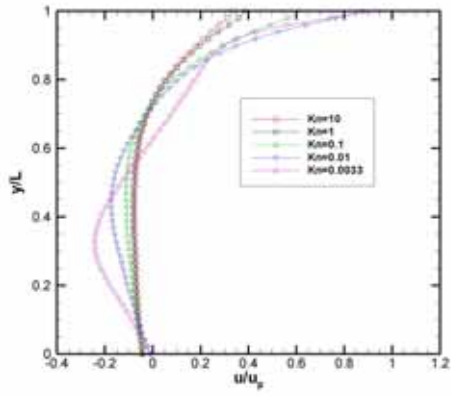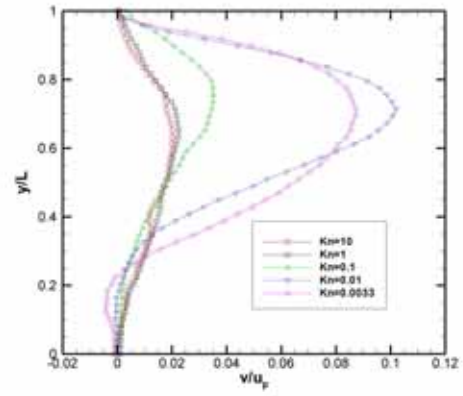
(a)   (b)
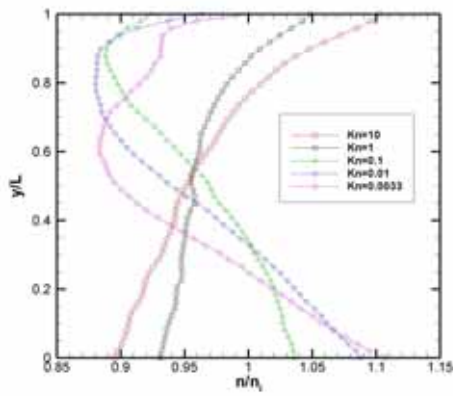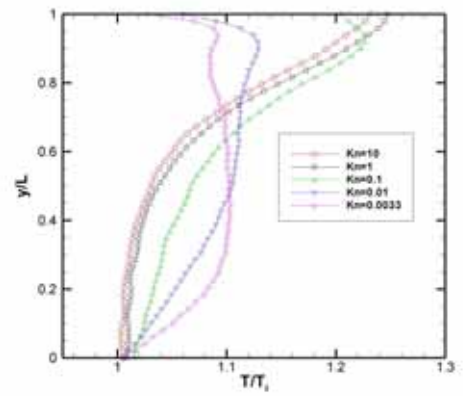
(c)   (d)

Fig. 3.52   Effect of Kn for M = 1.1 along vertical line through geometry center with
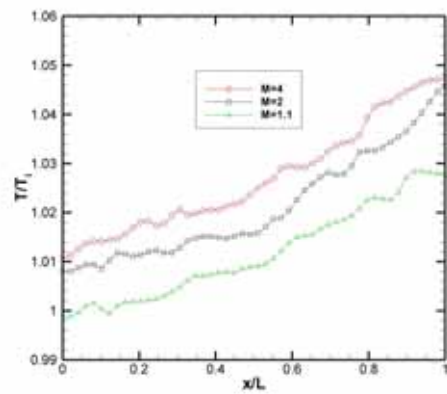
(a) u-velocity; (b) v-velocity; (c) number density (d) temperature
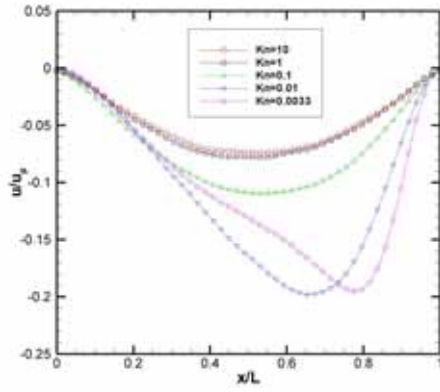
(a)
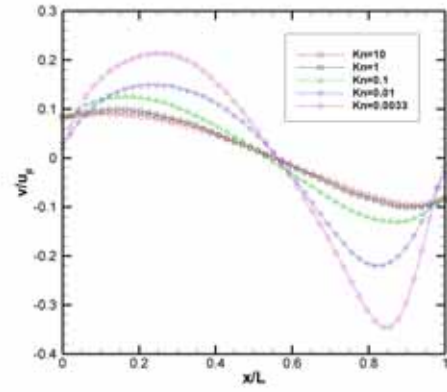
(b)
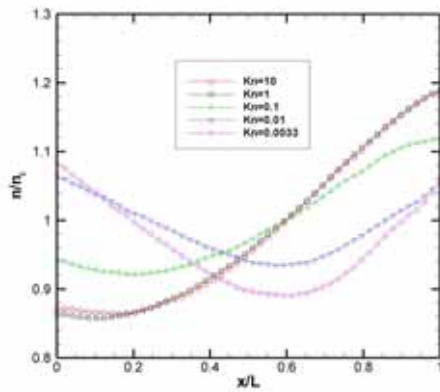
(c)
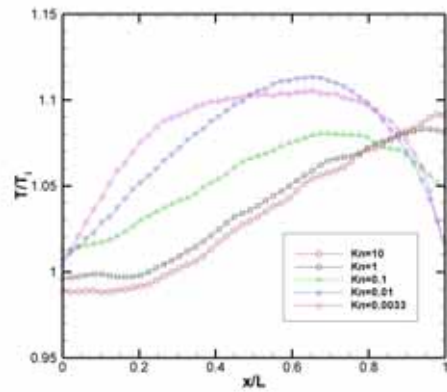
(d)

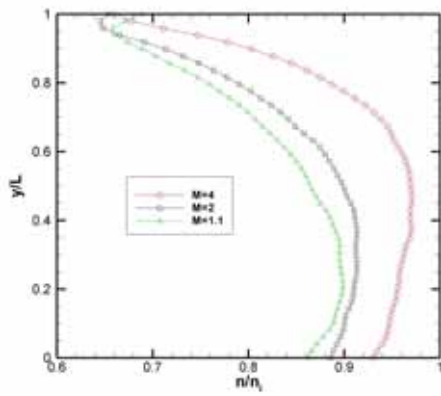**Fig. 3.53** Effect of Kn for M = 1.1 along horizontal line through geometry center with
(a) u-velocity; (b) v-velocity; (c) number density (d) temperature
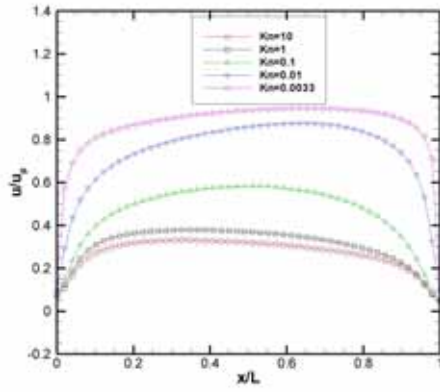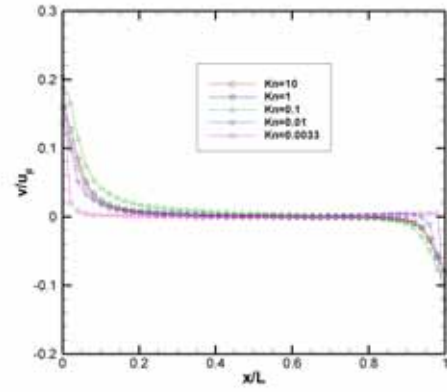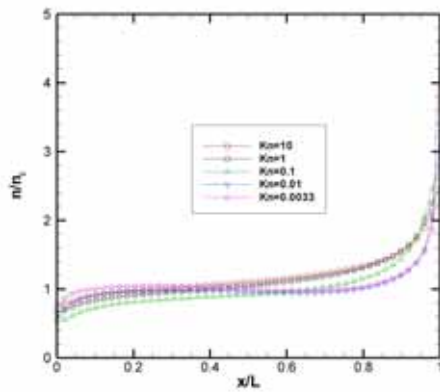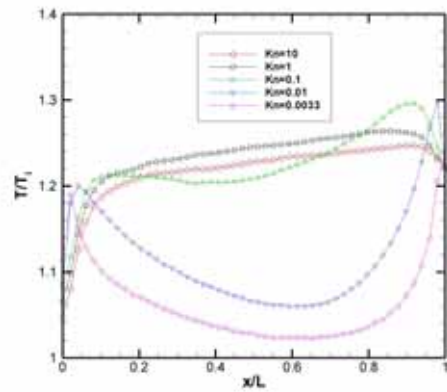
Fig. 3.54   Effect of Kn for M = 1.1 along horizontal line near top wall(y/L=1) with
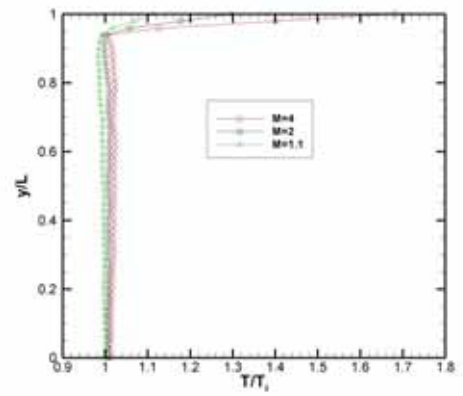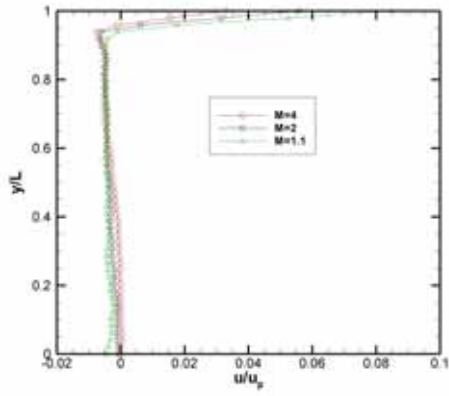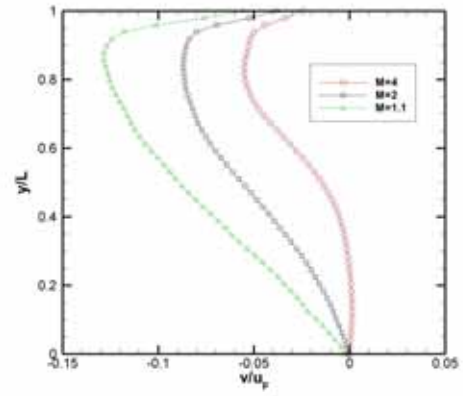(a) u-velocity; (b) v-velocity; (c) number density (d) temperature
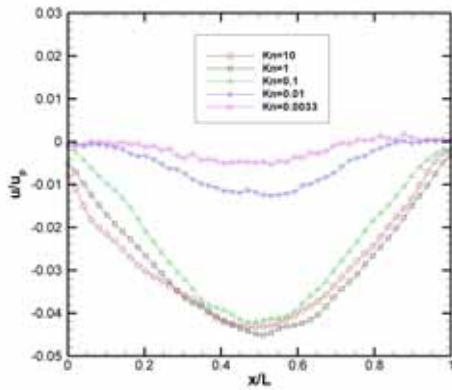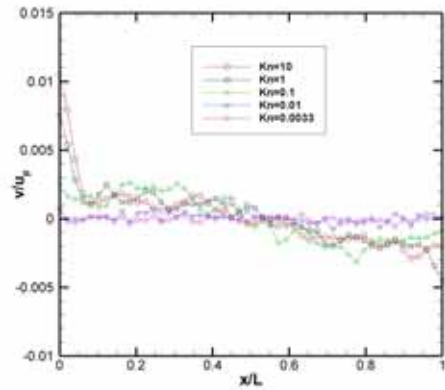
(a)   (b)
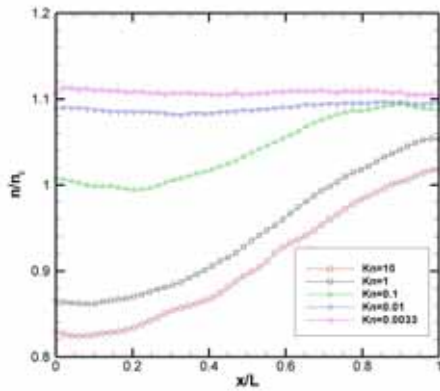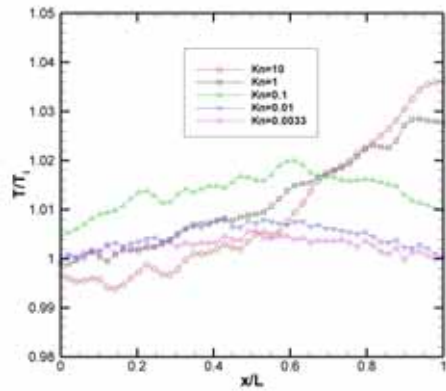
(c)   (d)

Fig. 3.55   Effect of Kn for M = 1.1 along horizontal line near bottom wall(y/L=0) with

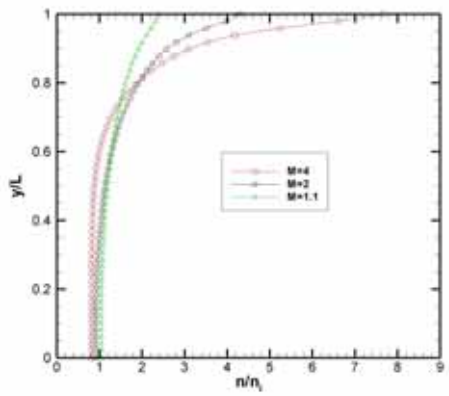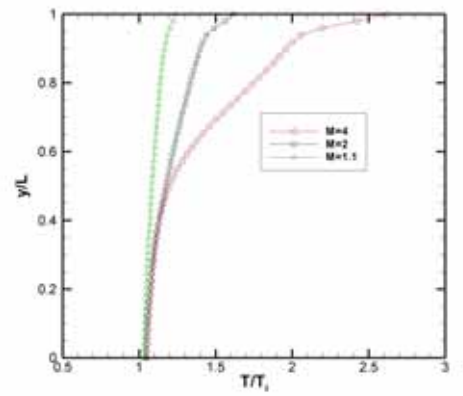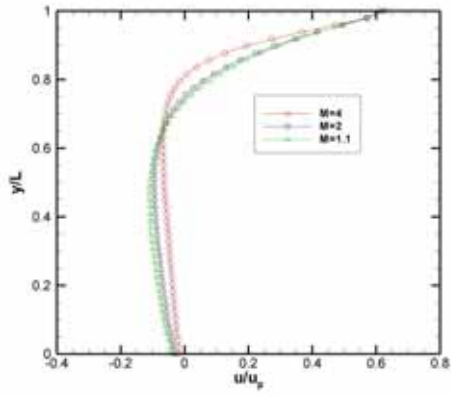(a) u-velocity; (b) v-velocity; (c) number density (d) temperature

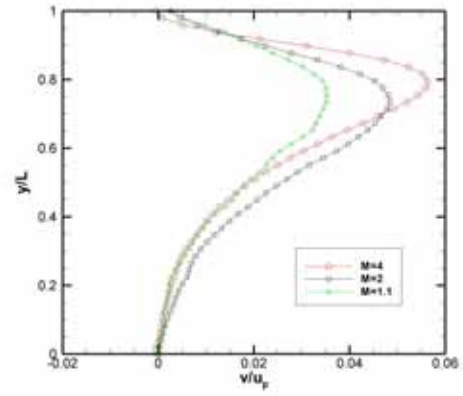(a)   (b)

(c)   (d)
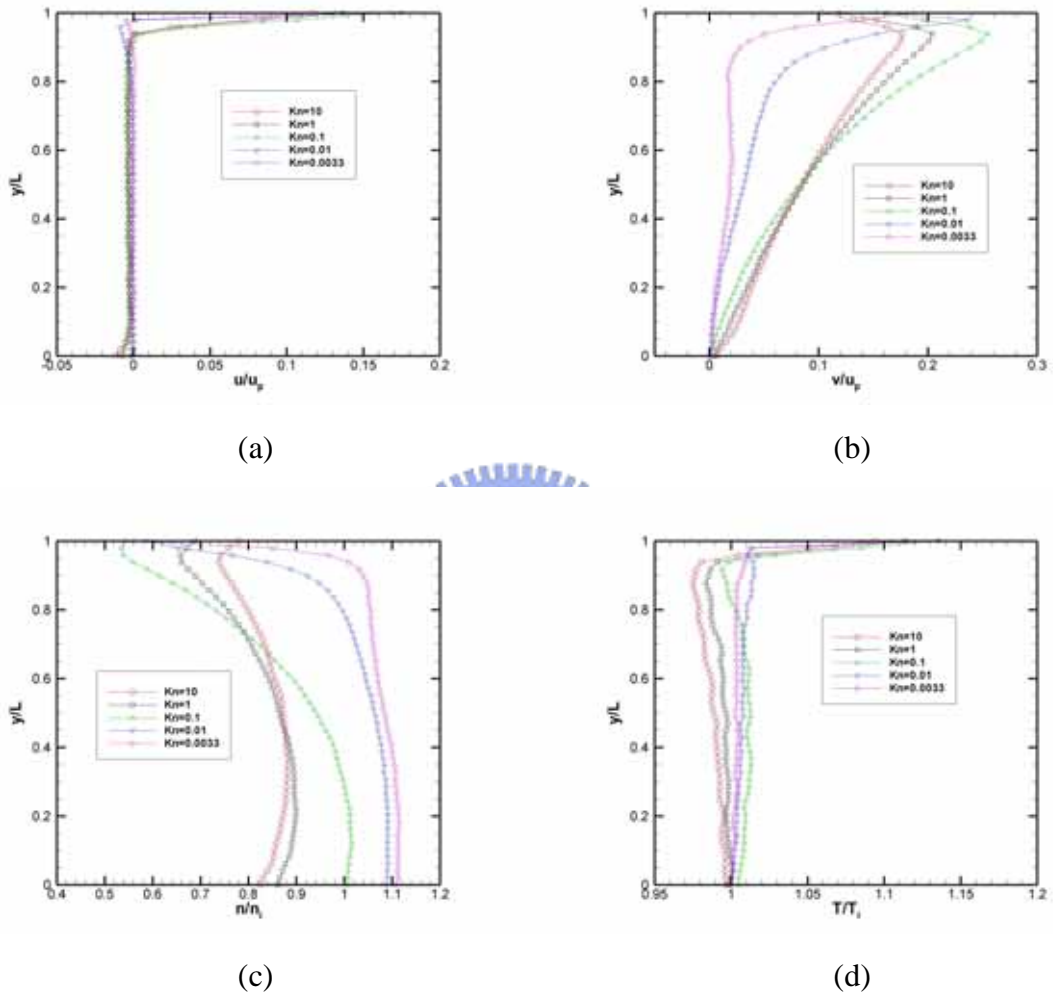
Fig. 3.56   Effect of Kn for M = 1.1 along vertical line near left wall(x/L=0) with
(a) u-velocity; (b) v-velocity; (c) number density (d) temperature
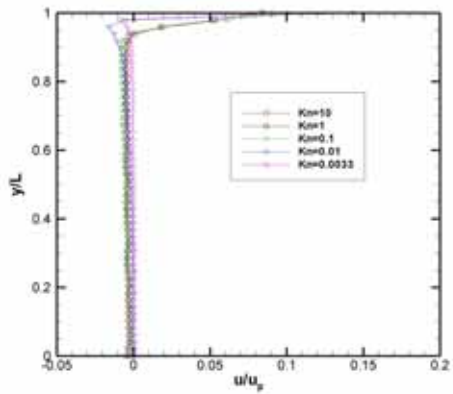
(a)
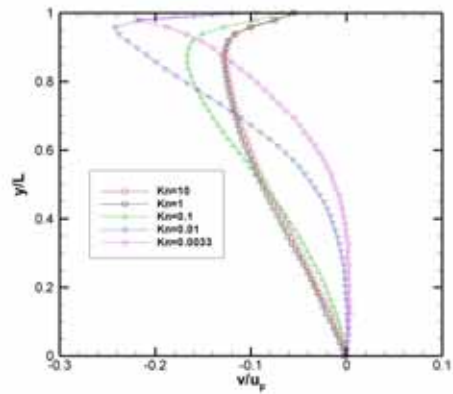
(b)
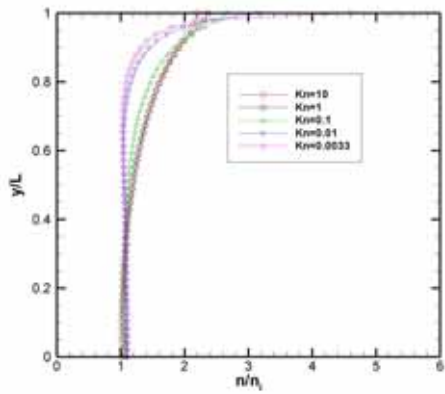
(c)
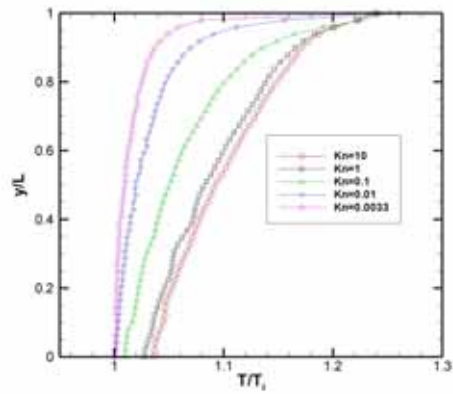
(d)
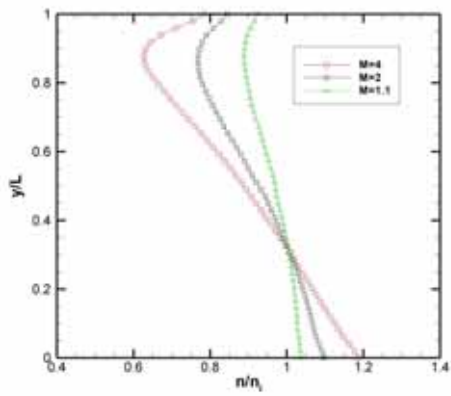
Fig. 3.57 Effect of Kn for M = 1.1 along vertical line near right wall(x/L=1) with (a) u-velocity; (b) v-velocity; (c) number density (d) temperature

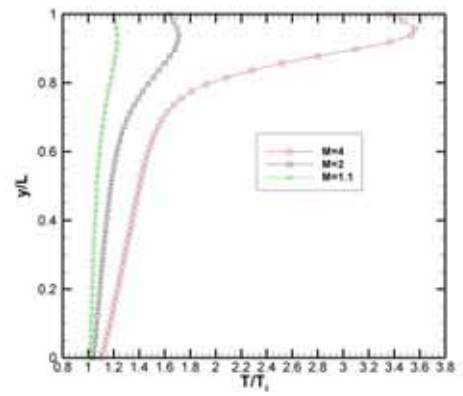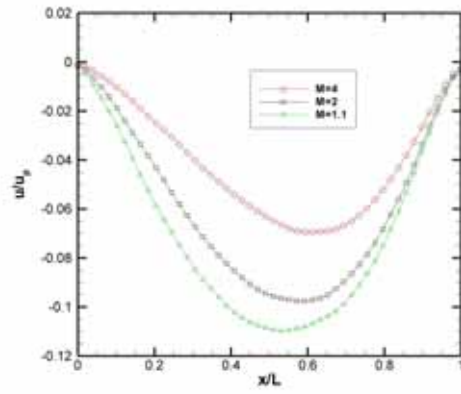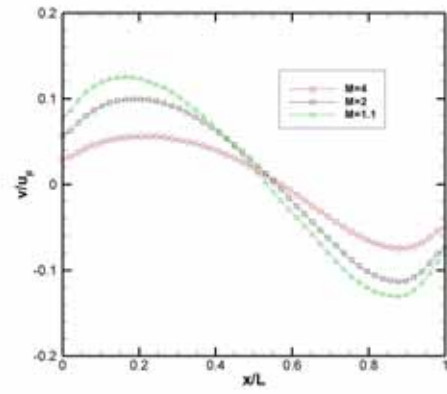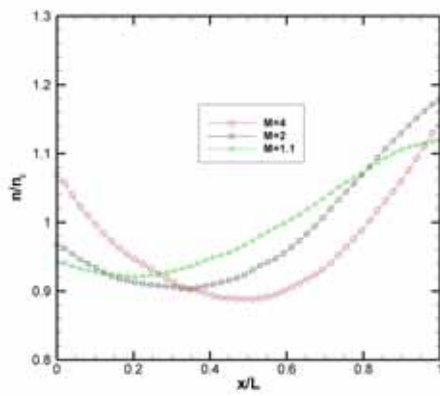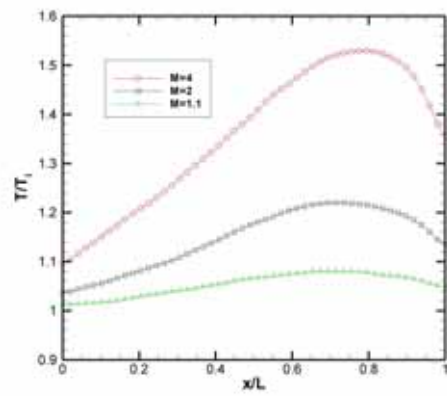(a)   (b)

(c)   (d)
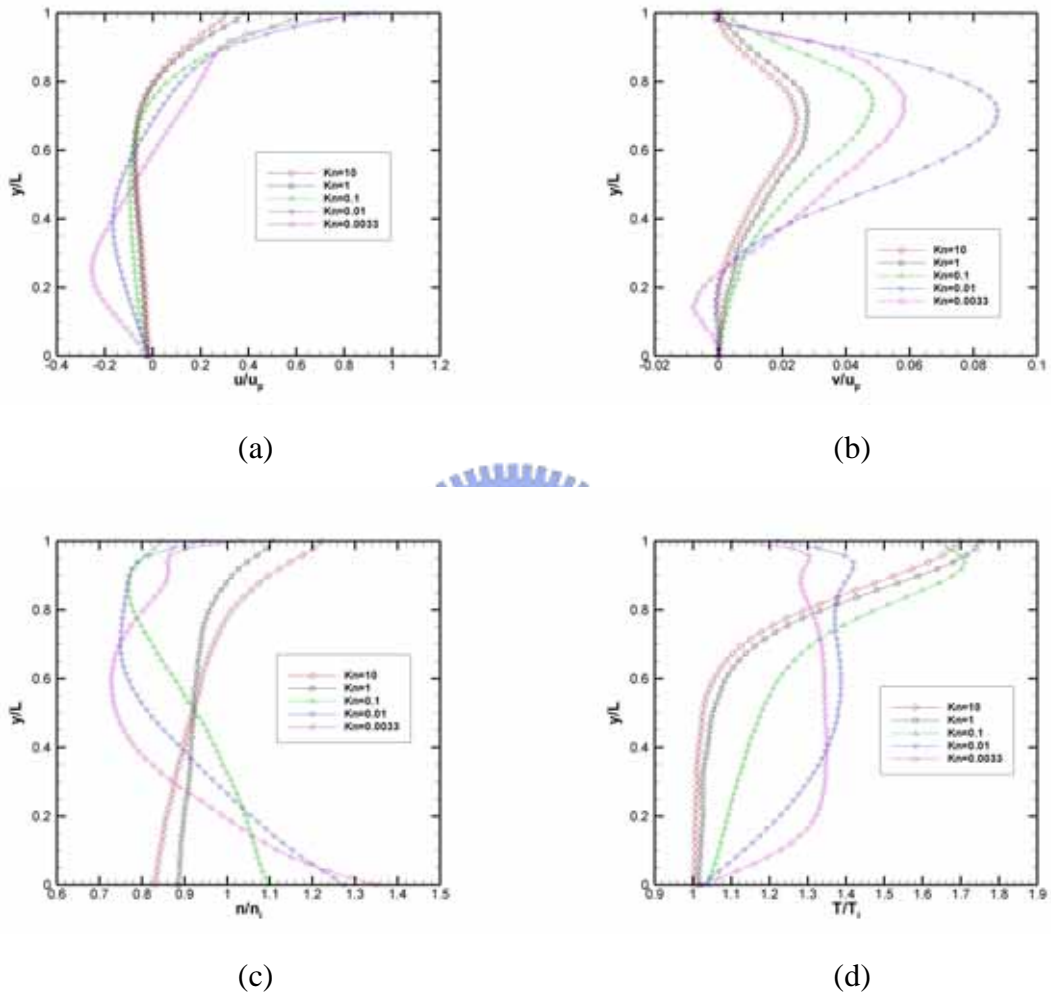
Fig. 3.58   Effect of Kn for M = 2 along vertical line through geometry center with

(a) u-velocity; (b) v-velocity; (c) number density (d) temperature
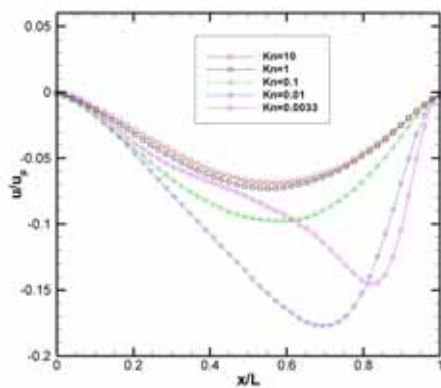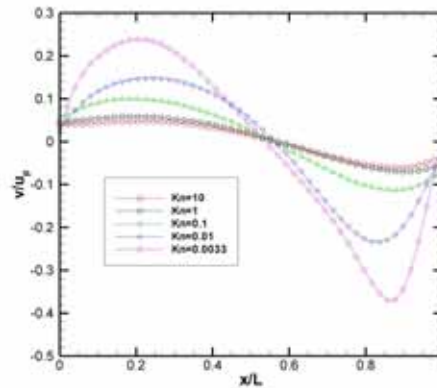
(a)   (b)
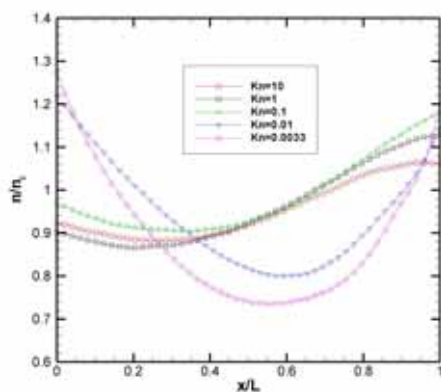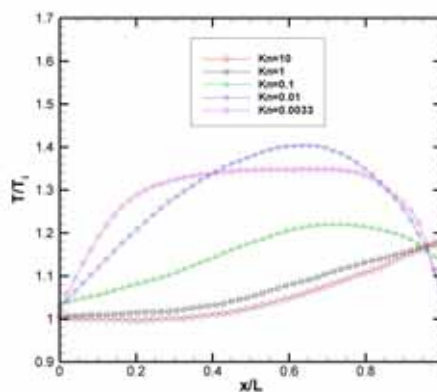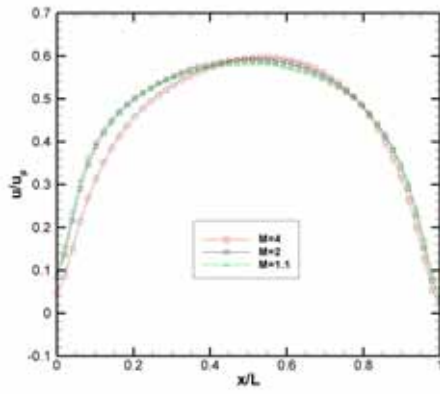
(c)   (d)

Fig. 3.59   Effect of Kn for M = 2 along horizontal line through geometry center with

(a) u-velocity; (b) v-velocity; (c) number density (d) temperature
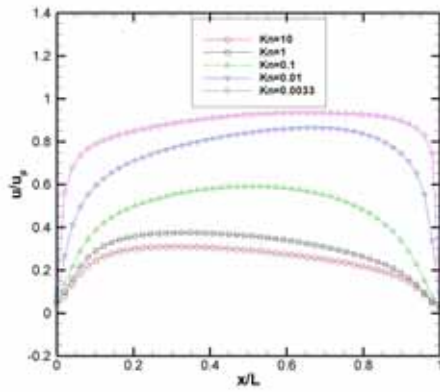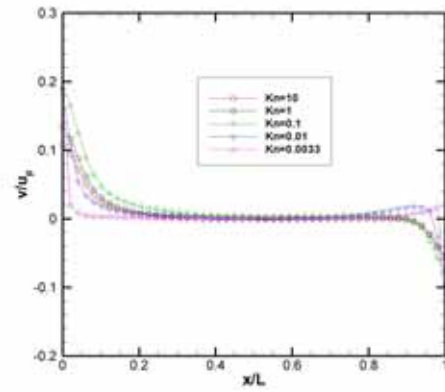
(a)   (b)
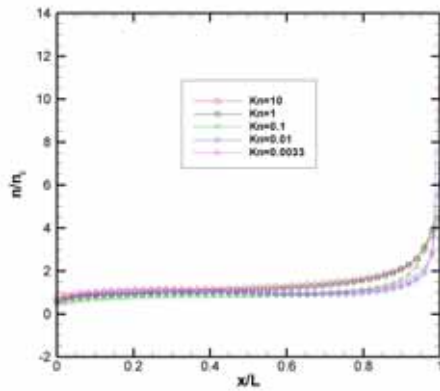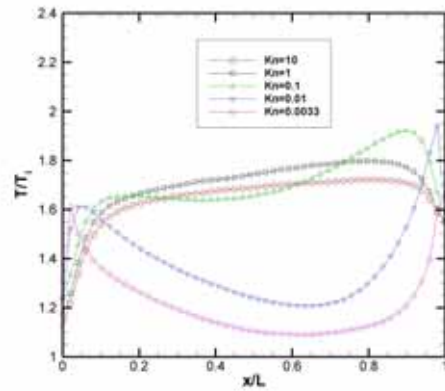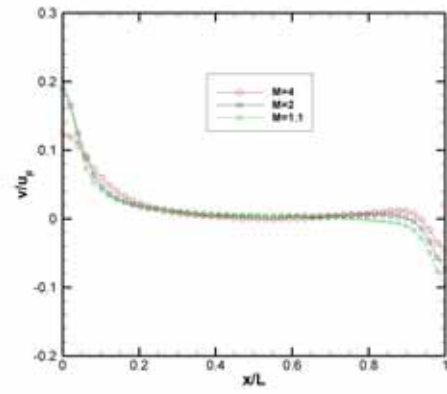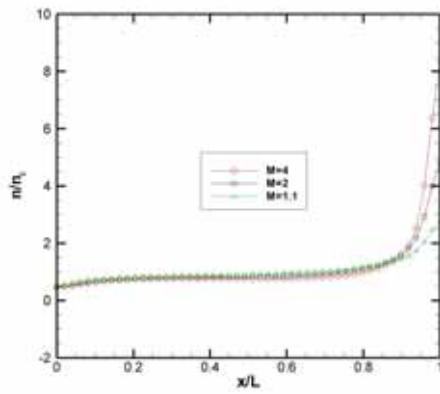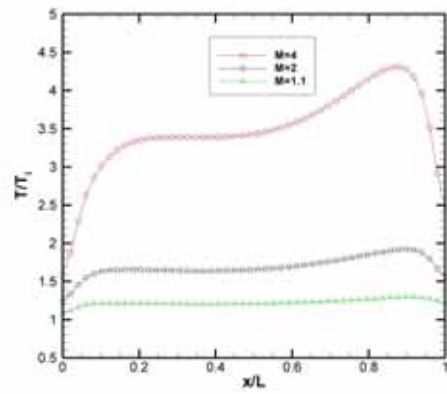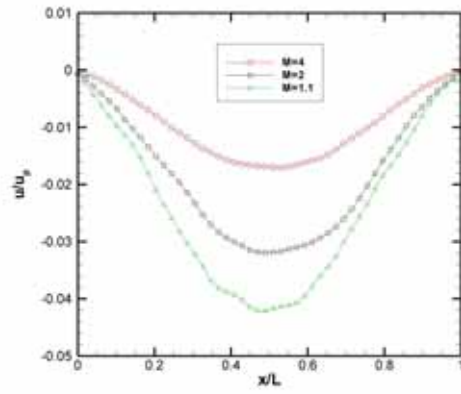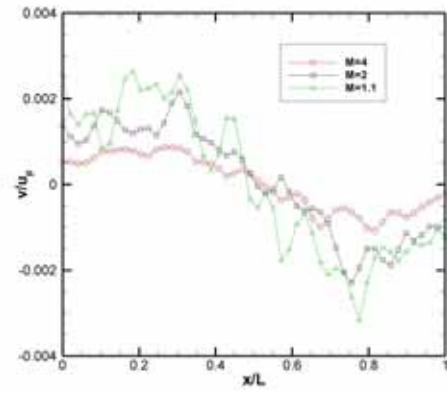

(c)   (d)

Fig. 3.60   Effect of Kn for M = 2 along horizontal line near top wall(y/L=1) with

(a) u-velocity; (b) v-velocity; (c) number density (d) temperature
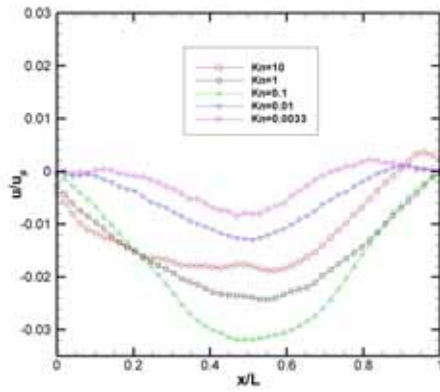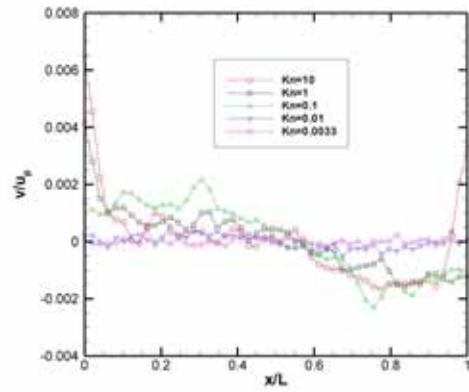
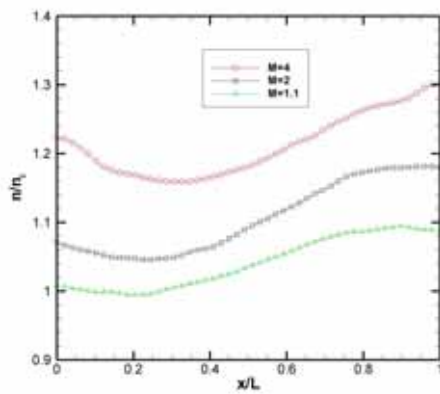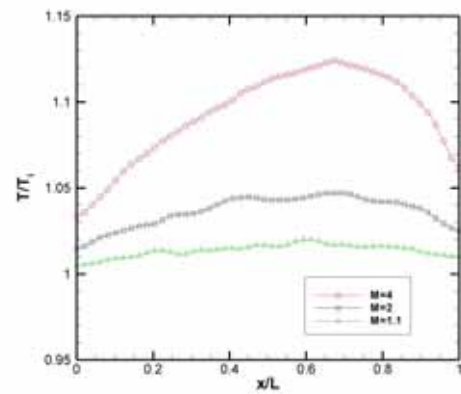(a)   (b)
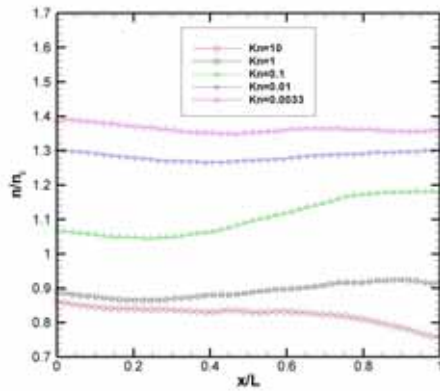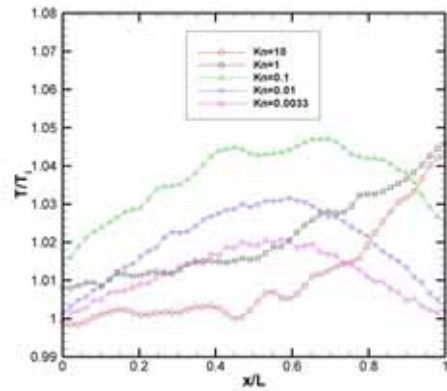
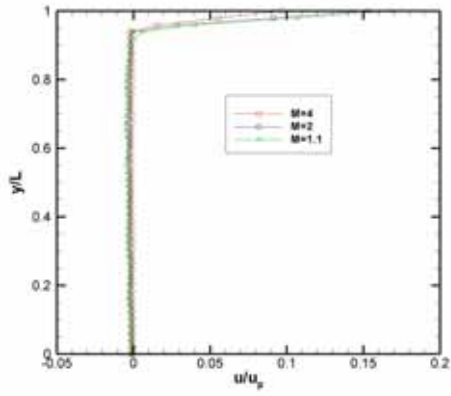(c)   (d)
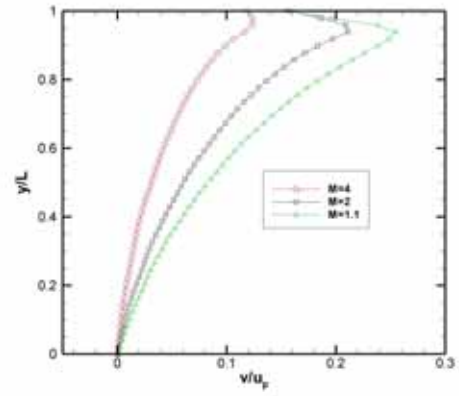
Fig. 3.61   Effect of Kn for M = 2 along horizontal line near bottom wall(y/L=0) with

(a) u-velocity; (b) v-velocity; (c) number density (d) temperature
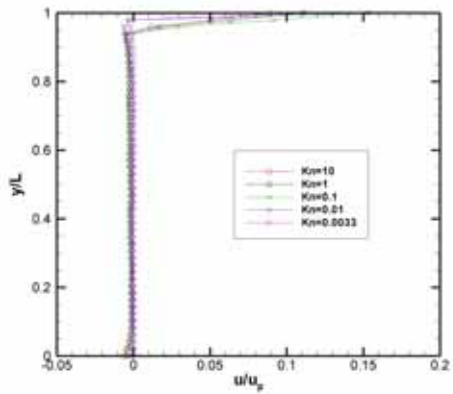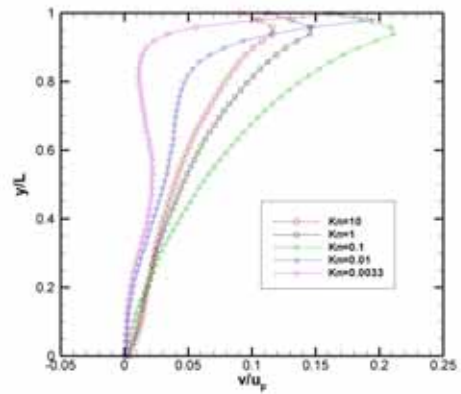
(a)   (b)
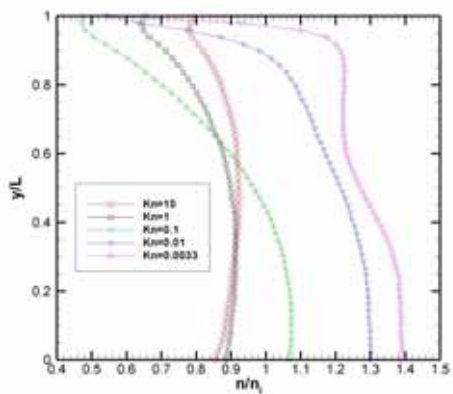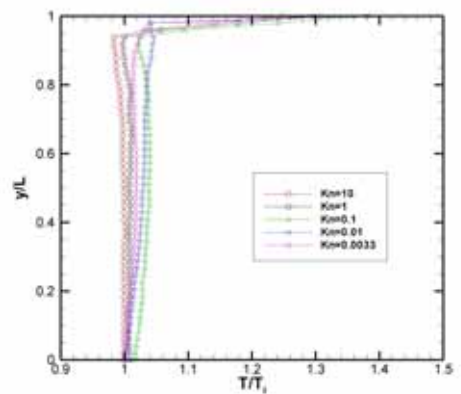
(c)   (d)

Fig. 3.62   Effect of Kn for M = 2 along vertical line near left wall(x/L=0) with

(a) u-velocity; (b) v-velocity; (c) number density (d) temperature
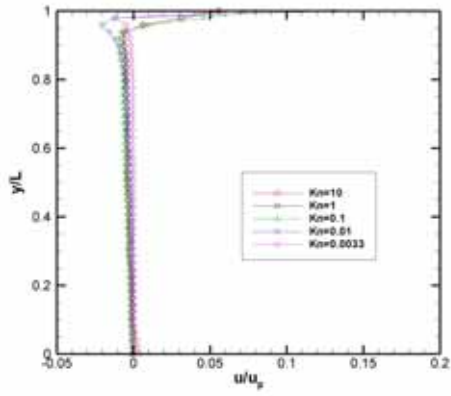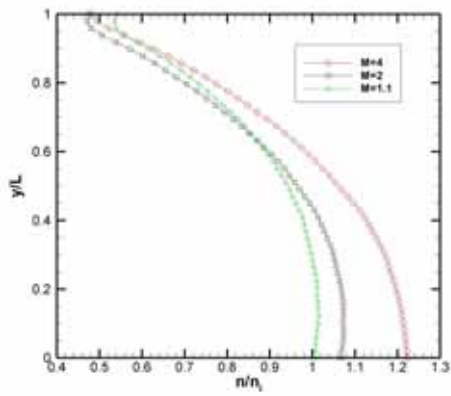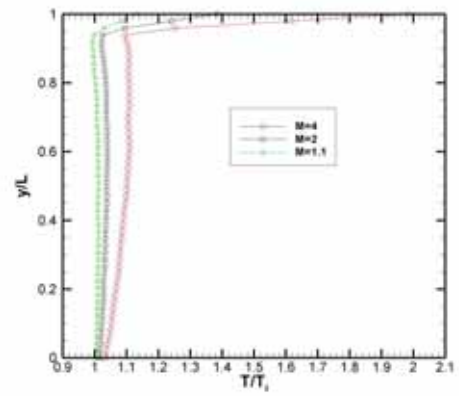
(a)
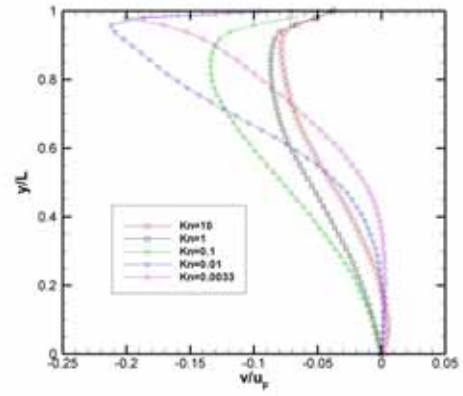
(b)

(c)
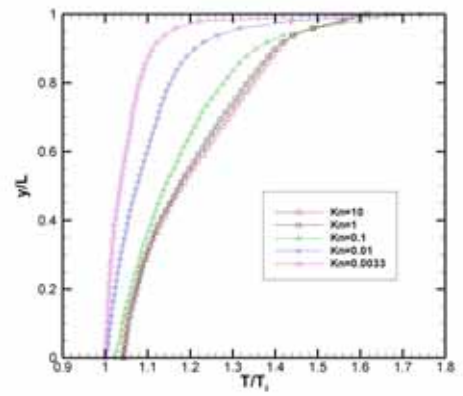
(d)

Fig. 3.63 Effect of Kn for M = 2 along vertical line near right wall(x/L=1) with

(a) u-velocity; (b) v-velocity; (c) number density (d) temperature

110
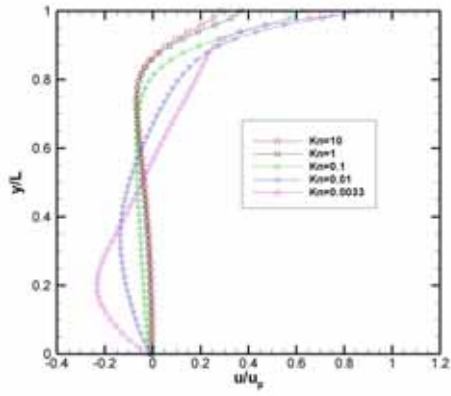
(a)
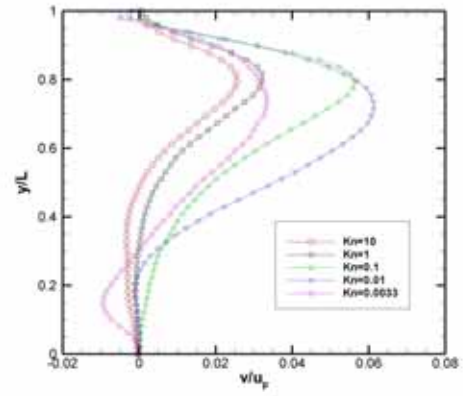
(b)

(c)
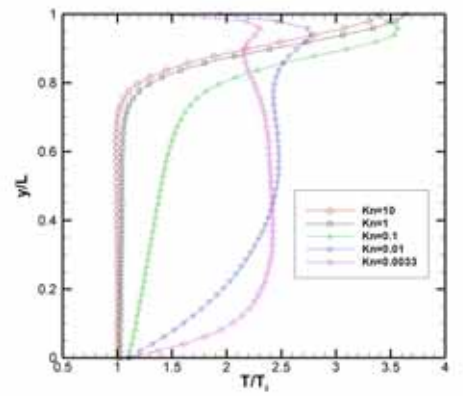
(d)

Fig. 3.64 Effect of Kn for M = 4 along vertical line through geometry center with

(a) u-velocity; (b) v-velocity; (c) number density (d) temperature
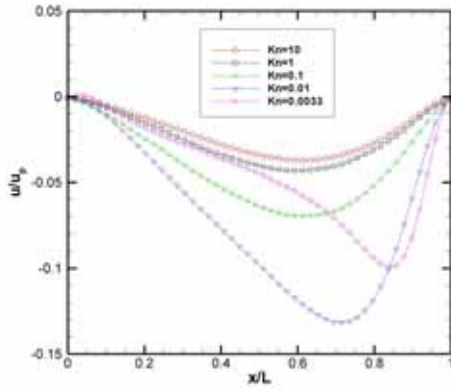
(a)
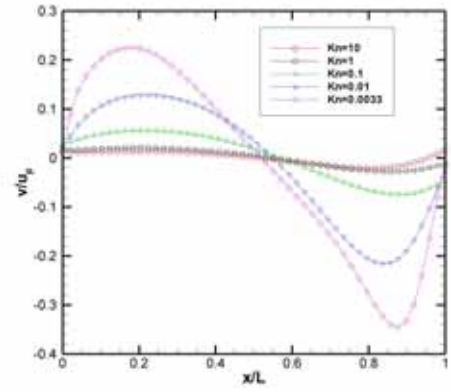
(b)
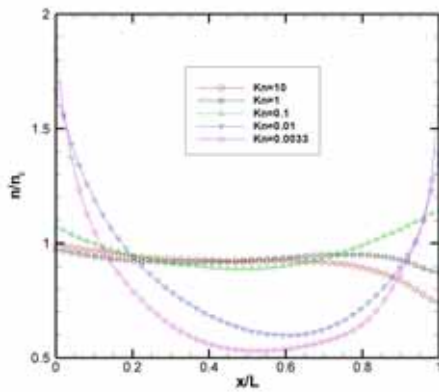
(c)
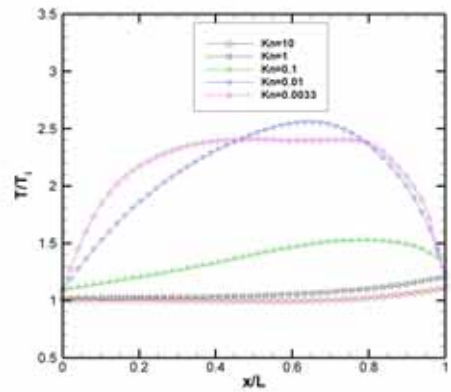
(d)

Fig. 3.65 Effect of Kn for M = 4 along horizontal line through geometry center with (a) u-velocity; (b) v-velocity; (c) number density (d) temperature

112
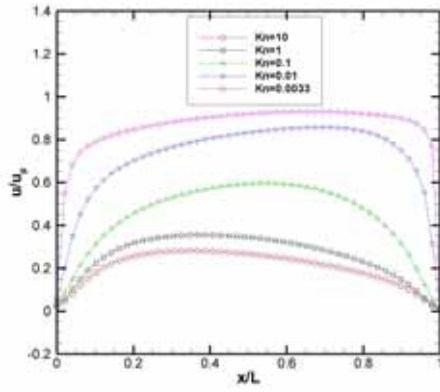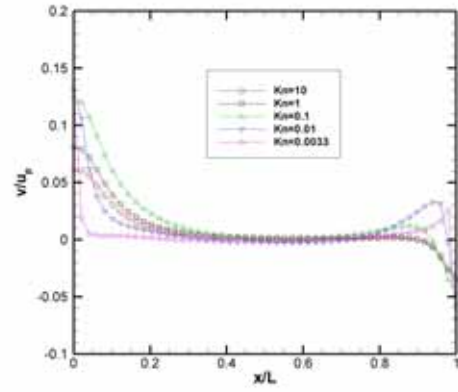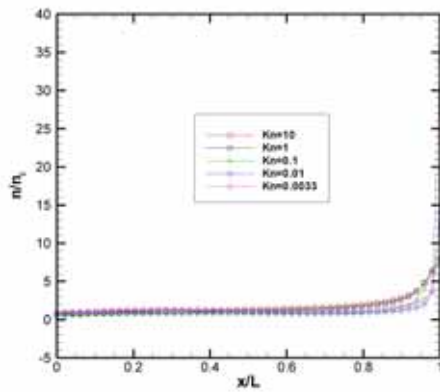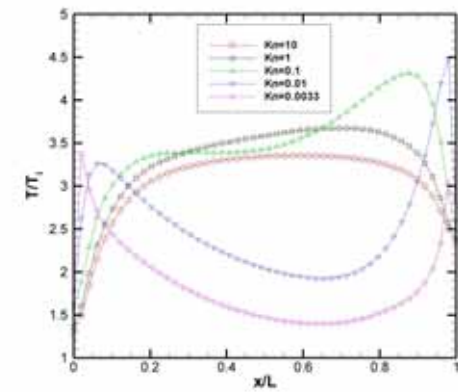
Fig. 3.66 Effect of Kn for M = 4 along horizontal line near top wall(y/L=1) with

(a) u-velocity; (b) v-velocity; (c) number density (d) temperature
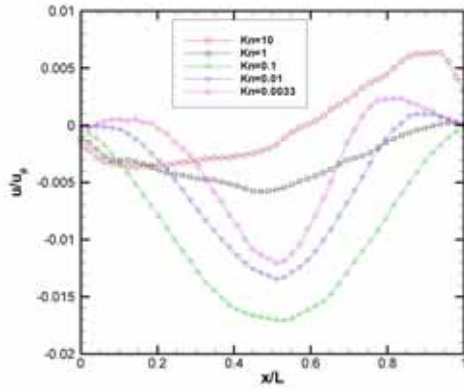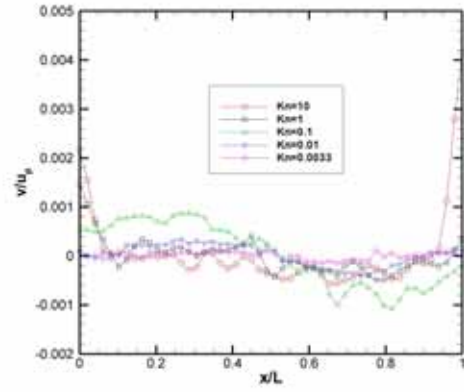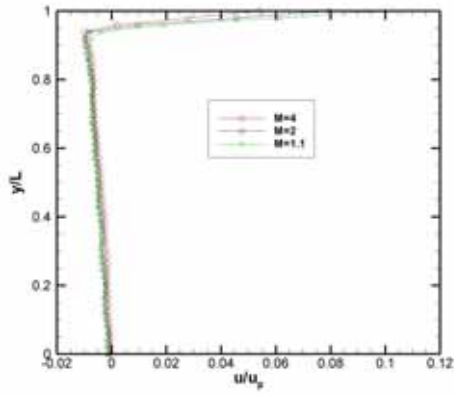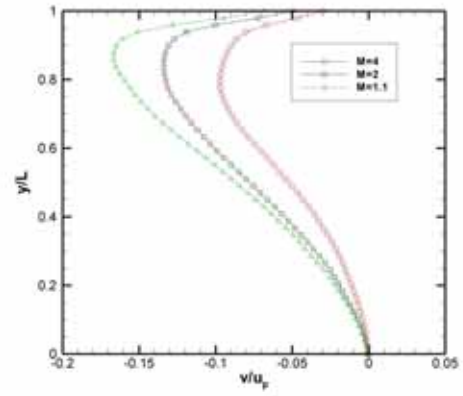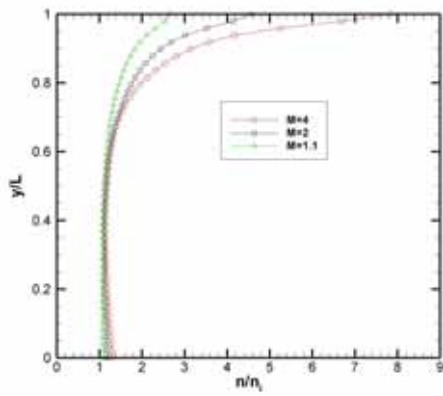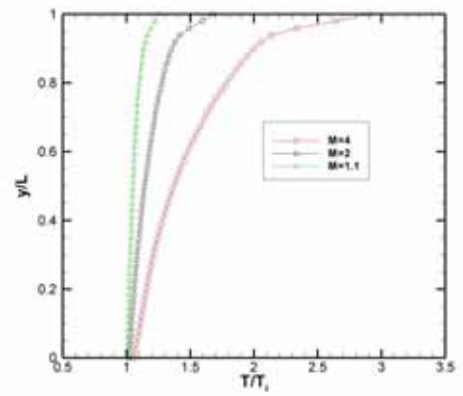
(a)   (b)
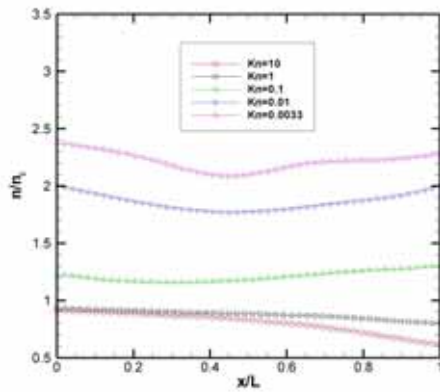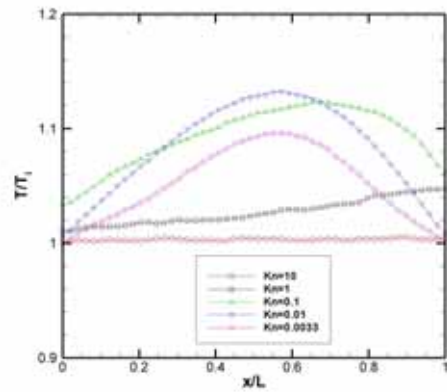
(c)   (d)

Fig. 3.67   Effect of Kn for M = 4 along horizontal line near bottom wall(y/L=0) with

(a) u-velocity; (b) v-velocity; (c) number density (d) temperature
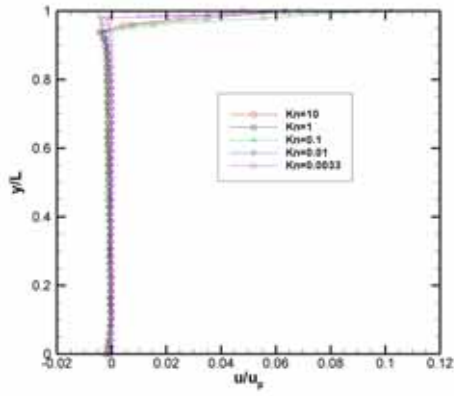
(a)
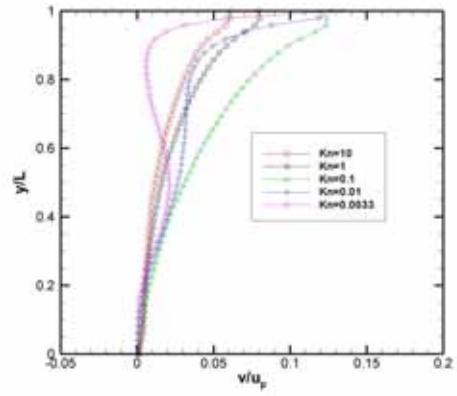
(b)
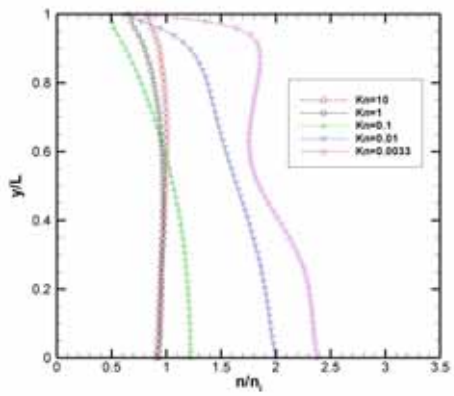
(c)
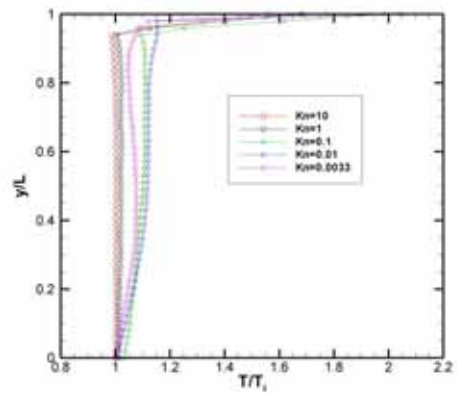
(d)

Fig. 3.68 Effect of Kn for M = 4 along vertical line near left wall(x/L=0) with

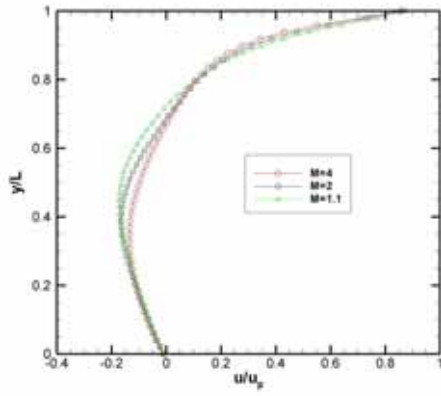(a) u-velocity; (b) v-velocity; (c) number density (d) temperature
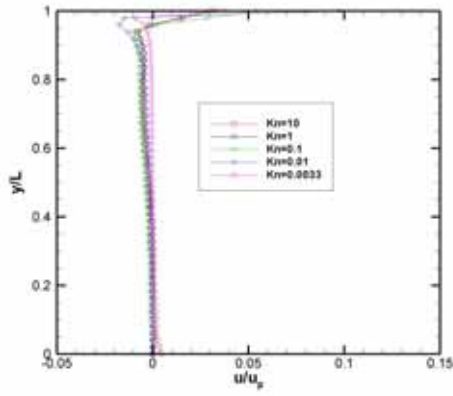
(a)
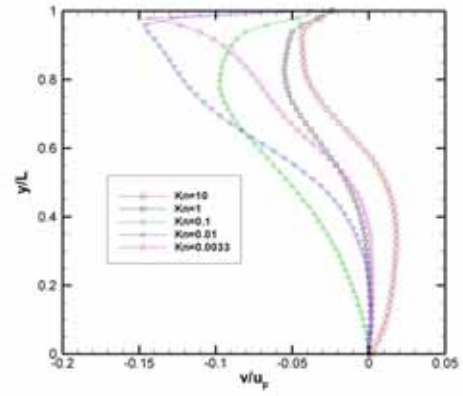
(b)
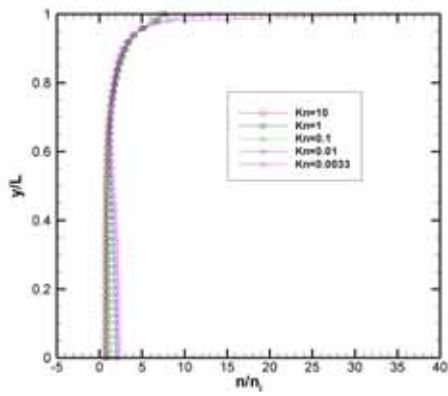
(c)
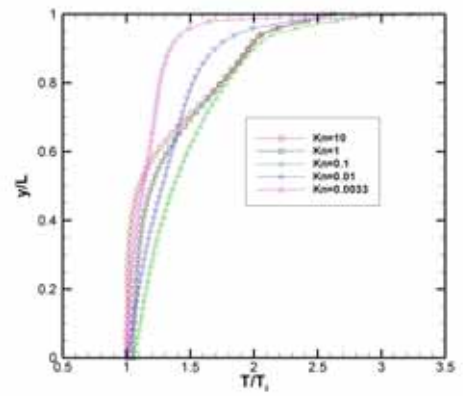
(d)

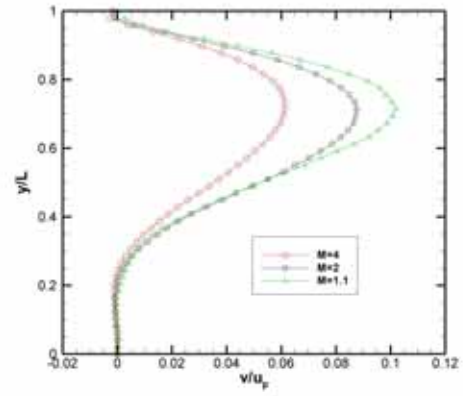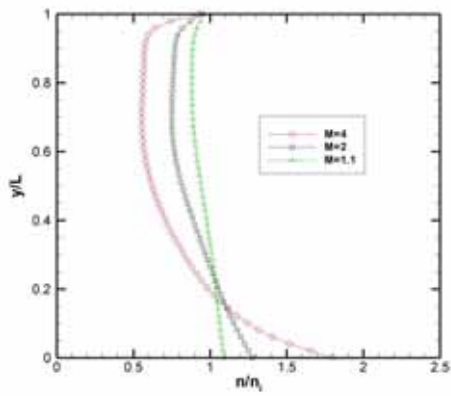**Fig. 3.69**   Effect of Kn for M = 4 along vertical line near right wall(x/L=1) with

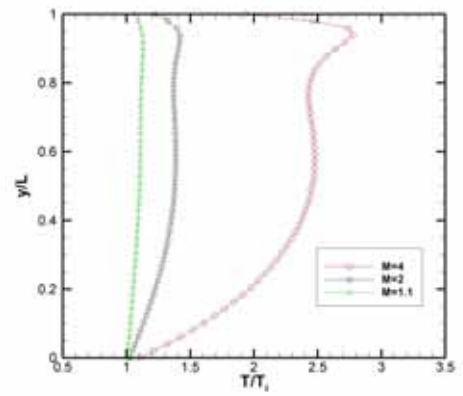(a) u-velocity; (b) v-velocity; (c) number density (d) temperature
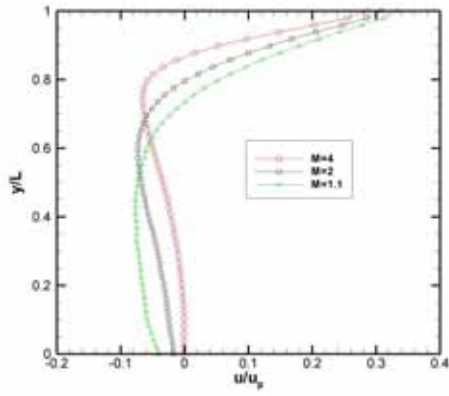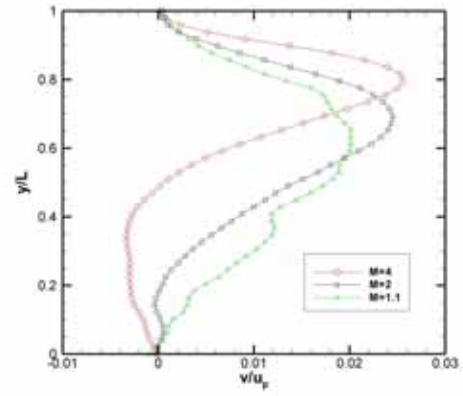
(a)   (b)
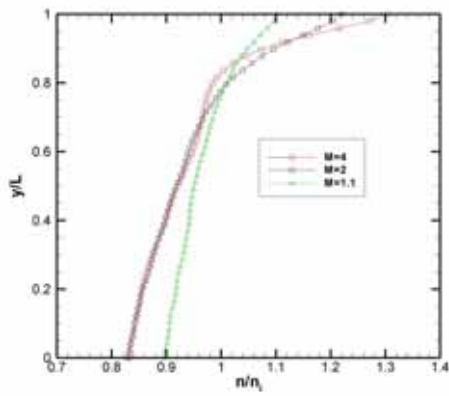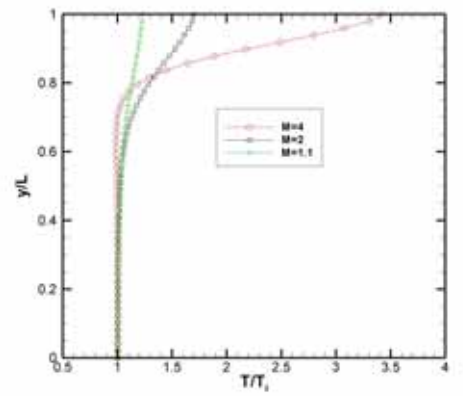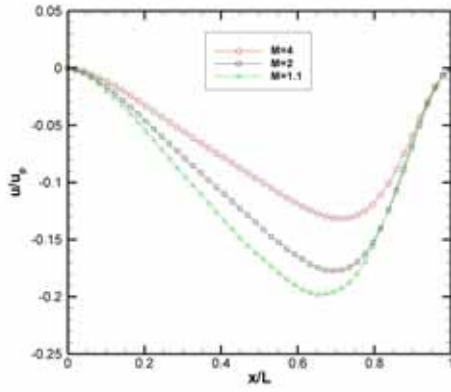

(c)   (d)
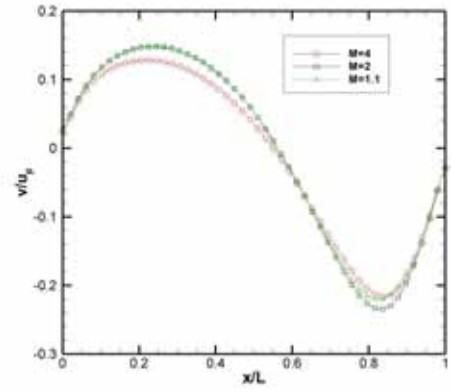
Fig. 3.70   Effect of M for Kn = 10 along vertical line through geometry center with
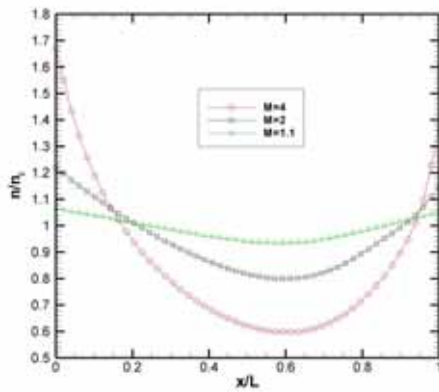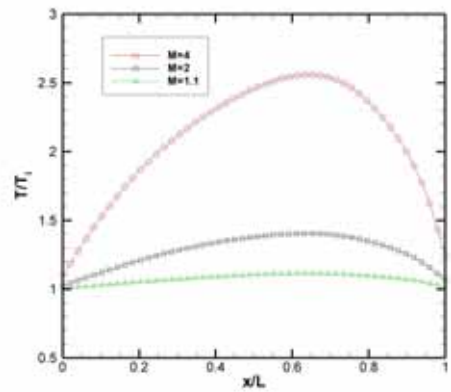(a) u-velocity; (b) v-velocity; (c) number density (d) temperature
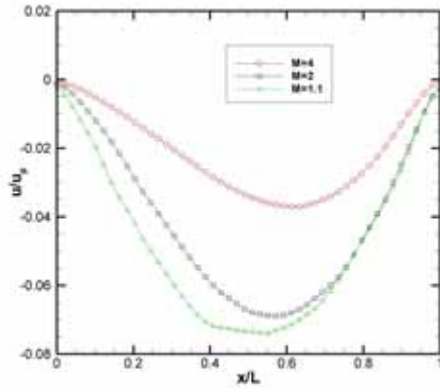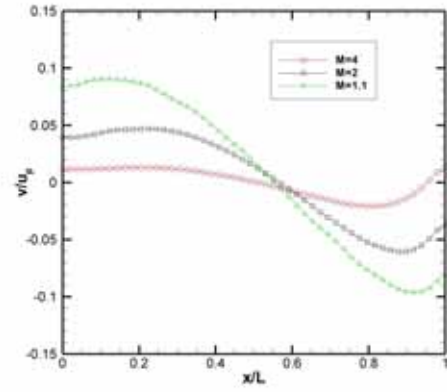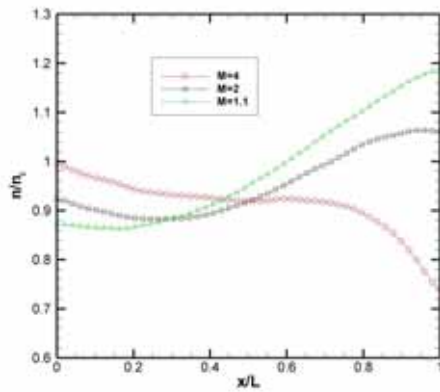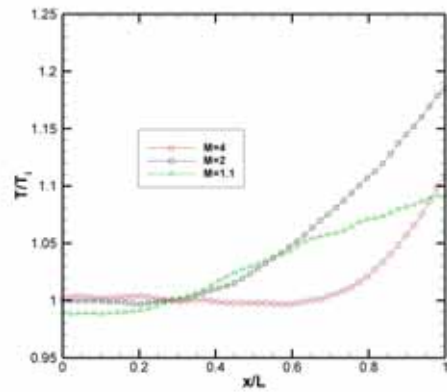
Fig. 3.71 Effect of M for Kn = 10 along horizontal line through geometry center with (a) u-velocity; (b) v-velocity; (c) number density (d) temperature
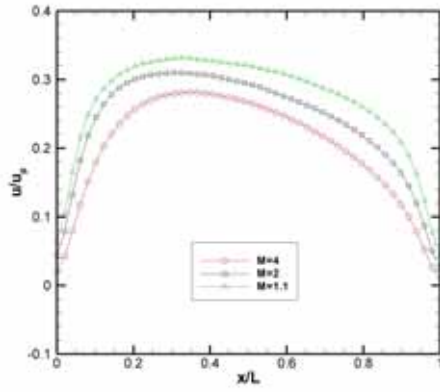
(a)
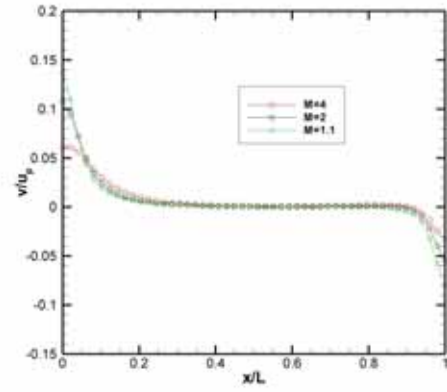
(b)
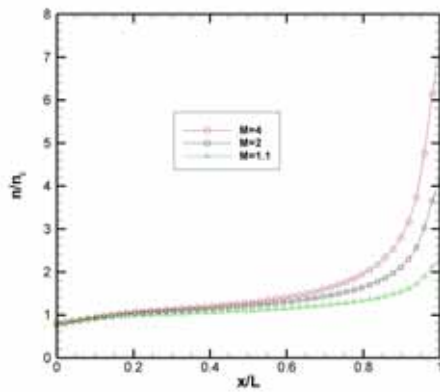
(c)
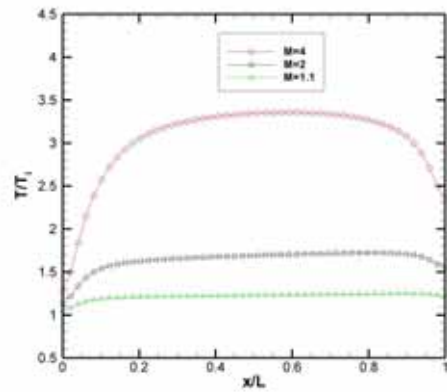
(d)
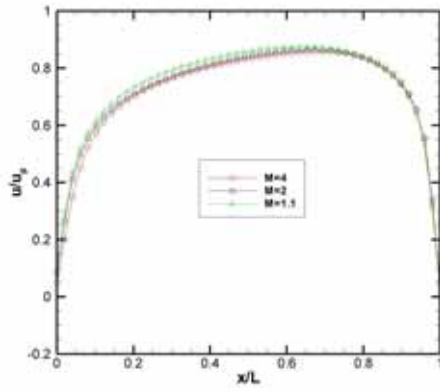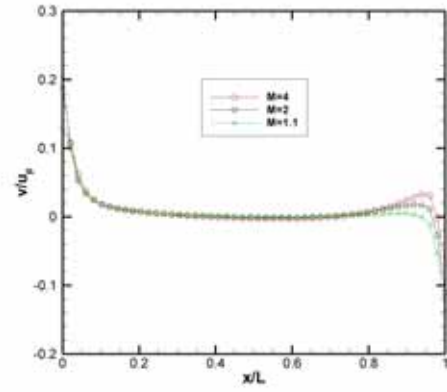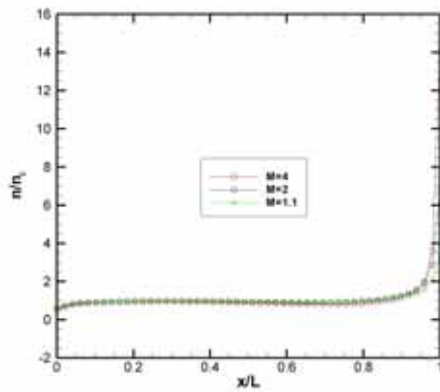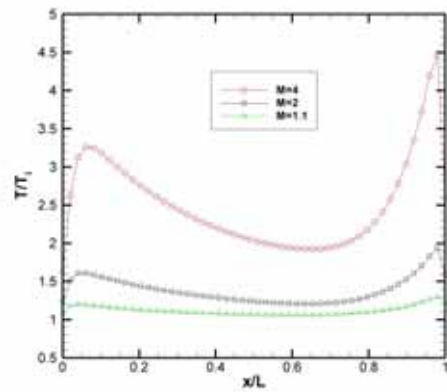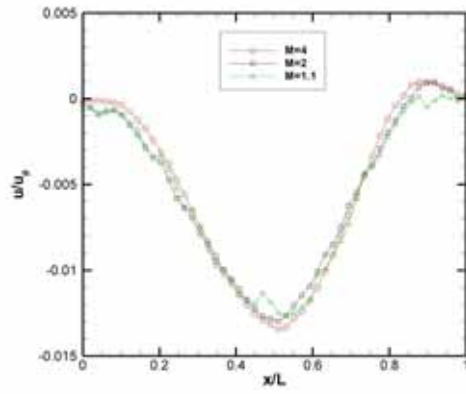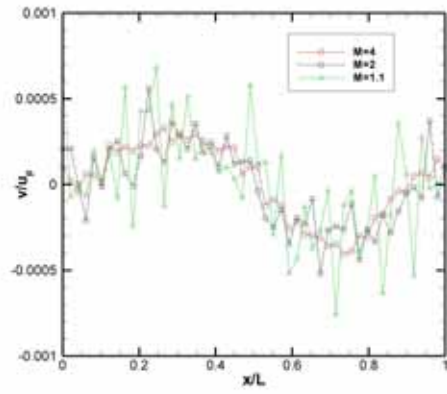
Fig. 3.72 Effect of M for Kn = 10 along horizontal line near top wall(y/L=1) with
(a) u-velocity; (b) v-velocity; (c) number density (d) temperature
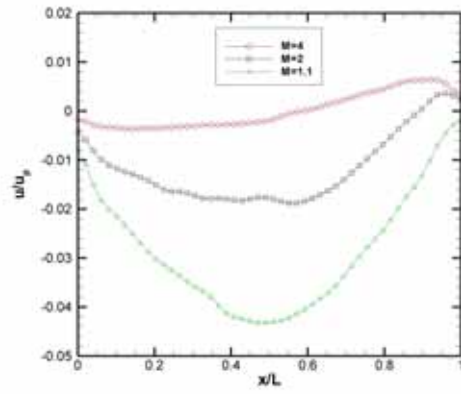
(a)
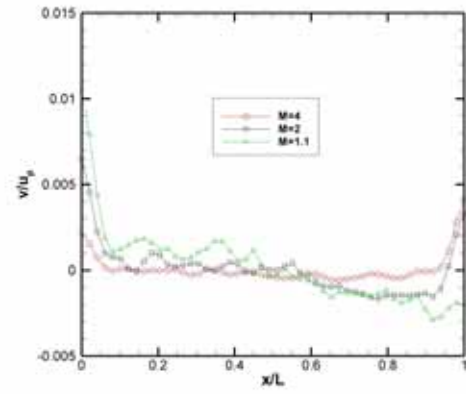
(b)
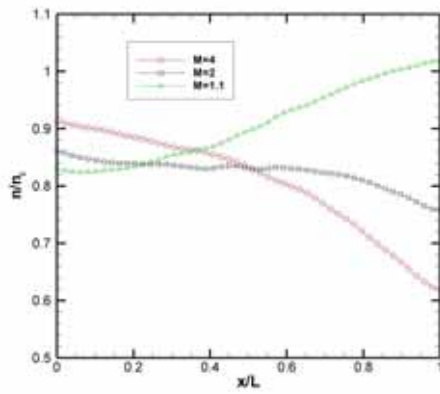
(c)
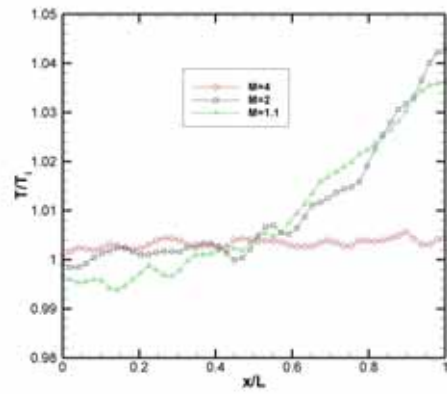
(d)

Fig. 3.73   Effect of M for Kn = 10 along horizontal line near bottom wall(y/L=0) with

(a) u-velocity; (b) v-velocity; (c) number density (d) temperature

120
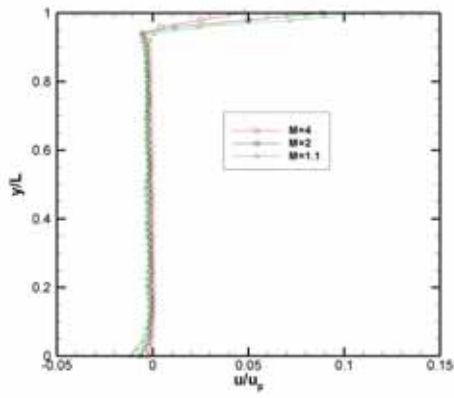
(a)
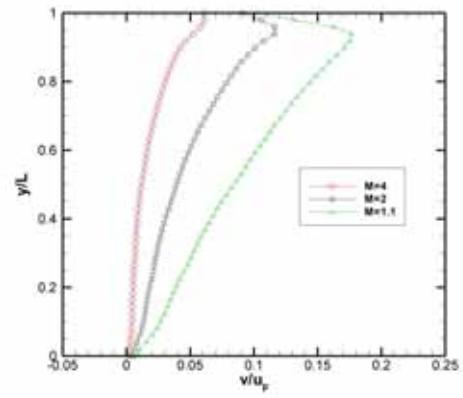
(b)
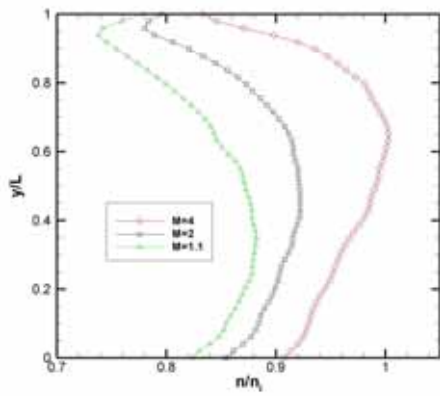
(c)
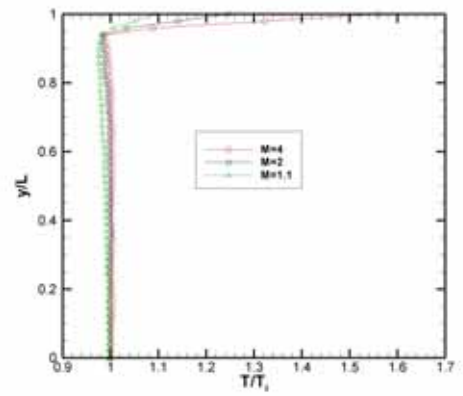
(d)

Fig. 3.74 Effect of M for Kn = 10 along vertical line near left wall(x/L=0) with
(a) u-velocity; (b) v-velocity; (c) number density (d) temperature
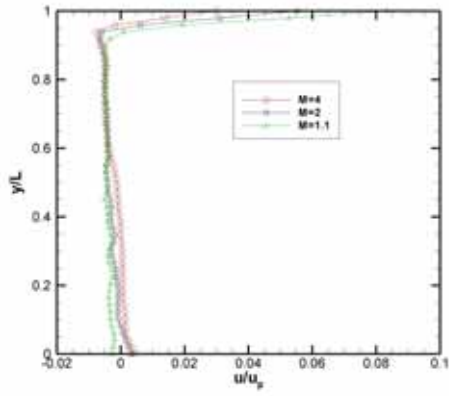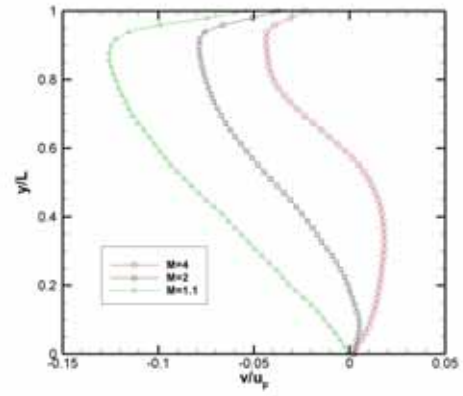
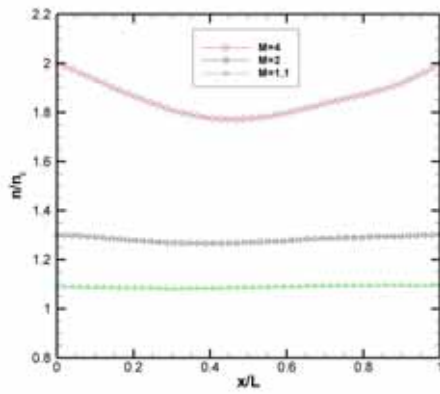(a)   (b)
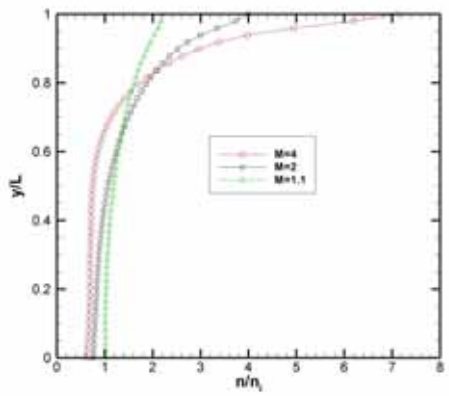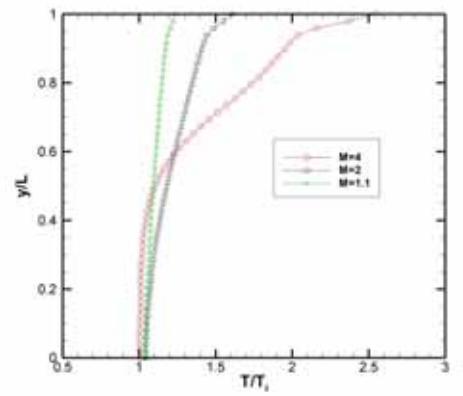
(c)   (d)

Fig. 3.75   Effect of M for Kn = 10 along vertical line near right wall(x/L=1) with

(a) u-velocity; (b) v-velocity; (c) number density (d) temperature
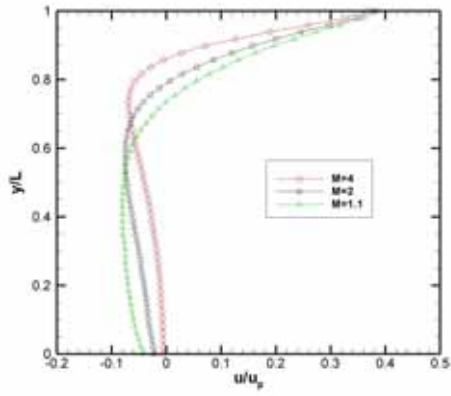
(a)
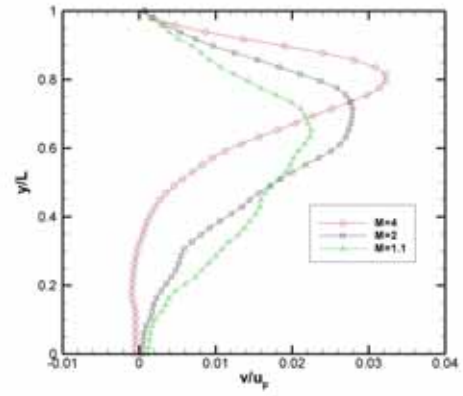
(b)
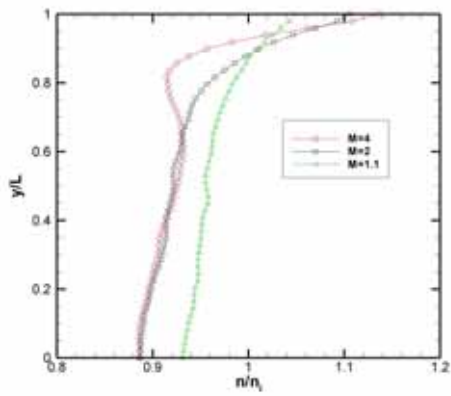
(c)
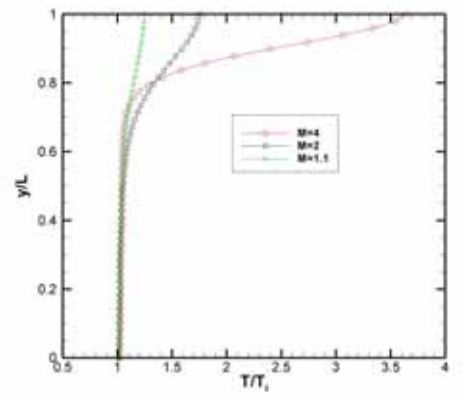
(d)

Fig. 3.76 Effect of M for Kn = 1 along vertical line through geometry center with
(a) u-velocity; (b) v-velocity; (c) number density (d) temperature

123
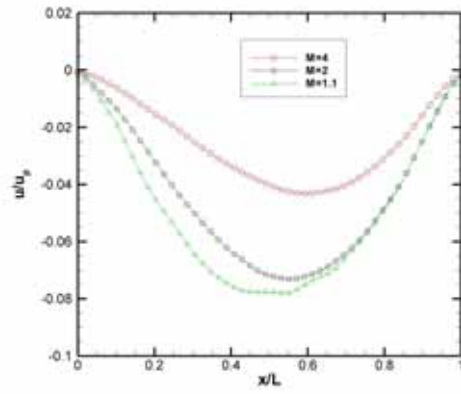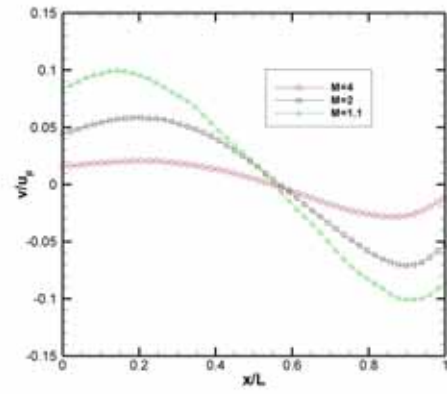
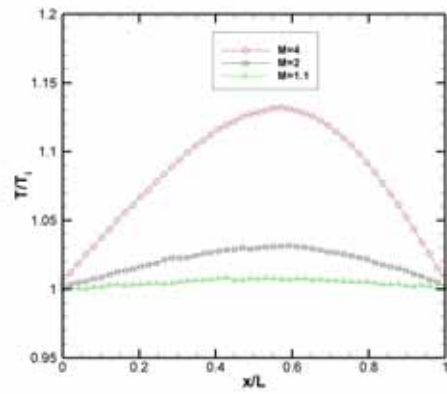(a)   (b)
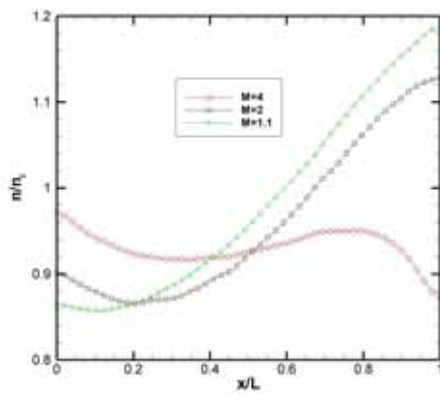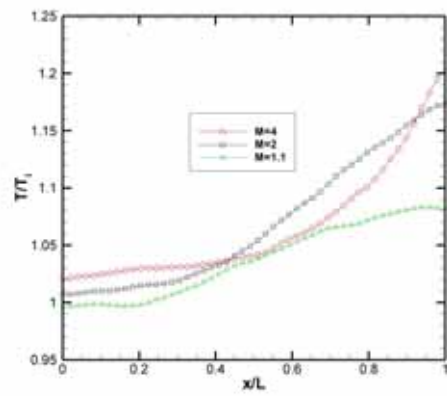
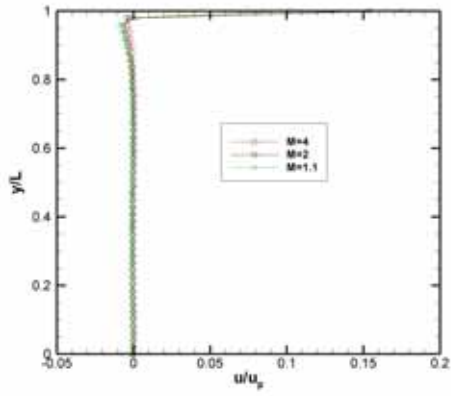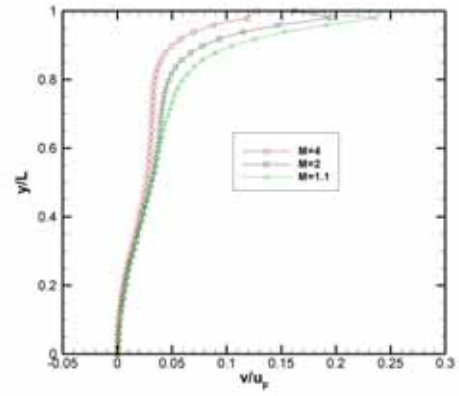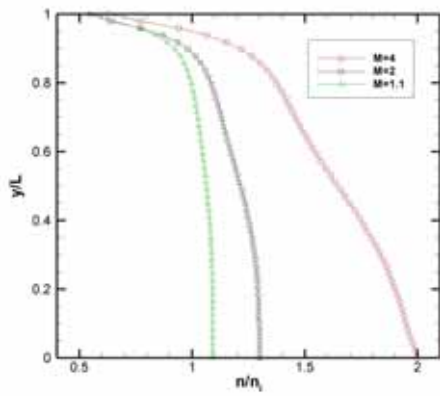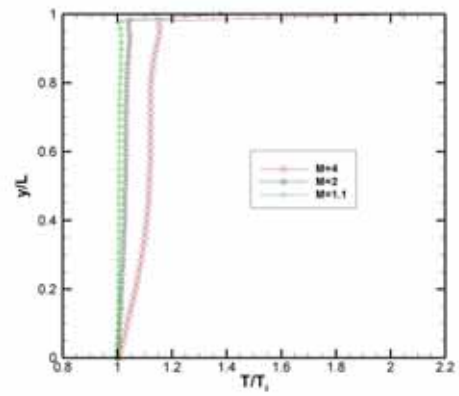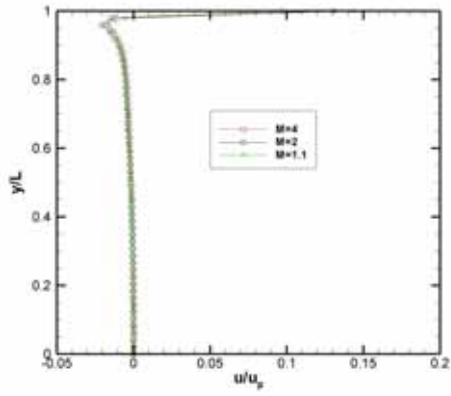(c)   (d)

Fig. 3.77   Effect of M for Kn = 1 along horizontal line through geometry center with

(a) u-velocity; (b) v-velocity; (c) number density (d) temperature
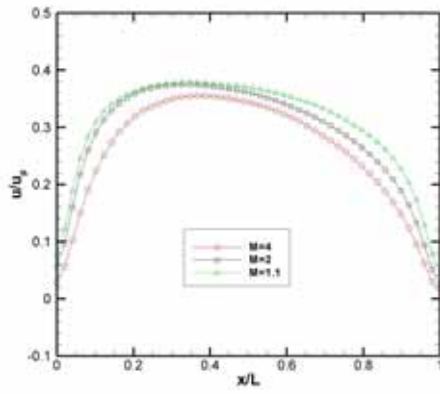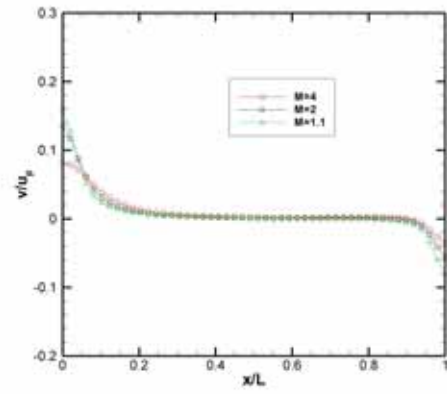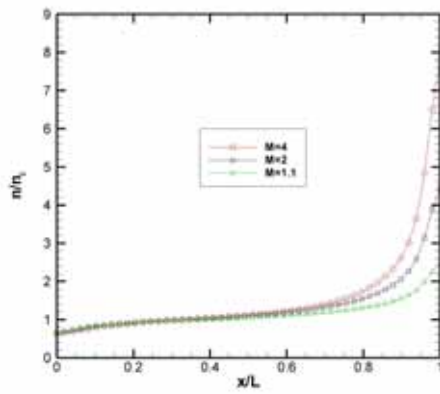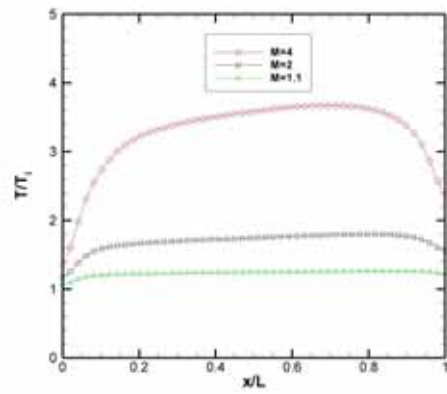
Fig. 3.78   Effect of M for Kn = 1 along horizontal line near top wall(y/L=1) with
(a) u-velocity; (b) v-velocity; (c) number density (d) temperature
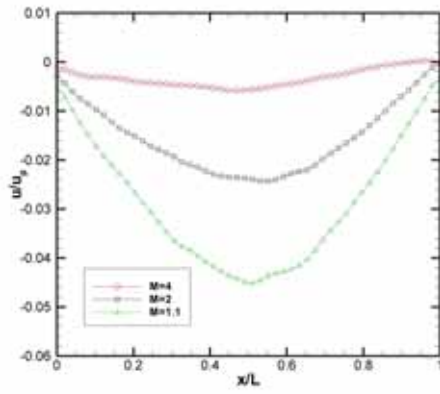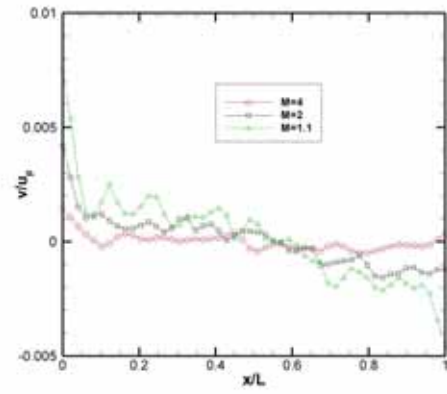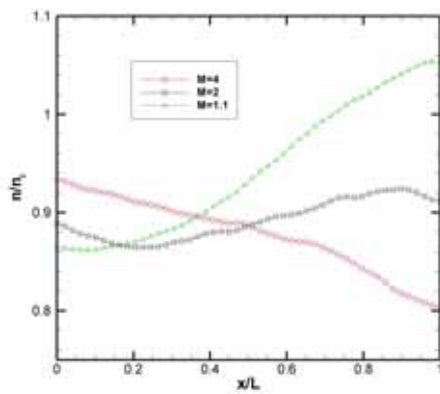
Fig. 3.79   Effect of M for Kn = 1 along horizontal line near bottom wall(y/L=0) with
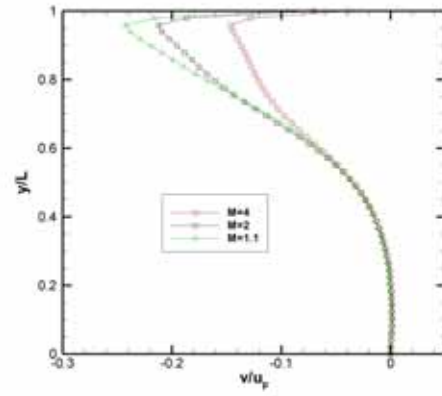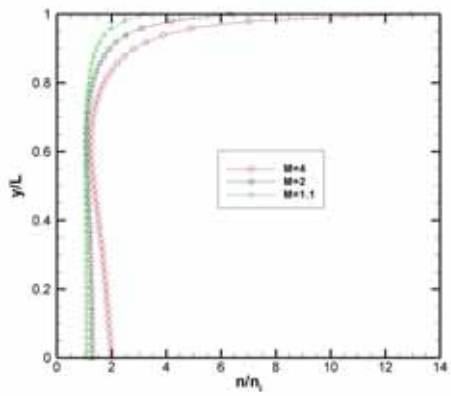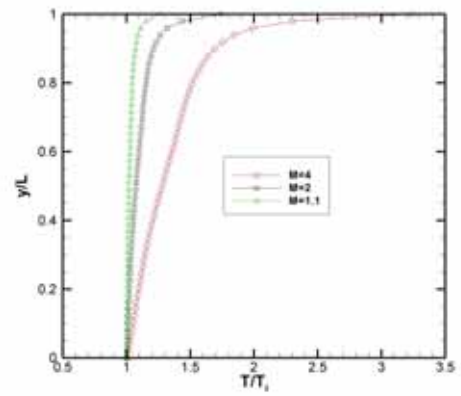
(a) u-velocity; (b) v-velocity; (c) number density (d) temperature
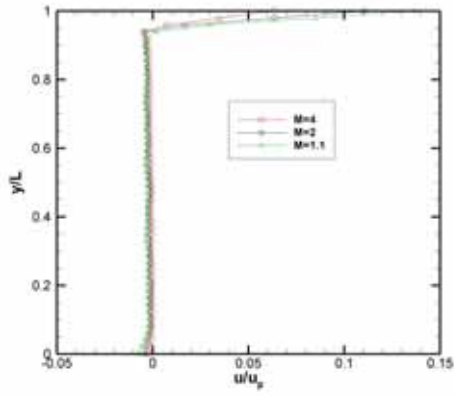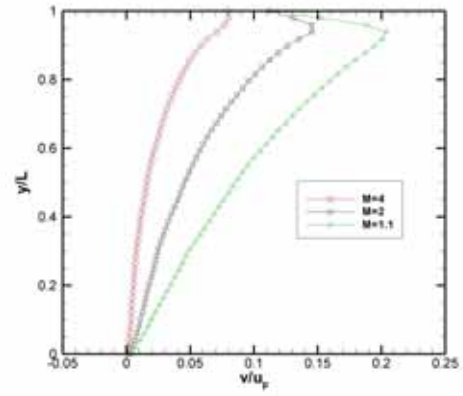
Fig. 3.80 Effect of M for Kn = 1 along vertical line near left wall(x/L=0) with
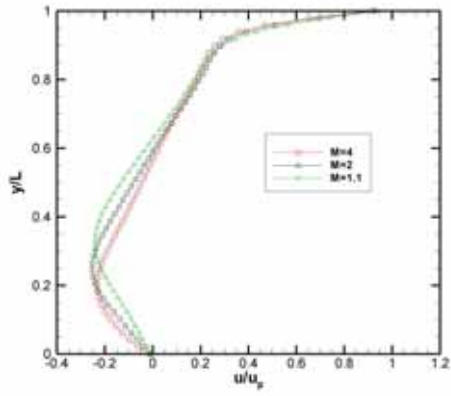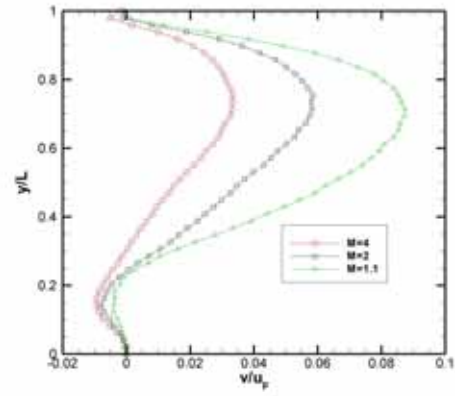(a) u-velocity; (b) v-velocity; (c) number density (d) temperature

Fig. 3.81 Effect of M for Kn = 1 along vertical line near right wall(x/L=1) with
(a) u-velocity; (b) v-velocity; (c) number density (d) temperature

128

Fig. 3.82 Effect of M for Kn = 0.1 along vertical line through geometry center with
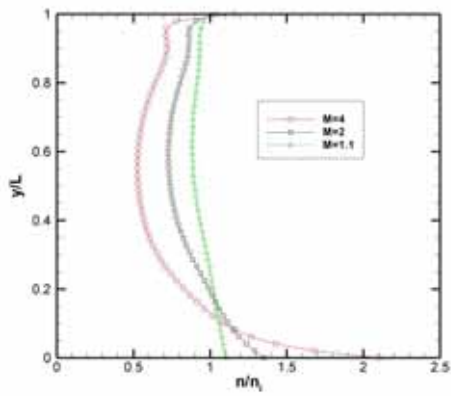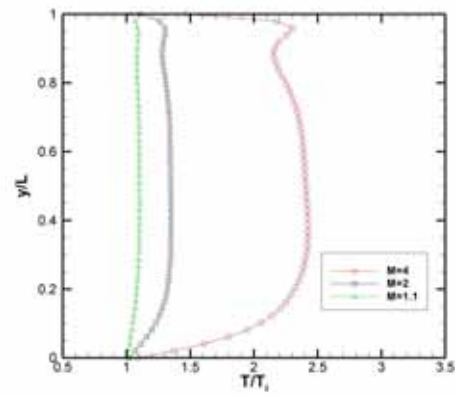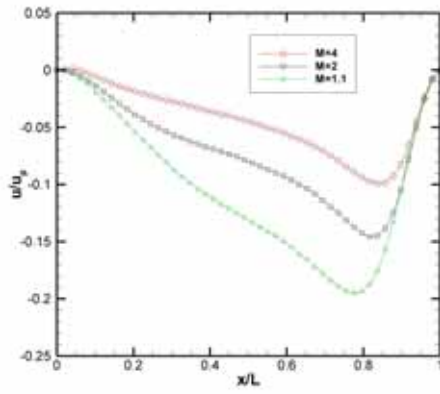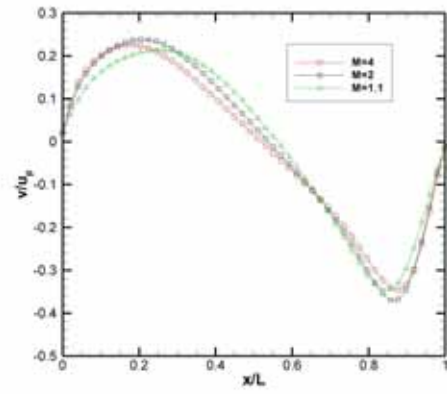(a) u-velocity; (b) v-velocity; (c) number density (d) temperature

(a)

(b)

(c)

(d)

Fig. 3.83 Effect of M for Kn = 0.1 along horizontal line through geometry center with (a) u-velocity; (b) v-velocity; (c) number density (d) temperature
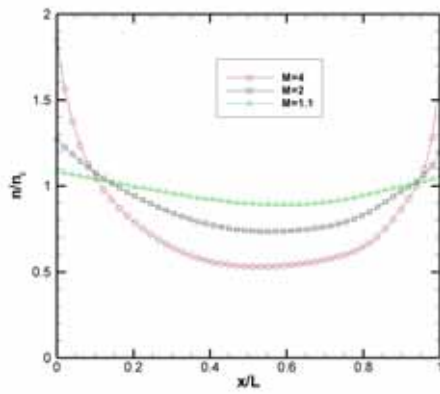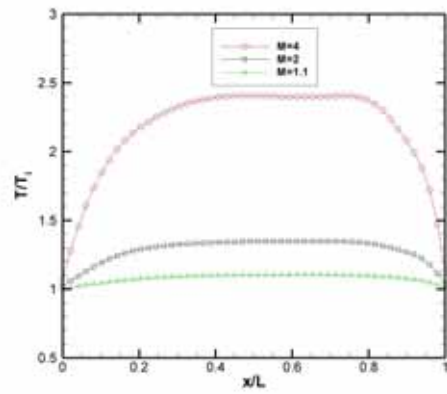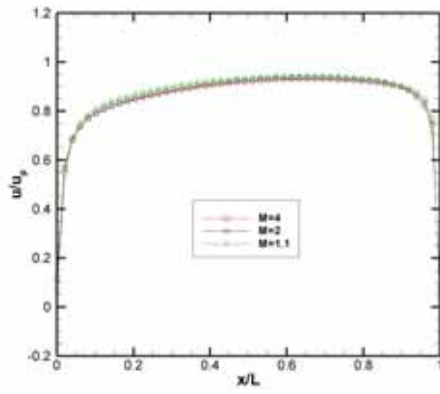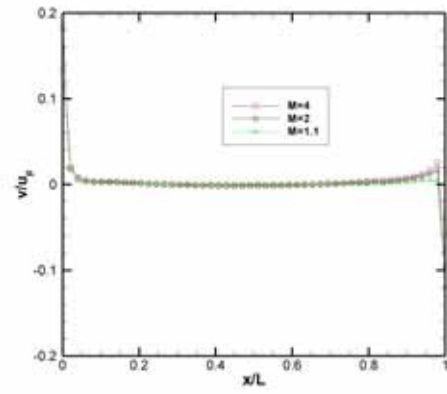
(a)

(b)

(c)

(d)

Fig. 3.84   Effect of M for Kn = 0.1 along horizontal line near top wall(y/L=1) with
(a) u-velocity; (b) v-velocity; (c) number density (d) temperature

Fig. 3.85   Effect of M for Kn = 0.1 along horizontal line near bottom wall(y/L=0) with
(a) u-velocity; (b) v-velocity; (c) number density (d) temperature

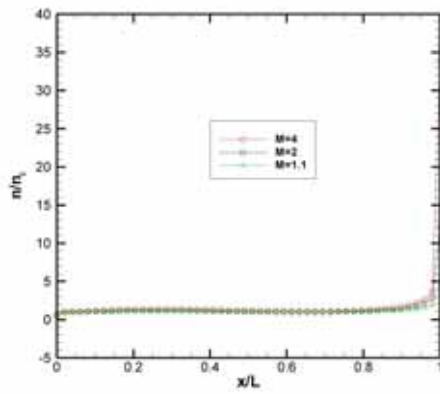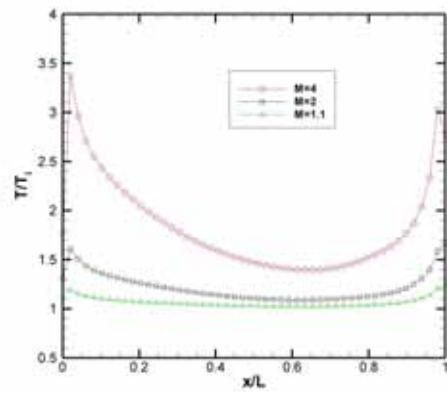(a)   (b)

(c)   (d)

Fig. 3.86   Effect of M for Kn = 0.1 along vertical line near left wall(x/L=0) with

(a) u-velocity; (b) v-velocity; (c) number density (d) temperature

(a)

(b)

(c)

(d)

Fig. 3.87 Effect of M for Kn = 0.1 along vertical line near right wall(x/L=1) with
(a) u-velocity; (b) v-velocity; (c) number density (d) temperature

(a)

(b)

(c)

(d)

Fig. 3.88 Effect of M for Kn = 0.01 along vertical line through geometry center with

(a) u-velocity; (b) v-velocity; (c) number density (d) temperature

(a)

(b)

(c)

(d)
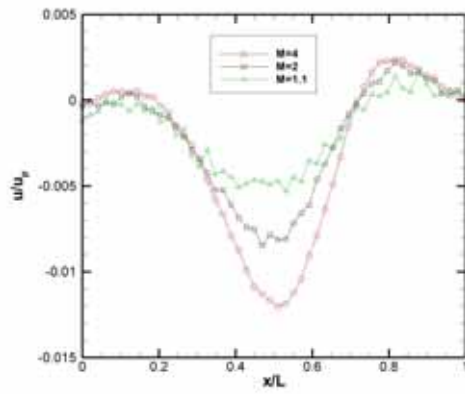
Fig. 3.89 Effect of M for Kn = 0.01 along horizontal line through geometry center with

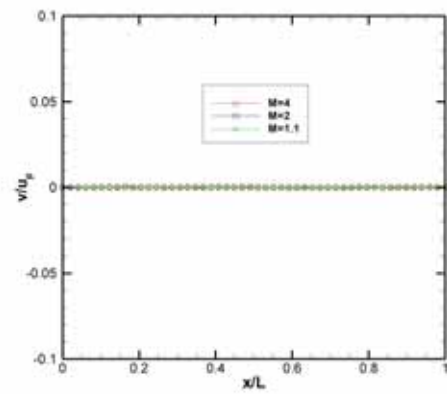(a) u-velocity; (b) v-velocity; (c) number density (d) temperature

Fig. 3.90 Effect of M for Kn = 0.01 along horizontal line near top wall(y/L=1) with (a) u-velocity; (b) v-velocity; (c) number density (d) temperature

(a)

(b)

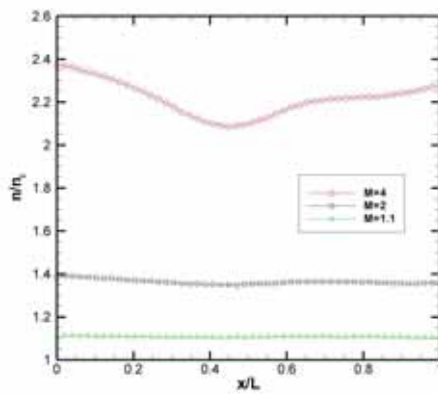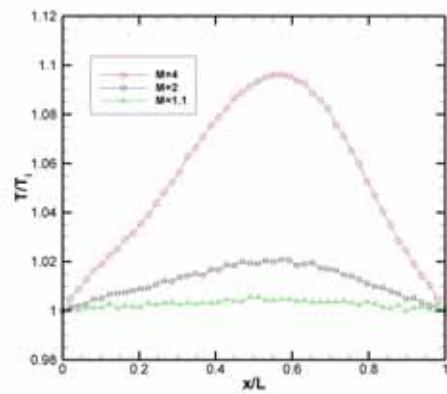(c)

(d)
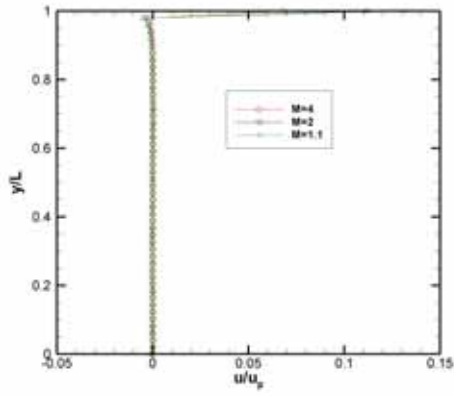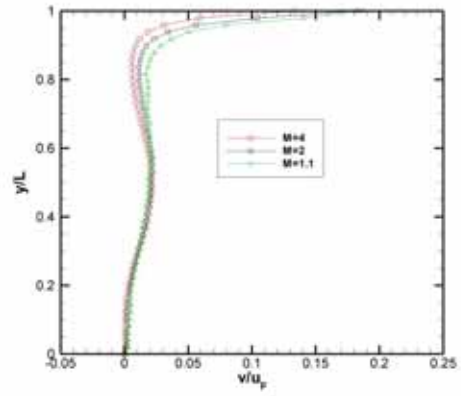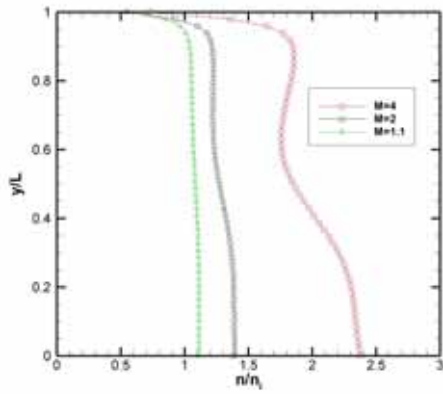
Fig. 3.91   Effect of M for Kn = 0.01 along horizontal line near bottom wall(y/L=0) with

(a) u-velocity; (b) v-velocity; (c) number density (d) temperature

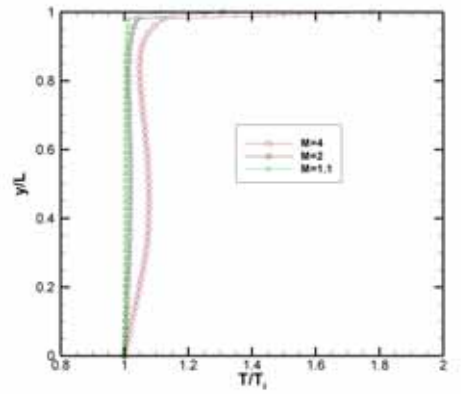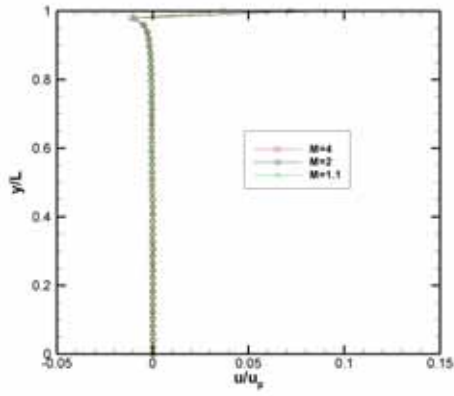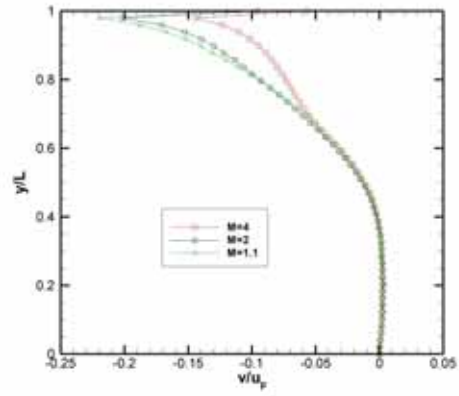**Fig. 3.92** Effect of M for Kn = 0.01 along vertical line near left wall(x/L=0) with
(a) u-velocity; (b) v-velocity; (c) number density (d) temperature

Fig. 3.93   Effect of M for Kn = 0.01 along vertical line near right wall(x/L=1) with

(a) u-velocity; (b) v-velocity; (c) number density (d) temperature
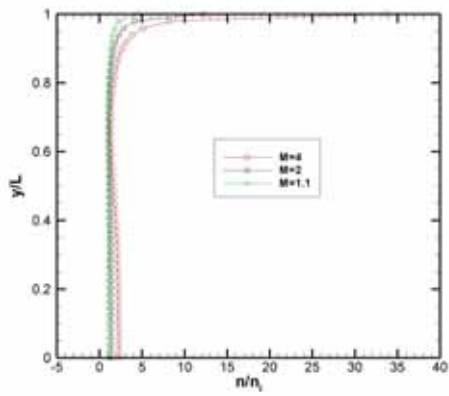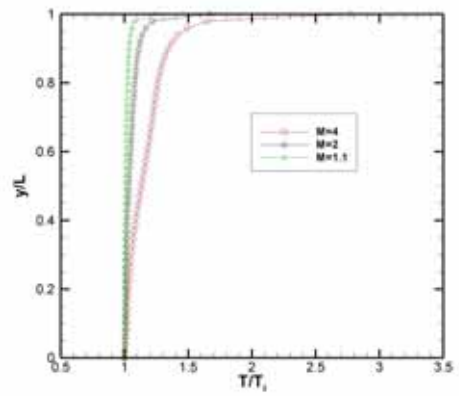
(a)   (b)

(c)   (d)

Fig. 3.94   Effect of M for Kn = 0.0033 along vertical line through geometry center with

(a) u-velocity; (b) v-velocity; (c) number density (d) temperature

141

(a)

(b)

(c)

(d)

Fig. 3.95   Effect of M for Kn = 0.0033 along horizontal line through geometry center with

(a) u-velocity; (b) v-velocity; (c) number density (d) temperature

Fig. 3.96 Effect of M for Kn = 0.0033 along horizontal line near top wall(y/L=1) with (a) u-velocity; (b) v-velocity; (c) number density (d) temperature

(a)

(b)

(c)

(d)

Fig. 3.97   Effect of M for Kn = 0.0033 along horizontal line near bottom wall(y/L=0) with

(a) u-velocity; (b) v-velocity; (c) number density (d) temperature

(a)   (b)

(c)   (d)

Fig. 3.98   Effect of M for Kn = 0.0033 along vertical line near left wall(x/L=0) with

(a) u-velocity; (b) v-velocity; (c) number density (d) temperature

(a)

(b)

(c)

(d)

Fig. 3.99 Effect of M for Kn = 0.0033 along vertical line near right wall(x/L=1) with

(a) u-velocity; (b) v-velocity; (c) number density (d) temperature

(a)

(b)

(c)

(d)

(e)
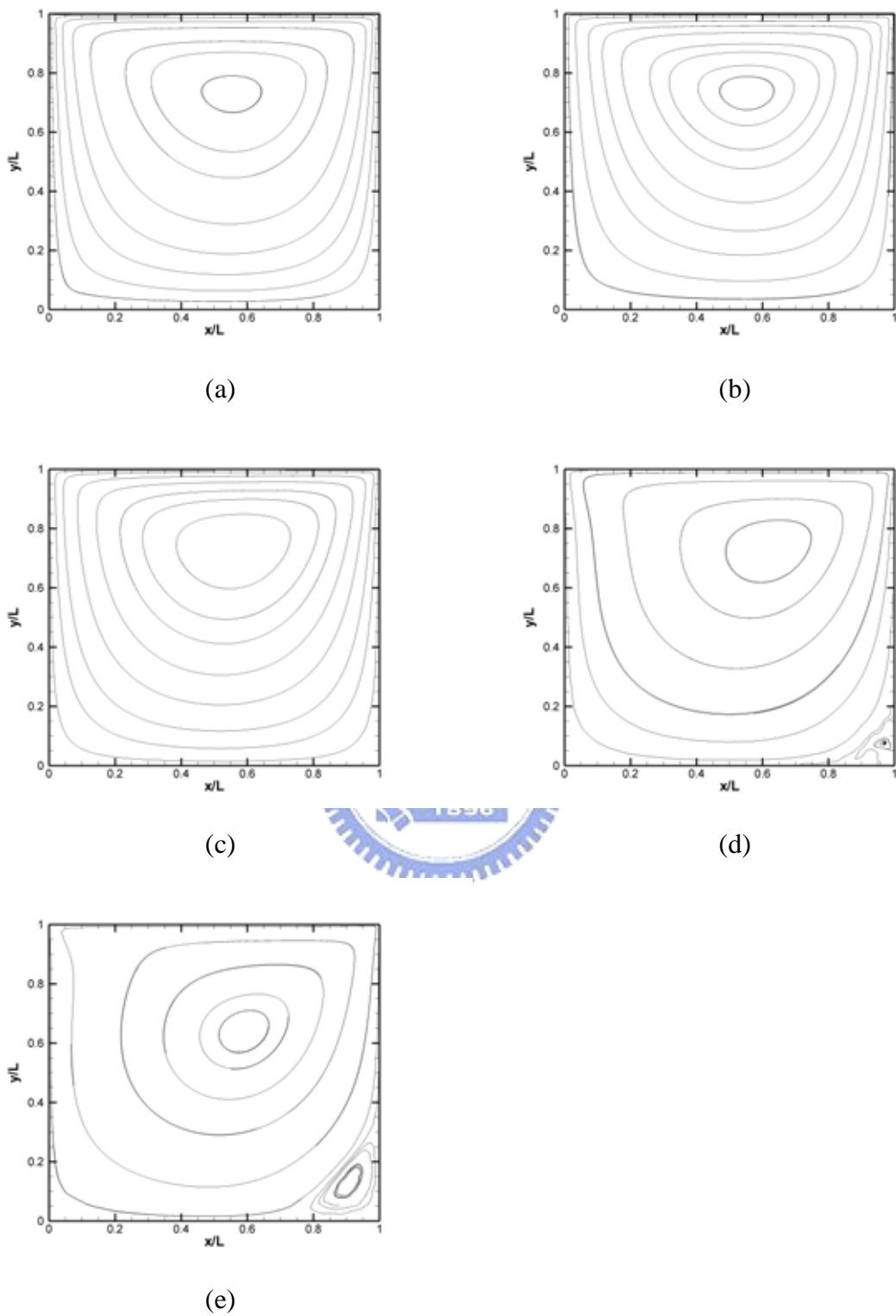
Fig. 3.100 Streamline for M=1.1 (a) Kn=10; (b) Kn=1; (c) Kn=0.1; (d) Kn=0.01; (e) Kn=0.0033

147
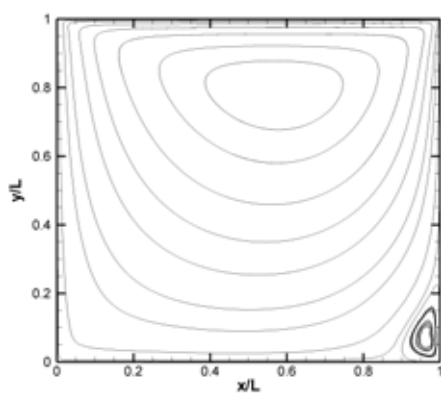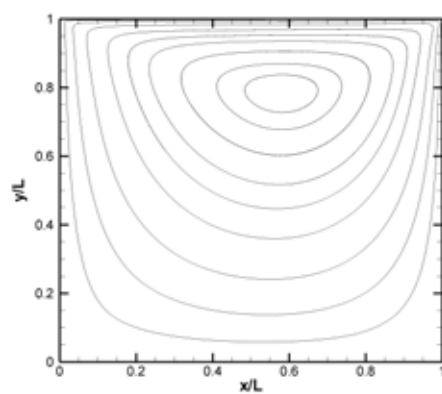
(a)   (b)
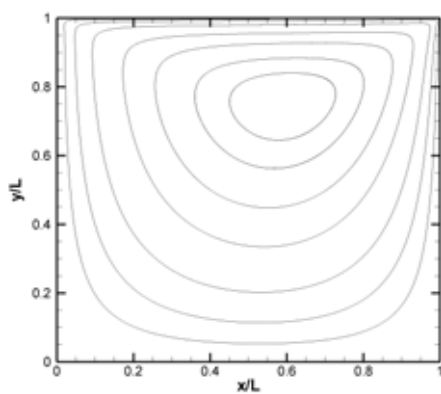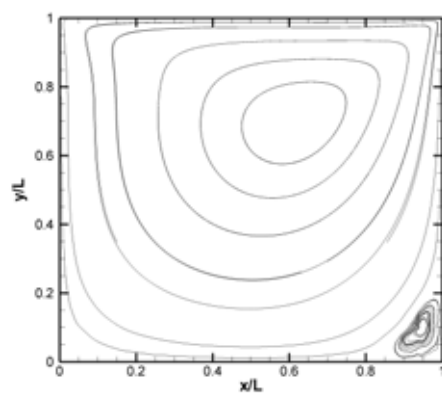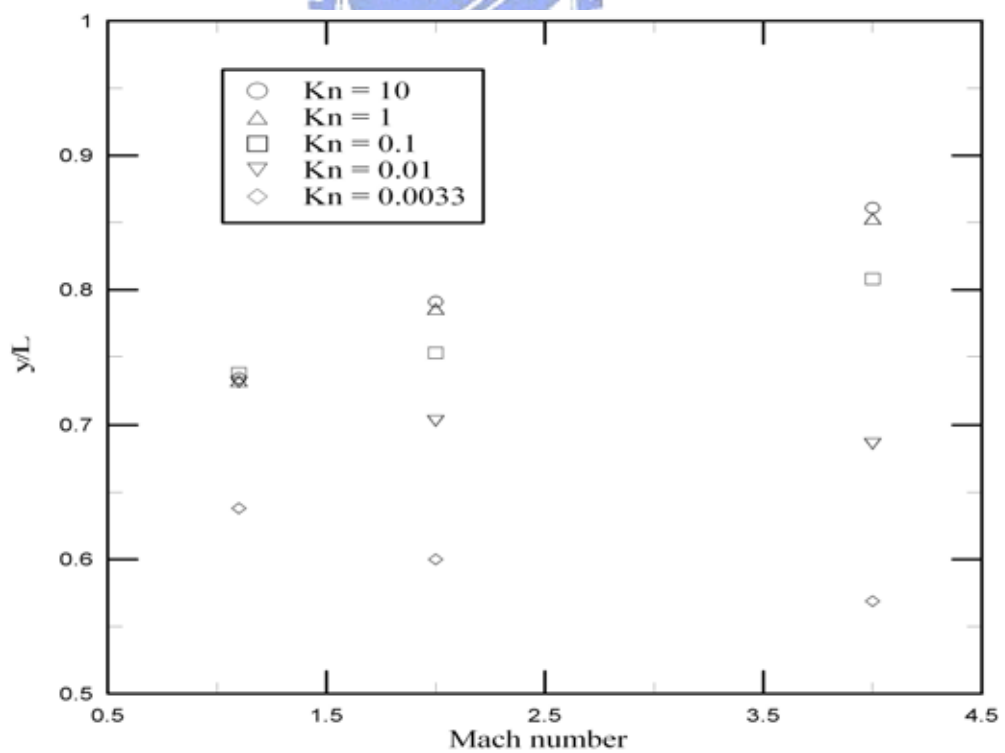

(c)   (d)
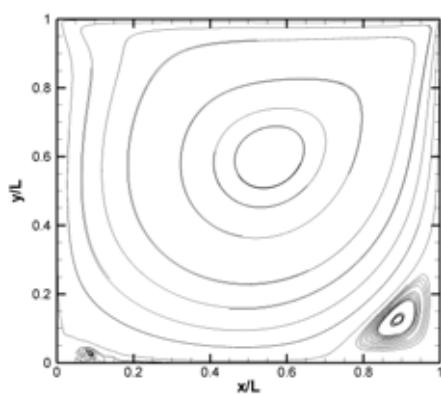
(e)

Fig. 3.101 Streamline for M=2 (a) Kn=10; (b) Kn=1; (c) Kn=0.1; (d) Kn=0.01; (e) Kn=0.0033

148

(a)   (b)

(c)   (d)

(e)
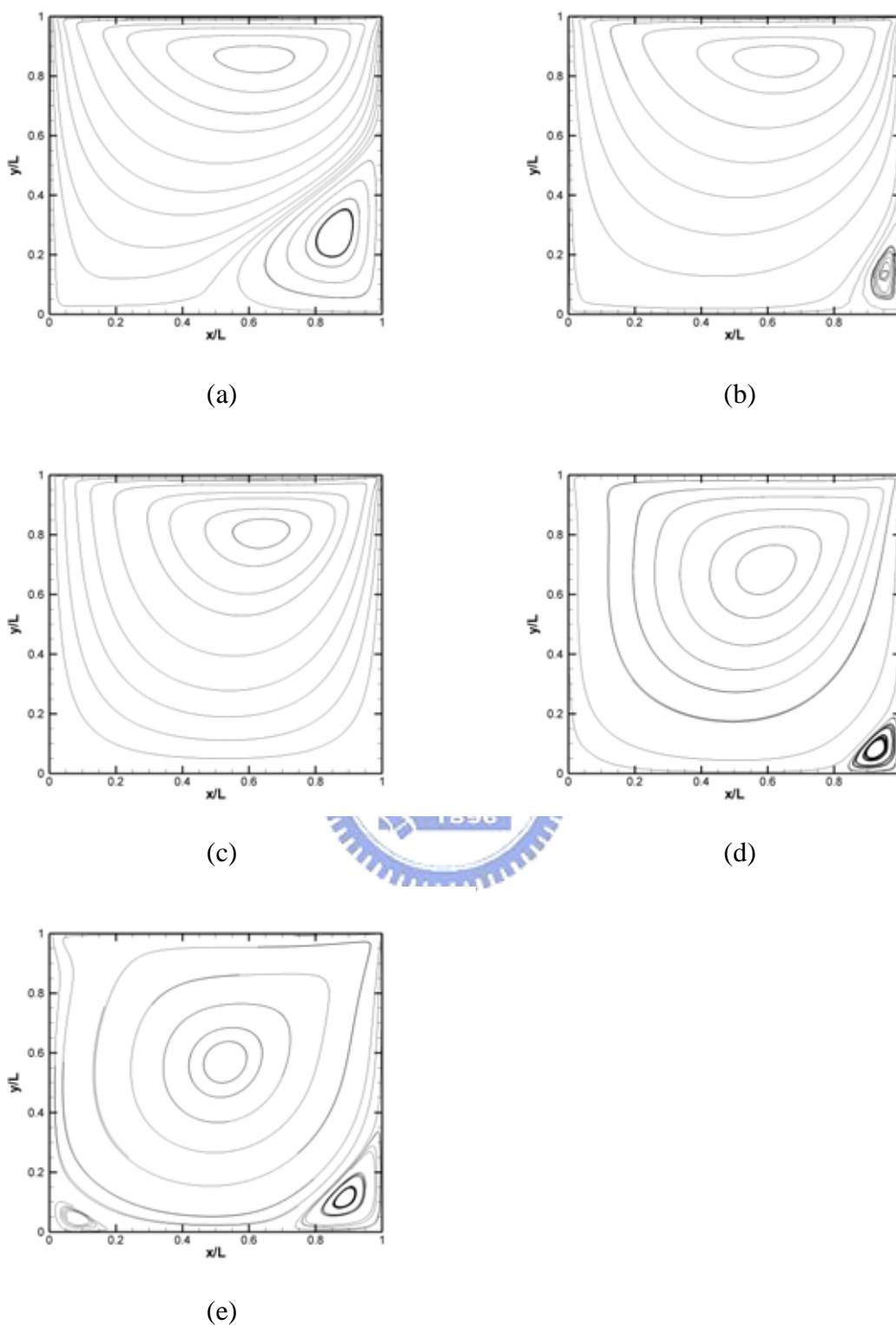
Fig. 3.102 Streamline for M=4 (a) Kn=10; (b) Kn=1; (c) Kn=0.1; (d) Kn=0.01; (e) Kn=0.0033

149
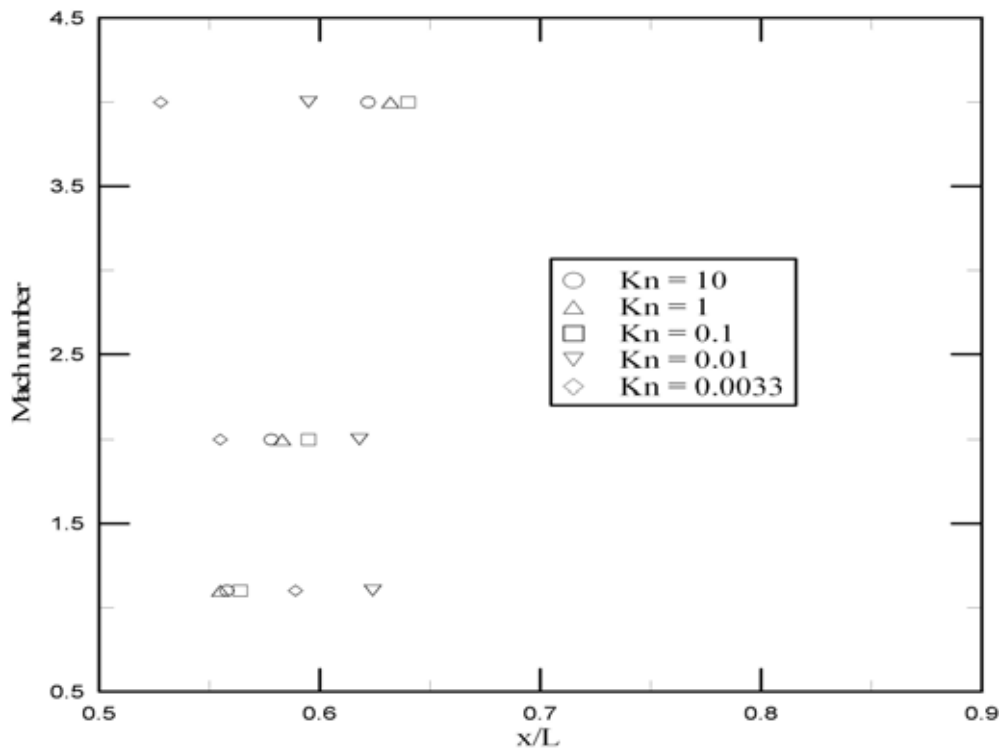
Fig. 3.103   Relative horizontal distance (x/L) of vortex center for various value of Knudsen

number and Mach number

Fig. 3.104   Relative horizontal distance (y/L) of vortex center for various value of Knudsen
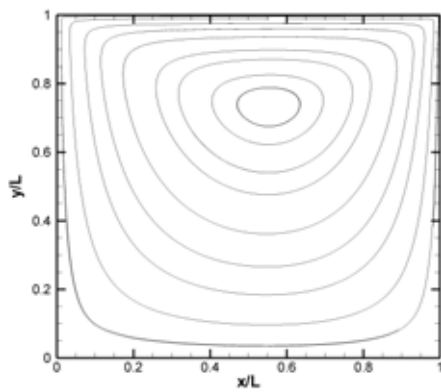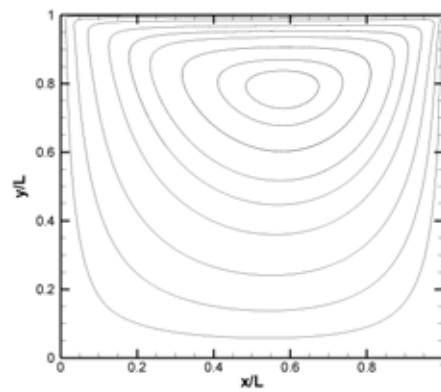
number and Mach number
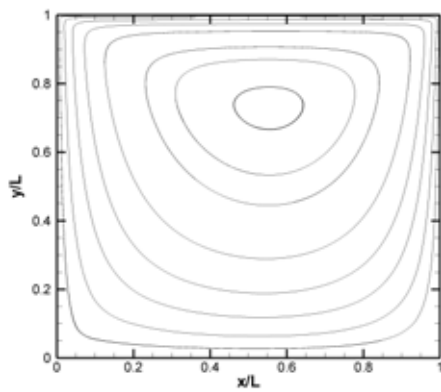
(a)
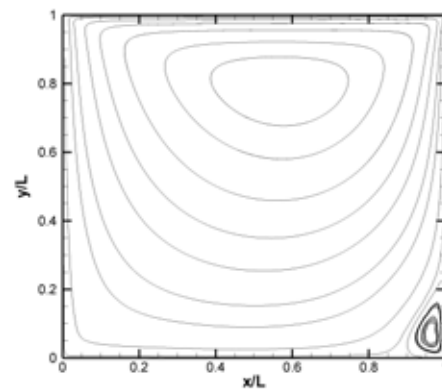
(b)
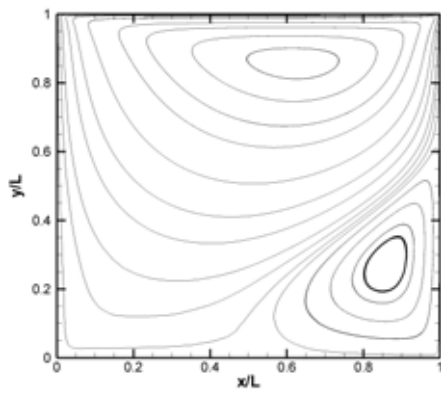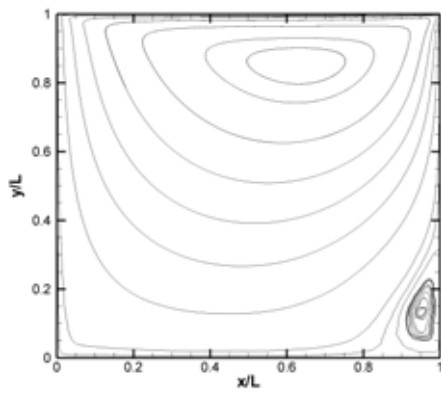

(c)

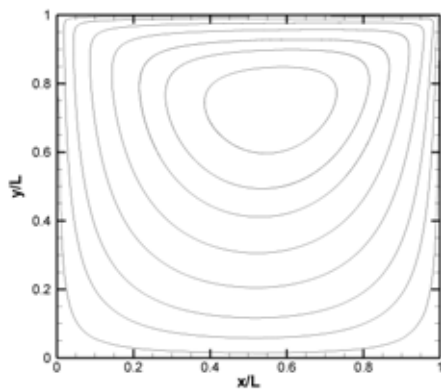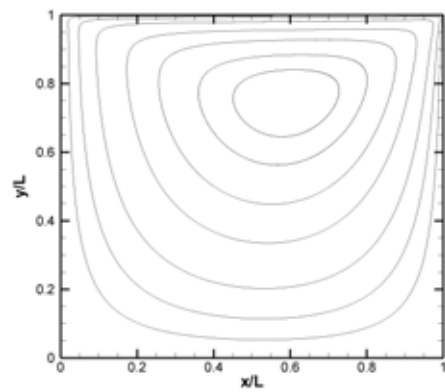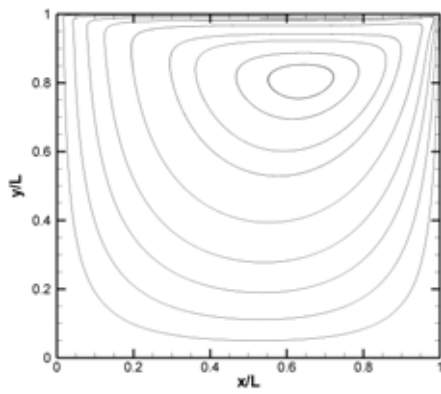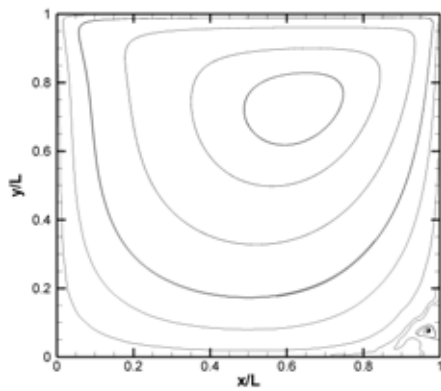**Fig. 3.105**   Streamline for Kn=10 (a) M=1.1; (b) M=2; (c) M=4

(a)

(b)

(c)

Fig. 3.106 Streamline for Kn=1 (a) M=1.1; (b) M=2; (c) M=4

(a)

(b)
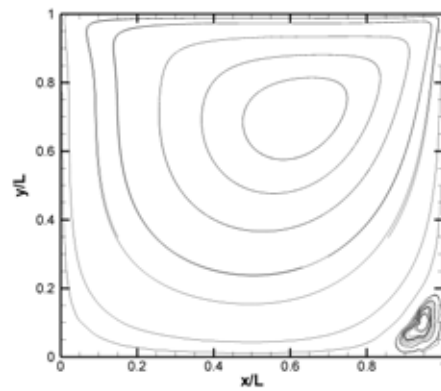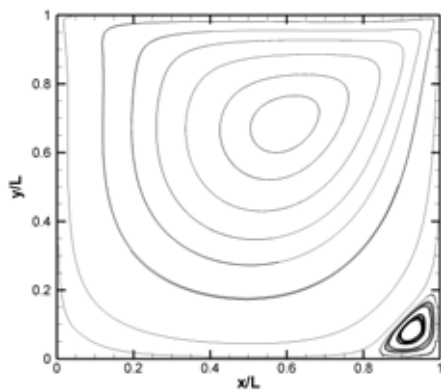

(c)

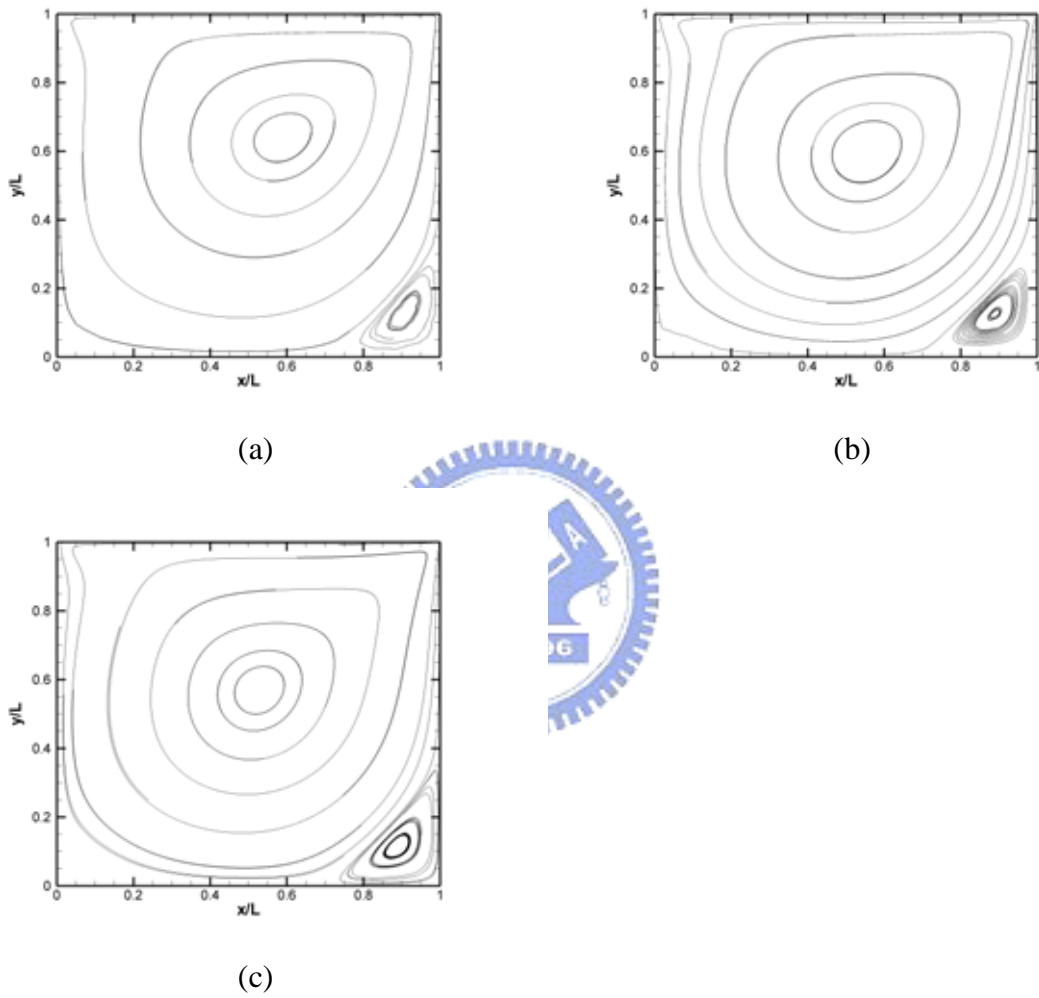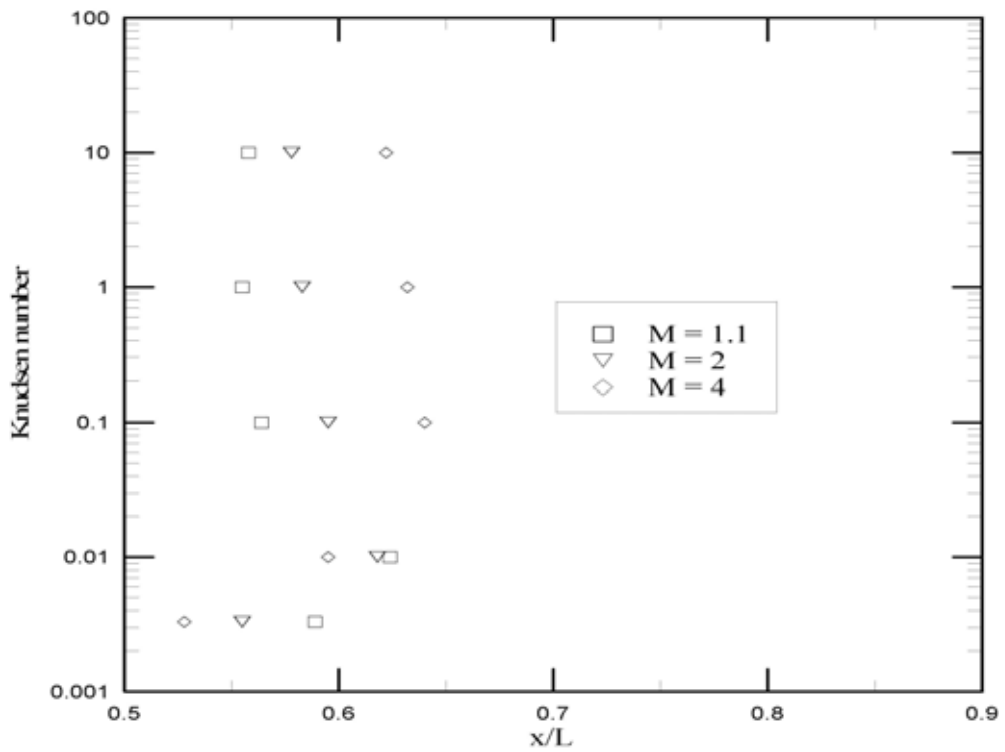**Fig. 3.107**   Streamline for Kn=0.1 (a) M=1.1; (b) M=2; (c) M=4

(a)

(b)

(c)

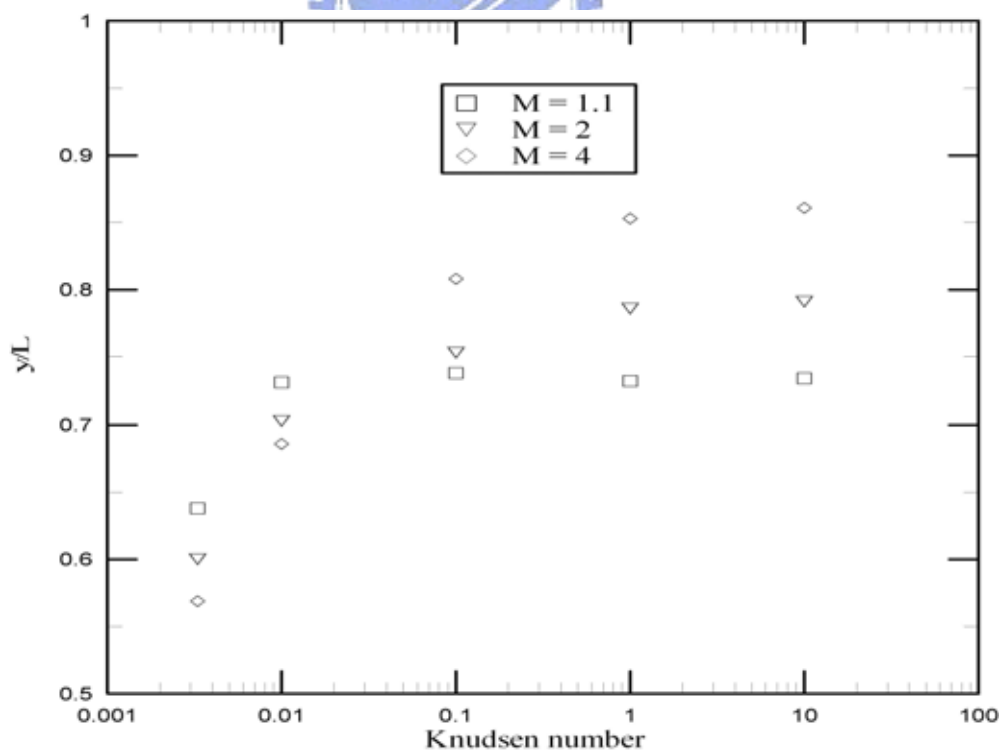**Fig. 3.108**   Streamline for Kn=0.01 (a) M=1.1; (b) M=2; (c) M=4

(a)

(b)

(c)

Fig. 3.109   Streamline for Kn=0.0033 (a) M=1.1; (b) M=2; (c) M=4

Fig. 3.110 Relative horizontal distance (x/L) of vortex center for various value of Mach

number and Knudsen number

Fig. 3.111 Relative horizontal distance (y/L) of vortex center for various value of Mach

number and Knudsen number